UNIVERSIDAD MICHOACANA DE SAN NICOLÁS DE HIDALGO

DIVISION OF GRADUATE STUDIES

FACULTY OF ELECTRICAL ENGINEERING

THESIS

MODEL PREDICTIVE CONTROL FOR POWER CONVERTERS: A STUDY IN THE LINEAR COMPLEMENTARITY FRAMEWORK

In partial fulfillment of the requirements for the degree of

DOCTOR OF SCIENCE IN ELECTRICAL ENGINEERING

Presents

Rodrigo Morfín Magaña

Thesis Advisor

Dr. J. Jesús Rico Melgoza

Thesis Co-Advisor

Dr. Fernando Ornelas Tellez

Morelia, Michoacán, March 2019

MODEL PREDICTIVE CONTROL FOR POWER CONVERTERS: A STUDY IN THE LINEAR COMPLEMENTARITY FRAMEWORK

Los Miembros del Jurado de Examen de Grado aprueban la **Tesis de Doctorado en Ciencias en Ingeniería Eléctrica, Opción en Sistemas de Control** de ***Rodrigo Morfín Magaña.***

Dr. Norberto García Barriga
Presidente del Jurado

Dr. J. Jesús Rico Melgoza
Director de Tesis

Dr. Fernando Ornelas Téllez
Co-director

Dr. Roberto Tapia Sánchez
Vocal

Dr. Luís Eduardo Ugalde Caballero
Revisor Externo (ITM-Morelia)

Dr. Roberto Tapia Sánchez
Jefe de la División de Estudios de Posgrado de la Facultad de Ingeniería Eléctrica. UMSNH
(Por reconocimiento de firmas)

UNIVERSIDAD MICHOACANA DE SAN NICOLÁS DE HIDALGO
Marzo 2019

Acknowledgments

To my parents María de Jesús Magaña Gonzales and Salvador Morfín Rodriguez, Who have always supported me more than I expected and They have been the fundamental base that has allowed me to obtain the present degree.

To my sister Shelby Edith Morfín Magaña, who has always support me and help me whenever I have needed it.

To my family, my wife Maricruz Tinoco Navarrerte, my daughter Miranda Arelí Morfín Tinoco, my son Leonardo Morfín Tinoco, Who are my main motivation to stay strong and never give up.

To my advisors J. Jesús Rico Melgoza and Fernando Ornelas Tellez, Who share with me their experience in the academic research field and always had a good advice for me during my studies.

To the *Consejo Nacional de Ciencia y Tecnología* **CONACYT** and the Mexican Government, which funded the present research and my Doctor in Sciences studies.

Resumen

Esta tesis propone el uso del marco de referencia complementario, desarrollado recientemente en la literatura para el modelado de convertidores de potencia. Se puede considerar que el convertidor de potencia consiste en elementos lineales (resistencias, condensadores e inductores), fuentes de voltaje y corriente, y dispositivos electrónicos (ED) como diodos e interruptores (tiristor, transistor, etc.). Una forma típica de modelar sistemas basados en convertidores de potencia es asumir las características no lineales de los EDs como ideales. En este contexto, los modelos de complementariedad han demostrado ser un enfoque apropiado para modelar y analizar convertidores de potencia. Dado que estos modelos, a diferencia de otras técnicas de modelado, representan el convertidor de potencia en todos los modos de operación, sin enumerarlos o asumir una determinada secuencia de modos o tiempos de conmutación, además de que su naturaleza discreta constituye una herramienta eficiente para el diseño de técnicas de control avanzadas en tiempo discreto. La presente tesis propone el desarrollo de esquemas de control predictivo (MPC) para convertidores de potencia modelados en el marco de referencia complementario. MPC es una técnica de control óptimo basada en el modelo y se caracteriza por ser muy intuitiva y permite incorporar restricciones, tanto lineales como no-lineales, en su formulación. La combinación del MPC y el marco complementario (de naturaleza discreta) para el diseño de control en convertidores de potencia, obtiene como resultado un controlador en tiempo discreto. Los controladores en tiempo discreto, a diferencia de los controladores analógicos, presentan desafíos adicionales durante su implementación, relacionados con los tiempos de ejecución y conversión analógico-digital. Por lo tanto, el diseño de control digital requiere probar su desempeño en un ambiente de tiempo real, ya sea por medio de una implementación ó utilizando técnicas de simulación avanzada como hardware-in-the-loop (HIL). En el desarrollo de la presente tesis se presentan casos de estudios que ejemplifican el uso de las herramientas propuestas en convertidores de potencia. Particularmente, en la etapa de modelado se utilizan los convertidores boost, buck y buck-boost, durante la descripción de los esquemas de control predictivo se presenta un rectificador, y finalmente como casos de estudio se presenta un circuito para la conexión de un panel fotovoltaico con la red, y las implementaciones para un inversor monofásico conectado a la red, así como un convertidor boost usando una técnica HIL. En los casos de implementación, este trabajo de tesis propone metodologías

adicionales que permiten robustecer los controladores implementados.

La presente tesis inicia con la revisión del modelado de convertidores de potencia en el marco complementario, teoría que ha sido detalladamente desarrollada en la literatura. Posteriormente como aportaciones originales en este marco se proponen esquemas de control predictivo que involucran entradas de control binarias y con modulación de ancho de pulso, así como su implementación en tiempo real, donde métodos para robustecer el controlador ante variaciones paramétricas son propuestos. Además de un estudio y diseño de control para un circuito completo de un panel fotovoltaico conectado a la red en el marco complementario.

Palabras clave: Modelo de control predictivo, sistemas híbridos,convertidores de poder, sistemas complementarios lineales, Lógica-Mixta dinámica.

Abstract

This thesis proposes the use of the complementary framework, which has been recently developed in the literature for modeling power converters. The power converter can be assumed to consist of linear elements (resistors, capacitors, and inductors), voltage and current sources, and electronic devices (EDs) such as diodes and switches (thyristor, transistor, etc.). A typical way to modeling power converters based systems is to assume the non-linear characteristics of EDs to be ideals. In this context, the complementarity models have proved an outstanding approach to modeling and analyzing power converters. Since these models, unlike other modeling techniques, represent the power converter in all modes without enumerating them or assuming a given sequence of modes or switching times, besides that the discrete nature of this models constitutes an efficient methodology for the design of advanced control techniques in discrete time. Therefore, this thesis proposes the development of model predictive control (MPC) schemes for power converters modeled in the complementary framework. MPC is an optimal control technique model-based that is characterized by being very intuitive and stands out, among other things, for the possibility to incorporate constraints, linear and non-linear, in the control formulation. The combination of the MPC and the complementary framework (of discrete nature) for the control design in power converters, results in a discrete-time controller. The controllers in discrete time, unlike the analog controllers, present additional challenges during their implementation, related to the execution times and analog-digital conversion, and in some cases (when an analog control signal is required) digital-analog conversion. Therefore, digital control design requires testing the controller performance in a real-time environment, either through implementation or using advanced simulation techniques such as hardware-in-the-loop (HIL). In the development of this thesis, case studies are presented that exemplify the use of the proposed methodology in power converters. Particularly, in the modeling part the boost, buck, and buck-boost converters are modeled, during the description of the model predictive control schemes a rectifier is presented, and finally as case studies a circuit for the connection of a photovoltaic panel with the grid is presented, and the implementations for a single-phase inverter connected to the grid as well as a boost converter using a HIL technique. In the implementation cases, this thesis work proposes additional methodologies that endowed robustness to the implemented controllers.

This thesis begins with the revision of the modeling of power converters in the complementary framework, a theory that has been developed in detail in the literature. Subsequently, as original contributions in this framework, predictive control schemes are proposed that involve binary control inputs and pulse width modulation, as well as their implementation in real time, where methods to given robustness to the controller against parametric variations are proposed. In addition to a study and control design for a complete circuit of a photovoltaic panel connected to the grid in the complementary framework.

Key words: Model predictive control, Hybrid systems, Power converters, Linear complementary systems, Mixed-Logical dynamical.

Table of content

List of figures

List of tables

List of acronyms

CCM Continuous conduction mode

CCS-MPC Continuous control set - MPC

DCM Discontinuous conduction mode

DMC Dynamic matrix control

DSP Digital signal processor

ED Electronic device

FACTS Flexible AC transmission system

FCS-MPC Finite control set - MPC

FPGA Field programmable gate array

GPC Generalized predictive control

HIL Hardware in the loop

LC Linear complementarity

LCP Linear complementarity problem

LCS Linear complementarity system

LQR Linear quadratic regulator

MAC Model algorithmic control

MI Mixed integer

MILFP	Mixed integer feasibility problem
MIP	Mixed integer problem
MIQP	Mixed integer quadratic problem
MLD	Mixed logical dynamical
MPC	Model predictive control
MPPT	Maximum power point tracking
PC	Power converter
PI	Proportional integral
PID	Proportional integral derivative
PLCP	Parametric linear complementarity problem
PLL	Phase locked loop
PV	Photovoltaic
PWA	Piecewise affine
PWM	Phase width modulation
PO	Perturbation and observation
QDMC	Quadratic dynamic matrix control
QP	Quadratic problem
RDS	Resistors diodes sources
PI	Proportional integral
RHC	Receding horizon control
RLS	Recursive least squares
VSS	Variable structure system

Chapter 1

Introduction

Power converters and drives technologies have been in constant development for several decades to enable the most precise use of electricity. Currently, the use of power converters includes low, medium and high power applications. Finding accurate mathematical frameworks is one of the main steps, especially when advanced control techniques are to be applied. Linear complementarity framework is a new perspective to modeling power converters, which emerges from the hybrid system theory to efficiently capture all operation modes in power converters. On the other hand, the model predictive control (MPC) is an advanced control strategy based on the mathematical model of the plant. The MPC has great acceptance in the industrial processes due to its simple implementation and effectiveness. Recently, the MPC has attracted the interest of research and academic communities, thanks to its optimization capabilities and the growing need of more accurate mathematical models of the plant, incorporating nonlinearities. Today, its application to electronic power converters and electrical drives is increasing [Rodriguez and Cortes, 2012, Vazquez *et al.*, 2014], since it can help fulfill the growing performance, efficiency, and safety demands and meet the standards and operational limits demanded by the evolving industry applications.

Modeling of Power Converters

Power converters can be assumed to consist of linear elements (resistors, inductors, capacitors), current and voltage sources, and electronic devices (EDs) such diodes and

electronic switches (thyristors, transistors, IGBTs, etc.). From the viewpoint of control engineering, power converters (PC) belong to a very special class of circuits to be controlled. Due to switching action (which is common to every PC), the structure of a PC model switches periodically between a set of ordinary differential equations. The whole model is then a differential equation system with discontinuous right-hand side function (resulting in a non-linear system). In the control literature, they are also called variable structure systems (VSS). Then, VSS control theory would be an immediate choice for control objective of PC. But this is not the widely adopted approach as described in [Sun and Grotstollen, 1992]. Recalling the history of power electronics, one can find that averaging has been a dominant technique for analysis and control of the PC. In average methods, the discontinuity of the original discontinuous models are smoothed and continuous, so that control methods for continuous systems become applicable. The most important technique is the space state average method proposed in [Middlebrook and Cuk, 1976], which is now a standard technique for analysis and control of PC. But it still has the following shortcoming: application to PWM converters working under discontinuous conduction mode or with current programmed control is not straightforward, application to resonant and quasi-resonant converters is impossible because small ripple assumption is not satisfied by the state variables of these converters, and a complete justification of validity of method has yet not been provided.

Another more accurate technique consist of assuming the diodes and switches to be ideal, discriminating among the different modes of the converter, building for each mode a linear time-invariant dynamic model, and determining the conditions for the computation among the different modes [Maksimovic *et al.*, 2001]. The resulting model is usually called as switched model. In this technique, the commutation conditions can depend on the state variables, and the switched model eventually becomes rather complex also for simple PC topologies [Burdio and Martinez, 1995]. In general, a switched model that describes all possible operations conditions is very difficult to obtain.

Another approach for power converters is given in the area of hybrid systems, this class of system involves continuous dynamics and discrete events. These continuous and discrete dynamics not only coexist but interact and changes occur both in response to discrete, instantaneous events and in response to dynamics, described by differential or

difference equations in time [van der Schaft, 1999, Branicky, 1998]. A special class of hybrid system is the complementarity model [Heemels *et al.*, 1999]. These models are characterized by a linear dynamic part and a suitable set of so-called complementarity variables (interpreted as inputs and outputs of the dynamic part of the model), which are constrained not to be nonzero at the same time [van der Schaft and Schumacher, 1998, Camlibel, 2001]. Complementarity systems have been proposed as a framework for modeling (static) resistors diodes sources (RDS) circuits [Camlibel *et al.*, 2003], which include only linear resistor, independent voltage, and current sources and ideal diodes [Vandenberghe *et al.*, 1989]. More recently, complementarity systems have been used to model switched electrical networks that contain ideal diodes and ideal switches [Vasca *et al.*, 2009]. Using the complementarity framework the PC can be modeled from a different perspective with respect to the classical approaches as average and switched models. In this framework the EDs are considered as external elements and modeled separately, then the entire model of the converter is obtained by integrating the EDs representation with the dynamic equations of the power converter circuit. The complementarity model is simple to build, captures in a very simple way all modes of the converter and allows the idealization of the EDs characteristics at the desired level of abstraction. In this thesis, the complementarity framework theory is used to modeling power converters. This allows capturing all operation modes of the PC by means of a generalized procedure for every PC topology, which is an advantage from another kind of hybrid systems.

Model Predictive Control

The development of modern control concepts can be traced back to the work of Kalman in the early 1960s with the linear quadratic regulator (LQR), designed to minimize an unconstrained quadratic objective function of states and inputs. The infinite horizon endowed the LQR algorithm with powerful stabilizing properties. However, how is mentioned in [Cavalcanti, 2001], this control had little impact on the control technology development in the process industries. The reason for this lies in the absence of constraints in its formulation, the nonlinearities of the real systems, and above all the culture of the industrial

process control community in that time, in which instrument technicians and control engineers either had no exposure to optimal control concepts or regarded them as impractical. Thus the early proponents of model predictive control (MPC) for process control proceeded independently, addressing the needs of the industry, with a intuitive optimal control scheme that can be solved by numeric algorithms, taking advantage of the available computational technology in that time.

In the late 1970s, various articles reported successful applications of MPC in the industry, in [Richalet *et al.*, 1978] the authors presenting a Model Predictive Heuristic Control (later known as Model Algorithmic Control (MAC)). The first model predictive control algorithm was introduced by Cutler and Ramaker in early 1980s as Dynamic Matrix Control (DMC). The common theme of MPC strategies was the idea of using a dynamic model of the process to predict the effect of the future control actions, then the best control action is determined by minimizing the predicted error subject to operational restrictions. The optimization is repeated at each sampling period with updated information from the process. These formulations are algorithmic and also heuristic, and took advantage of the increasing potential of digital computers from that time.

Later, the second generation of MPC arrived, where the control problem is presented as an optimization problem, such as quadratic dynamic matrix control (QDMC), in [Garcia and Morshedi, 1986] the authors used quadratic programming to solve the constrained open-loop optimal control problem, where the system is linear, the cost function quadratic, the control and state constraints are defined by linear inequalities. Later in the early 1990s, in [James and Kenneth, 1993] the authors developed an infinite horizon controller in a receding feedback strategy, where the controller's implementation requires only the solution of finite-dimensional quadratic optimization programs. This MPC approach was of great interest for a whole range of interesting applications in the engineering field. In particular, the MPC as a control technique for PC takes advantage of their inherent discrete nature, but only when the mathematical model of PC preserves their characteristic no-linear behavior. This thesis purposes MPC schemes based on the power converter dynamics, because the MPC characteristics which allow to incorporating the constraints that result in the PC complementarity model. This allows that the resulting controller range

includes all operation modes of the PC.

1.1. Problem statement

The control of PC is an area that continues in constant development due to their multiple applications, in which they can be applied in a current technological context, such as the integration of alternative energy sources and electric vehicles, to name a few. In PC, one of the most used modeling techniques until now is averaged models, where classic control techniques as PIDs can be used. However, these modeling and control techniques are effective for a small operation range, limiting the possible conduction modes in the PC. In this sense, advance control techniques requires accurate non-linear models of power converters, in order to design controllers that can operate efficiently in a wide operation range.

1.2. Background

Model predictive control (MPC) has now approximately four decades of sustained development [Morari and Lee, 1999, Lee, 2011], and its considered one of the most important advances in control process. However it had few applications in power converters control due to the high amount of calculations needed in order to solve the optimization problem online, which is incompatible with the small sampling times used in converter control. But this restriction has begun to fade out, thanks to the explosive evolution of digital control platforms over the last decades, such as digital signal processors (DSPs) or field programmable gate arrays (FPGAs), enabling the implementation of emerging and, usually, more complex control techniques [Bordons and Montero, 2015]. MPC schemes have been applied to the control of specific power electronic systems. An MPC has been used in [Cheng *et al.*, 2018] to control a boost converter to maintain the output voltage while avoiding large peak inductor current. MPC has also been used in DC-AC inverters, in the reference [Cortes *et al.*, 2009] which shows an inverter with a passive filter. The controller uses the model of the system to predict the behavior of the output voltage for each possible swit-

ching state. Since the switching strategy is based on space vector and the number of possible switching states are a few, the selection of the best switching sequence can be easily done by comparing the results of each of the possible sequences. The reference [Cortes *et al.*, 2009] has proven that the MPC is useful in the control of multilevel converters. The MPC had also found application in power converters for flexible AC transmission system (FACTS), the reference [Geyer *et al.*, 2015] presents a predictive controller for a STATCOM that provides quality voltage to a three phase load. In reference [Shi *et al.*, 2013] three phase voltage source rectifiers under unbalanced grid voltage conditions are controlled via MPC to ensure stable dc-side voltage. The term MPC does not designate a specific control strategy but rather an ample range of control methods that makes explicit use of a model of the system in order to predict the future behavior of the variables over a time frame (integer multiple of the sample time). These predictions are evaluated based on a cost function, and then, the sequence that minimizes the cost function is chosen, obtaining, in this way, the sequence of optimized control actions. Only the first value of the sequence is applied, and the algorithm is calculated again every sampling period. MPC presents several features that make it suitable for controlling PC. Apart from being intuitive and easy to understand, constraints, nonlinearities, and multivariable case can easily be included in the formulation [Kouro *et al.*, 2009a]. The MPC technique applied to power converters have been classified into two main categories [Cortes *et al.*, 2008, Linder *et al.*, 2010]: continuous control set MPC (CCS-MPC) and finite control set MPC (FCS-MPC). Reference [Cheng *et al.*, 2018] is an example of a CCS-MPC. FCS-MPC approaches for power converters have emanated from the hybrid systems theory. MPC techniques have been widely applied in power electronics [Kouro *et al.*, 2009b]. A comparison between CCS-MPC and FCS-MPC is presented in [Ahmed *et al.*, 2018] for an induction machine in terms of their design performance. In the first group, a modulator generates the switching states starting form the continuous output of the predictive controller. On the other hand, the FSC-MPC approach takes advantage of the limited number of switching states of the power converter for solving the optimization problem. A discrete model is used to predict the behavior of the system of every admissible actuation sequence up to prediction horizon. The switching action that minimizes a predefined cost function is finally selected to be applied in the next sampling instant. The main

advantages of the FCS-MPC lies in the direct application of the control action to the converter, without requiring a modulation stage [Rodriguez *et al.*, 2013]. Practical operative scenarios of power converters usually determine the converter to operate in continuous and discontinuous conduction modes which contribute to the difficulties for their control design. Indeed, MPC requires the prediction of the system state whose evolution depends on the sequence of configurations of the circuit which are not directly controllable in many situations, such as for the conducting and blocking states of the diodes [Cheng *et al.*, 2018]. A possible solution for obtaining a power converter model valid for all operating conditions consists of using a mixed logical dynamical (MLD) model. Within the MLD modeling framework the MPC problem can be formulated as a mixed-integer quadratic program (MIQP).

MLD models have been used for the MPC of DC-DC boost converters and for realizing MPC through MIQP approaches [Hai-Peng *et al.*, 2015], in the case of step-down DC-DC converters [Hejri and Giua, 2011, Almer and Morari, 2013]. A finite control set MPC (FCS-MPC) based on a MLD model of an inverter has been proposed in [Li *et al.*, 2014]. The equivalence between MLD and linear complementarity (LC) models has been shown in [Heemels and Schutter, 2000]. On the other hand, the advantage of LC model is the compact and modular procedure for the construction of this type of power converters model. Indeed, LC systems describe the converter dynamic behavior in all operating modes without enumerating them or assuming a given sequence of modes or switching times [Vasca *et al.*, 2009]. The usefulness of LC models in the power electronics field has been confirmed in [Tant *et al.*, 2012, Addi and Goeleven, 2017]. Specific PC topologies such as single-phase diode bridges [Acary *et al.*, 2011], resonant converters [Iannelli *et al.*, 2011] and three-phase rectifiers [Rico-Melgoza *et al.*, 2009] have been modeled and analyzed within the complementarity framework. Recently, those models have been extended also to closed-loop power converts [Batlle *et al.*, 2005, Sessa *et al.*, 2014, Lopez-Castillo and Rico-Melgoza, 2014, Sessa *et al.*, 2016]. However, in the MPC design for power converters, the LC model does not be exploited yet despite their modeling advantages. In this thesis, the modeling of power converters is proposed in the complementarity framework, and then an FCS-MPC is formulated based in this model.

1.3. Justification

The theory of hybrid systems as well the complementarity framework has been described in the literature. The modeling of power converters in the complementarity framework has been clearly presented as an accurate technique that model all the operation modes of the power converter in compact structures. However, this powerful framework has not been exploited in model-based control designs where these accurate models can be a compressive method for analyzing the control performance of power converters considering their entire behavior. This thesis aims to take the complementarity framework to the next step in the design of model predictive control schemes for power converters.

1.4. Motivation

New emerging frameworks for modeling power converters as linear complementarity systems actually have been demonstrated a powerful methodology for transient and steady-state analysis. The main advantage of this modeling technique is that represent any power converter topology in all operation modes without enumerating them or assuming a given sequence of modes or switching times, and they constitute a pretty accurate model for the power converters. This general processes to modeling any power converter topology can be exploited into a next step, for advanced model-based control techniques, like MPC, where one of the main advantages is that can handle constraints, and these can be nonlinear. The combination of the complementarity models and the MPC schemes brings to us a complete framework for the power converter analysis and control.

1.5. Hypothesis

The complementarity framework can be used as the basis for modeling power converters, where all operation modes of the real converter are modeled. Then, by defining general transforms, the complementarity model can be rewritten to another hybrid system, where schemes of model predictive control that includes a quadratic objective function can be designed. This allows the establishment of an entire framework for power converter analy-

sis and control, where the involved methodology does not depend on the power converter topology.

1.6. Objectives

1.6.1. General Objective

Development of a complete methodology for modeling, analysis, simulation, and control of power converters in the complementarity framework, where all operation modes and non-linear behavior are preserved.

1.6.2. Particular Objectives

- Modeling of power converters in the complementarity framework.
- Control designs for power converters, in particular advance model-based predictive control techniques.
- Implementation of controllers based on MPC schemes for practical power converter applications.

1.7. Methodology

The thesis methodology consists of a literature review that allows to describe in detail the steps to modeling power converters in the complementarity framework. After, three paths to formulating the control predictive problem are explored, where optimization algorithms as exahustive search, Nelder-Mead and mixed integer quadratic problems are used. Finally, in the implementation of the controller, techniques as hardware in the loop and recursive least square are used.

1.8. Thesis contributions

The main contributions of this thesis are:

- A detailed process for the modeling power converter in the complementarity framework.
- Methods to transform LC models into another hybrid system, that can be useful in MPC schemes with quadratic objective functions.
- Original MPC schemes for power converters control, including phase-width modulation inputs and without any modulation signal.
- A comparative study of the advantages and disadvantages of including PWM signal in MPC schemes.
- A Hardware-in-the-loop method for testing a boost converter controller in a real-time environment.
- The development of techniques for given robustness to the MPC controllers during their implementations.
- A complete study case of a grid-connected photovoltaic source for residential microgrid applications.

1.9. Thesis Outline

- Chapter 2 introduces the optimization concepts, which are the basis for modeling and transient simulation of power converters in the complementarity framework, and for the MPC formulations that have been addressed in the following chapters.
- Chapter 3 describes a method to model power converters in the linear complementarity framework. In this chapter, the LC model is used for transient simulation, and other hybrid system representations, as a piecewise system and a mixed logical dynamical system, are derived from this model. Each model is validated by means of a comparison with the commercial simulator SystemModeler.
- Chapter 4 presents the MPC schemes for power converters modeled in the complementarity framework. Different FCS-MPC formulations are introduced, where the models

described in chapter 3 are used. Additional formulations are described to model the control input as PWM signals, which can be included in the FCS-MPC formulation. Additionally, a comparison of the control performance when including and not a PWM signal is presented.

- Chapter 5 applies the LC modeling and MPC schemes in practical examples of power converters. A study case of a grid-connected photovoltaic cell and two real-time implementations of FCS-MPC are presented. Additionally, in the implementation cases, methods to given robustness to the FCS-MPC controller are presented.

- Chapter 6 concludes the thesis and future work is proposed.

Chapter 2

Linear complementarity system of power converters

In this chapter, the linear complementarity framework is introduced as a modeling technique capable of capture all the non-linear characteristics of the power converter, a description of how to modeling power converters into a linear complementarity system, and the use of these models in transient simulation for power converters is presented. Additionally, methods to transform the linear complementarity system into other hybrid system are presented, particularly in a piecewise and mixed-logical-dynamical system. In order to prove the effectiveness of these systems to capture all the power converter dynamics, a comparison with the simulator SystemModeler is performed by means of transient simulations of the power converters: boost, buck, and buck-bost.

2.1. Complementarity models of electronic devices

The idealized voltage–current characteristics of electronic devices can be represented in the complementarity framework by means of static LC models in the form

$$\varphi = B_s z + E_s u \tag{2.1a}$$

$$w = C_s \lambda + D_s z + F_s u + h_s \tag{2.1b}$$

$$0 \leq w \perp z \geq 0 \tag{2.1c}$$

where (φ, λ) is the voltage–current or current–voltage pair of the electronic device, $w \in \mathbb{R}_+^{N_z}$ and $z \in \mathbb{R}_+^{N_z}$ are complementarity variables, $u \in \{0, 1\}$ is the external control input of the switch, and B_s, E_s, C_s, D_s, F_s, h_s are constant matrices of suitable dimensions. The symbol "$\perp$" represents the orthogonality condition, i.e., $w \perp z$ stands for $w^\top z = 0$, and inequalities among vectors are componentwise. The variable λ can be interpreted as the input of the device model while φ can be seen as the corresponding output. A typical model of an

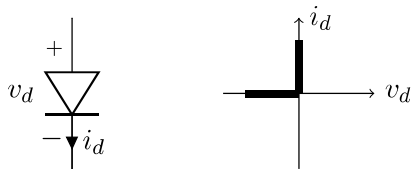

Figure 2.1: (a) Diode symbol. (b) Voltage-current characteristic.

ideal diode in the voltage–current plane consists of two halflines: the voltage is zero and the current takes any positive value when the device is conducting, the current is zero and the voltage is negative under blocking operating conditions. The diode characteristic can be directly represented through a pair of complementarity variables. Figure 2.1 shows the ideal diode schematic and its set-valued voltage–current characteristic. This is a non-controlled device and then $E_s = F_s = 0$. The characteristic can be represented in the LC framework with a pair of complementarity variables. If the diode current is considered as an output variable, say $\varphi_{dc} = i_d$, and the diode voltage as an input variable, say $\lambda_{dv} = v_d$, the complementarity diode model can be expressed as

$$\varphi_{dc} = z_d, \quad w_d = -\lambda_{dv} \tag{2.2}$$

with $0 \leq w_d \perp z_d \geq 0$, which is in the form (2.1) with $B_s = 1$, $C_s = -1$, $D_s = 0$ and $h_s = 0$. The subscripts "dc" and "dv" are used to indicate that the variable refers to a diode current (first subscript) or a diode voltage (second subscript), respectively. Conversely, if the output is the voltage $\varphi_{dv} = v_d$ and the input is the diode current $\lambda_{dc} = i_d$, it is obtained the complementarity model

$$\varphi_{dv} = -z_d, \quad w_d = \lambda_{dc} \tag{2.3}$$

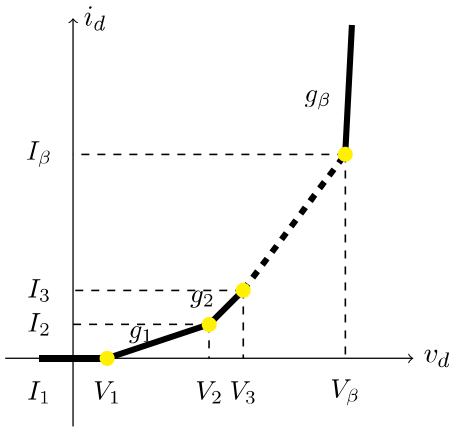

Figure 2.2: Piecewise linear approach of the diode voltage-current characteristic.

with $0 \leq w_d \perp z_d \geq 0$, which is in the form (2.1) with $B_s = -1$, $C_s = 1$, $D_s = 0$ and $h_s = 0$.

An alternative piecewise linear characteristic of a diode is shown in Fig. 2.2. Say β the number of breakpoints in the voltage-current characteristic, (V_i, I_i), $i = 1, \ldots, \beta$ the coordinates of the i-th breakpoint, ρ_i the slope of the i-th linear piece of the characteristic, i.e.

$$\rho_i = \frac{I_{i+1} - I_i}{V_{i+1} - V_i}, \tag{2.4}$$

with $i = 1, \ldots, \beta$, $(V_{\beta+1}, I_{\beta+1})$ a generic point of the last linear piece of the characteristic. If the last piece of the characteristic is vertical, then $V_{\beta+1} = V_\beta$ and $\rho_\beta = +\infty$. Let us define the admittance in the i-th linear part of the voltage-current characteristic as follows

$$g_i = \rho_i - \rho_{i-1}, \tag{2.5}$$

where $i = 1, \ldots, \beta$, $\rho_0 = 0$ (the first piece is horizontal).

If the diode current is considered as an output variable, $\varphi_{dc} = i_d$, the diode voltage as an input variable, $\lambda_{dv} = v_d$ the diode characteristic can be expressed in the following

linear complementarity form

$$\varphi_{dc} = z_1 + \cdots + z_\beta \tag{2.6a}$$

$$w_1 = -\lambda_{dc} + \frac{1}{g_1} z_1 + V_1 \tag{2.6b}$$

$$\vdots$$

$$w_\beta = -\lambda_{dc} + \frac{1}{g_\beta} z_\beta + V_\beta \tag{2.6c}$$

with the complementarity condition $0 \leq w \perp z \geq 0$ where w and z are vectors collecting the corresponding complementarity variables. The model (2.6) is in the form (2.1) with $B_s = \begin{pmatrix} 1 & \dots & 1 \end{pmatrix}$, $C_s = -B_s^\top$,

$$D_s = \begin{pmatrix} \frac{1}{g_1} & \dots & 0 \\ \vdots & \ddots & 0 \\ 0 & \dots & \frac{1}{g_\beta} \end{pmatrix}, \quad h_s = \begin{pmatrix} V_1 \\ \vdots \\ V_\beta \end{pmatrix},$$

G_s and H_s zero matrices of suitable dimensions.

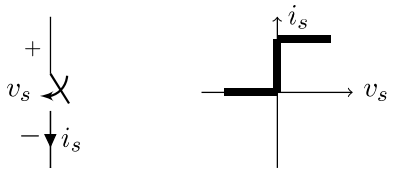

(a) (b)

Figure 2.3: (a) Switch symbol. (b) Voltage-current characteristic.

The model (2.1) can be used to represent the idealized characteristics of controlled electronic devices in the LC form. Let us consider a bipolar junction transistor where i_s is the collector current, v_s is the collector-emitter voltage, I_M is the maximum collector current, $u \in [0, 1]$ is the normalized switch control signal proportional to the base current. In the following we assume $u \in \{0, 1\}$. Analogous physical meanings of i_s, v_s, I_M and u are possible for other electronic switches. When the switch is blocking (Off, $u = 0$) the switch current i_s is identically zero for any switch voltage v_s. When the switch is conducting (On,

$u = 1$) the voltage v_s is zero and the device can provide any current between 0 and $I_{\mathrm{M}}u$, see Figure 2.3.

Let us consider the switch as a subsystem whose output is the switch current, i.e. $\varphi_{sc} = i_s$, and input is the switch voltage, i.e. $\lambda_{sv} = v_s$. The subscripts "sc" and "sv" are used to indicate that the variable refers to a switch current (first subscript) or a switch voltage (second subscript), respectively. Then the voltage–current characteristic in Figure 2.3 can be represented with the following LC model

$$\varphi_{sc} = z_1 \quad w_1 = -\lambda_{sv} + z_2 \quad w_2 = -z_1 + I_{\mathrm{M}}u \tag{2.7}$$

with the complementarity condition $0 \leq w \perp z \geq 0$ where w and z are vectors collecting the corresponding complementarity variables. The model (2.7) is in the form (2.1) with

$$B_s = \begin{pmatrix} 1 \\ 0 \end{pmatrix}^{\top}, \; C_s = \begin{pmatrix} -1 \\ 0 \end{pmatrix}, \; D_s = \begin{pmatrix} 0 & 1 \\ -1 & 0 \end{pmatrix}, \; F_s = \begin{pmatrix} 0 \\ I_{\mathrm{M}} \end{pmatrix},$$

$E_s = 0$ and $h_s = 0$. The expressions (2.7) together with the complementarity constraint can be explained by looking at the possible values assumed by the input $\lambda_{sv} = v_s$. The following cases are possible:

$$\lambda_{sv} < 0 \Rightarrow w_1 > 0 \Rightarrow z_1 = 0 \Rightarrow \varphi_{sc} = 0 \tag{2.8a}$$

$$\lambda_{sv} > 0 \Rightarrow z_2 > 0 \Rightarrow w_2 = 0 \Rightarrow \varphi_{sc} = z_1 = I_{\mathrm{M}}u \tag{2.8b}$$

$$\lambda_{sv} = 0 \Rightarrow \{w_1 \geq 0, z_2 \geq 0\} \Rightarrow \; \varphi_{sc} = z_1 \in [0, \; I_{\mathrm{M}}u] \tag{2.8c}$$

with $u = \{0, 1\}$.

The LC model of the switch is different if the input of the model is the current, i.e. $\lambda_{sc} = i_s$, and the output is the voltage, i.e. $\varphi_{sv} = v_s$. In this case the LC model can be written as

$$\varphi_{sv} = -z_1 + z_2, \quad w_1 = \lambda_{sc}, \quad w_2 = -\lambda_{sc} + I_{\mathrm{M}}u \tag{2.9}$$

with the complementarity condition $0 \leq w \perp z \geq 0$, where w and z collects in vectors the corresponding complementarity variables. The model (2.9) is in the form (2.1) with

$$B_s = \begin{pmatrix} -1 \\ 1 \end{pmatrix}^{\top}, \; C_s = \begin{pmatrix} 1 \\ -1 \end{pmatrix}, \; F_s = \begin{pmatrix} 0 \\ I_{\mathrm{M}} \end{pmatrix}, \tag{2.10}$$

$D_s = 0$, $E_s = 0$ and $h_s = 0$. The expressions (2.9) can be explained by considering the different ranges for the input $\lambda_{sc} = i_s$. The following cases are possible:

$$\lambda_{sc} = 0 \Rightarrow \{w_1 = 0, w_2 = I_{\mathrm{M}} u\}$$
$$\Rightarrow \begin{cases} u = 1 & \Rightarrow z_2 = 0 \Rightarrow \varphi_{sv} = -z_1 \leq 0 \\ u = 0 & \Rightarrow \varphi_v = -z_1 + z_2 \in \mathbb{R} \end{cases} \tag{2.11a}$$

$$\lambda_{sc} = I_{\mathrm{M}} u \Rightarrow \begin{cases} u = 1 & \Rightarrow w_1 > 0 \Rightarrow z_1 = 0 \\ & \Rightarrow \varphi_{sv} = z_2 \geq 0 \\ u = 0 & \Rightarrow \text{see (2.11a)} \end{cases} \tag{2.11b}$$

$$0 < \lambda_{sc} < I_{\mathrm{M}} u \Rightarrow \{w_1 > 0,\ w_2 > 0\} \Rightarrow \varphi_{sv} = 0, \tag{2.11c}$$

with $u = \{0, 1\}$. Another electronic device which is commonly used in power converters

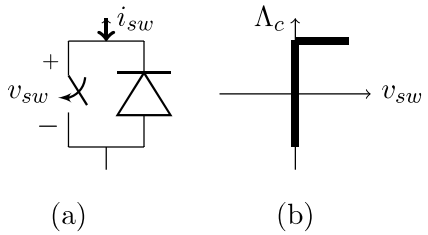

Figure 2.4: (a) Switch with antiparallel diode symbol. (b) Voltage-current characteristic.

consists of an antiparallel connection of an electronic switch and a diode, see Figure 2.4. The resulting characteristic has one breaking point and it can be modelled with one pair of complementarity variables. Assume that the input is $\lambda_{av} = v_{sw}$ and the output is $\varphi_{ac} = i_{sw} = i_s - i_d$ that is the difference between the switch and the diode currents. The subscripts "ac" and "av" are used to indicate that the variable refers to a antiparallel-switch (first subscript) current (second subscript) or an antiparallel-switch voltage, respectively. Then an LC model can be written as

$$\varphi_{ac} = -z + I_{\mathrm{M}} u, \quad w = \lambda_{av} \tag{2.12}$$

with $0 \leq w \perp z \geq 0$ and $u = \{0, 1\}$. The equations (2.12) are in the form (2.1) with $B_s = -1$, $E_s = I_M$, $C_s = 1$, $D_s = 0$, $F_s = 0$ and $h_s = 0$. In the case $\lambda_{ac} = i_{sw}$ and

$\varphi_{av} = v_{sw}$ the corresponding LC model can be written as

$$\varphi_{av} = z, \quad w = -\lambda_{ac} + I_{\mathrm{M}} u \tag{2.13}$$

with $0 \leq w \perp z \geq 0$, $u = \{0, 1\}$, which is in the form (2.1) with $B_s = 1$, $E_s = 0$, $C_s = -1$, $D_s = 0$, $F_s = I_M$ and $h_S = 0$.

The LC models of diodes and controlled switches are the basic elements from which more complex piecewise linear characteristics of electronic devices can be represented in the complementarity form. A general approach for more complex current–voltage characteristics can be obtained by an nondecreasing single break point as it described in [Vasca *et al.*, 2009]. The LC models of the different electronic devices can be collected in a complementarity representation in the form (2.1) with suitable block-diagonal matrices. Let us assume that the power converter under investigation has N_d diodes, N_s switches, N_a antiparallel switches. With some abuse of notation let us redefine the following variables: for the N_d diodes, say φ_{dc} (φ_{dv}) the column vector whose components are the currents (voltages) considered as outputs for the diodes model, with the corresponding λ_{dv} and λ_{dc} as inputs; for the N_s switches, say φ_{sc} (φ_{sv}) the column vector of the currents (voltages) considered as outputs for the swithces model, with the corresponding λ_{sv} (λ_{sc}) as inputs; for the N_a antiparallel switches, say φ_{ac} (φ_{av}) the column vector of the currents (voltages) considered as outputs for the antiparallel switches model, with the corresponding λ_{av} (λ_{ac}) as inputs. Then we can define the column vectors

$$\varphi = \mathrm{col}(\varphi_{dc}, \varphi_{dv}, \varphi_{sc}, \varphi_{sv}, \varphi_{ac}, \varphi_{av}), \tag{2.14a}$$

$$\lambda = \mathrm{col}(\lambda_{dc}, \lambda_{dv}, \lambda_{sv}, \lambda_{sc}, \lambda_{av}, \lambda_{ac}) \tag{2.14b}$$

where $\mathrm{col}(\cdot)$ indicates a vector obtained by stacking in a unique column the column vectors in its argument and $w \in \mathbb{R}_+^{N_z}$ and $z \in \mathbb{R}_+^{N_z}$ are the corresponding vectors of complementarity variables with $N_z = N_d + N_s + N_a$. The LC model in the form (2.1), including all electronic devices of the power converter, can be easily obtained by collecting all LC models of the electronic devices. This compact representation is useful for the formulation of the entire power converter LC model.

2.2. Linear complementarity system of power converters

Once all the electronic devices used in the power converter circuit are collected as (2.14), the next step is to deriving the state variables of the system dynamics and the input equations λ.

A power converter model can be derived by considering the interconnection of a dynamic system and a set of piecewise linear (φ, λ) characteristics representing the current-voltage characteristics of all electronic/switching devices. This approach can be synthesized with the block scheme in Figure 2.5. The dynamic subsystem considers as inputs the exogenous signals e and the vector φ of the devices currents and voltages, and can be written in the matrix form

$$\frac{\mathrm{d}}{\mathrm{d}t}x = A_c x + B_c \varphi + E_c e \tag{2.15a}$$

$$\lambda = C_c x + D_c \varphi + F_c e. \tag{2.15b}$$

The choice of considering the current or the voltage as the output of the device model is determined by the construction of the dynamic equations of the circuit. Then, the other device variable, i.e. λ, is chosen accordingly as an output of the dynamic subsystem and it will be an input for the device model. A minimal state space representation of the power converter can be obtained by circuit theory methods [Frasca *et al.*, 2010] or by bond graph approaches [Villa-Villaseor and Rico-Melgoza, 2018]. These methods are based tree and co-tree graph theory [Hyatt *et al.*, 2008]. The dynamic expressions can be obtained by firstly extracting the ideal to their ports and then by finding a proper tree, i.e. one that contains all the exogenous voltage (current) sources and the capacitors (inductors) in the network, but no inductors (capacitors) and no current (voltage) sources. A proper tree can be found if no loops of capacitors/voltage sources and no cut sets of inductors/current sources are present in the circuit. When this is the case, the complementarity model of a power converter can be found by artificially adding always open/closed ideal switches.

By combining the two subsystems representations (2.1) and (2.15), the whole LC

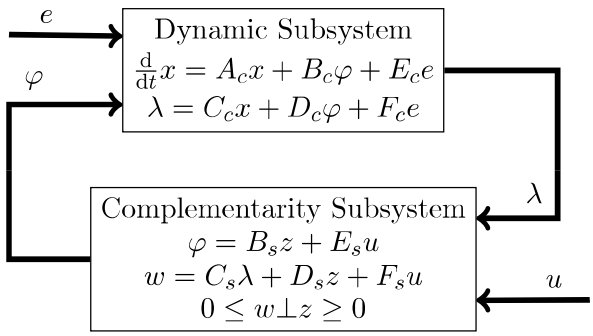

Figure 2.5: Dynamic and Complementarity Subsystem.

dynamic model can be written as

$$\frac{\mathrm{d}}{\mathrm{d}t}x = Ax + Bz + Ee + Gu \tag{2.16a}$$

$$w = Cx + Dz + Fe + Hu \tag{2.16b}$$

$$0 \le w \perp z \ge 0, \tag{2.16c}$$

where $x \in \mathbb{R}^{N_x}$ is the state vector, $u \in \{0,1\}^{(N_s+N_a)}$ is the control signal of the switches, $z \in \mathbb{R}^{N_z}$ and $w \in \mathbb{R}^{N_z}$, $e \in \mathbb{R}^{N_e}$ and the matrices are given by

$$A = A_c, \qquad B = B_c B_s, \tag{2.17a}$$

$$E = E_c, \qquad G = B_c E_s \tag{2.17b}$$

$$C = C_s C_c, \qquad D = D_s + C_s D_c B_s, \tag{2.17c}$$

$$F = C_s F_c, \qquad H = F_s + C_s D_c E_s \tag{2.17d}$$

with suitable dimensions. The set of expressions (2.16) is a continuous-time linear complementarity system. It represents in a compact form any mode of the power converter, i.e. it holds independently of the conducting or blocking states of the diodes and for continuous and discontinuous conduction modes too. It should be noticed that the model (2.16) represents an open-loop power converter in the sense that the swithces control signal are till considered as an input.

2.2.1. Discretization

The linear complementarity system (2.16) is composed by differential equations (2.16a), and static constraints (2.16b) and (2.16c), due to this hybrid nature, the system evolve must be calculated in discrete time. In [Camlibel, 2001] the author suggest the backward Euler discretization technique as the most suitable for linear complementarity systems. Let us consider the LC model (2.16) and a sampling period, say α. Without loss of generality one can assume $\alpha = P_s/N$, where P_s is the switching period assumed to be the same for all switches and N is a positive integer. In other words there are N samples for each switching period. Then, the continuous time instants multiple of the period, say $t_p = pP_s$ with p integer, will correspond to the discrete samples $k_p = pN$. The continuous-time state derivative at the continuous time instant $t = k\alpha$ with $k = 1, 2, ...$ can be approximated as $\frac{\mathrm{d}}{\mathrm{d}t}x \simeq (x(k) - x(k-1))/\alpha$, where $x(k)$ is the k-th sample of the discretized model vector state. Then, by using the backward Euler discretization technique with sampling period α, from (2.16) one obtains the following discrete-time system

$$x(k) = A_d x(k-1) + B_d z(k) + E_d e(k) + G_d u(k) \tag{2.18a}$$

$$w(k) = Cx(k) + Dz(k) + Fe(k) + Hu(k) \tag{2.18b}$$

$$0 \leq w(k) \perp z(k) \geq 0, \tag{2.18c}$$

with $A_d = (I - \alpha A)^{-1}$, $B_d = \alpha A_d B$, $E_d = \alpha A_d E$ and $G_d = \alpha A_d G$.

2.3. Linear complementarity problem

The discrete LC model (2.18) can be solved as an optimization problem, the immediate formulation is the linear complementarity problem (LCP), which optimization structure is suitable for transient simulation. The LCP is a generalization of the problem of finding a solution to a set of simultaneous linear equations. Although the extension is somewhat simple, the resulting problem provides an elegant framework for the theory of linear and quadratic programming and bimatrix games, it is sometimes termed the "fundamental problem" of mathematical programming [Cottle *et al.*, 1992a]. The LCP consists in determining the complementarity variables (w, z) for a given matrix M and a vector q in

(2.19). The LCP can be expressed as an optimization problem without objective function [Cottle *et al.*, January 1993b]. The LC model (2.18) can be written as a LCP by substituting (2.18a) in (2.18b), which in compact form can be expressed by the constraints

$$w(k) = q(k) + Mz(k) \tag{2.19a}$$

$$0 \leq w(k) \perp z(k) \geq 0 \tag{2.19b}$$

where

$$M = CBd + D$$
$$q(k) = CAdx(k-1) + (CEd + F)e(k) + (CGd + H)u(k).$$

At each time-step k, given $x(k-1)$, $e(k)$ and $u(k)$, the set of expressions (2.18b)–(2.18c) is a LC problem in terms of unknown $z(k)$. Then, starting from a given $x(0)$ and the knowledge of the inputs $e(k)$ and $u(k)$ for $k = 1, 2, ...$, the whole state evolution can be obtained by iteratively solving for $k = 1, 2, ...$ the sequence of LC problems.

The LCP has a unique solution for all $q(k)$ if and only if M is a matrix positive definite, [Cottle *et al.*, 1992a]. A matrix is positive definite if all its principal minors are non-negative. If the matrix is only positive semidefinite, there is not an unique solution for the LCP, but it is possible to prove that among all solutions of the LCP the least-norm one is unique [Han *et al.*, 2009], which means that solution minimizes the problem. The LCP (2.19) can be solved by using PATH Solver [Dirkse and Ferris, 1995], which is an algorithm based on the interior point method. This solver is available for Matlab™.

2.3.1. Numeric simulation - Boost converter

As an example, consider the boost converter whose circuit scheme is illustrated in Figure 2.6. This simple configuration exhibit different dynamics in relation to the switch position (On, or Off), and two operation modes: continuous conduction mode (CCM) and discontinuous conduction mode (DCM), in relation of the diode polarization, and their state variables exhibit the characteristic ripple in power converters. By applying Kirchoff laws,

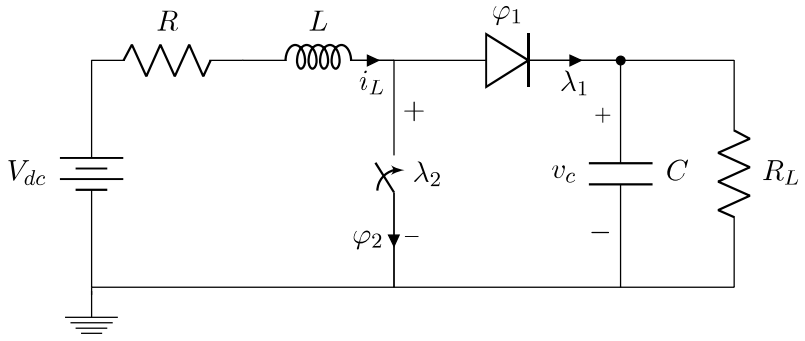

Figure 2.6: Boost converter scheme.

the following dynamic equations can be obtained

$$\begin{aligned} L\frac{di_L}{dt} =& V_{dc} - Ri_L + \varphi_1 - v_c \\ C\frac{dv_c}{dt} =& i_L - \varphi_2 - \frac{v_c}{R_L} \end{aligned}$$

where $\varphi = \begin{pmatrix} \varphi_1 & \varphi_2 \end{pmatrix}^\top$ are the output variables of the complementarity model of the electronic devices, this equations correspond to the (2.15a) with $x = \begin{pmatrix} i_L & v_c \end{pmatrix}^\top$ and the matrices

$$A_c = \begin{pmatrix} -R/L & -1/L \\ 1/C & -1/CR_L \end{pmatrix}, \quad E_c = \begin{pmatrix} 1/L \\ 0 \end{pmatrix}, \quad B_c = \begin{pmatrix} 1/L & 0 \\ 0 & -1/C \end{pmatrix}.$$

The output equations of the dynamic subsystem can be written as

$$\lambda_1 = i_L - \varphi_2, \qquad \lambda_2 = -\varphi_1 + v_c.$$

which correspond to (2.15b) with

$$C_c = \begin{pmatrix} 1 & 0 \\ 0 & 1 \end{pmatrix}, \; D_c = \begin{pmatrix} 0 & -1 \\ -1 & 0 \end{pmatrix}$$

and $F_c = 0$. The representation (2.1) can be obtained by collecting the diode model (2.3) for (φ_1, λ_1), and the switch model (2.7) for (φ_2, λ_2), thus obtaining the following matrices:

$$B_s = \begin{pmatrix} 1 & 0 & 0 \\ 0 & 1 & 0 \end{pmatrix}, \quad D_s = \begin{pmatrix} 0 & 0 & 0 \\ 0 & 0 & 1 \\ 0 & -1 & 0 \end{pmatrix}, \quad F_s = \begin{pmatrix} 0 \\ 0 \\ I_{\mathrm{M}} \end{pmatrix}$$

Table 2.1: Boost Converter parameters

Component, Parameter	value
Voltage supply, V_{dc}	12 V
Resistance, R	0.001 Ω
Inductance, L	80 µH
Capacitance, C	180 µF
Load Resistance, R_L	20 Ω
Switching period, P	100 µs
Integration step, α	1 µs

$C_s = -B_s^\top$ and $E_s = 0$. By using the matrices derived above in (2.17) the LC model (2.16) of the boost converter can be directly obtained.

In this case, the boost parameters are selecting for a DCM, this can be done by choosing the inductor value as lower as the critical value $L < L_{cr}$, where

$$L_{cr} = \frac{R_L(1-d)^2 d}{2} P. \tag{2.25}$$

The output voltage in DCM is expected to be greater than the output voltage in CCM, $V_{o_{CCM}} < V_{o_{DCM}}$, where

$$V_{o_{CCM}} = \frac{V_{dc}}{(1-d)} \tag{2.26}$$

and

$$V_{o_{DCM}} = \frac{\beta V_{dc}}{(\beta - d)}, \tag{2.27}$$

being $0 \leq \beta \leq 1$ the time fraction of the duty cycle where the current is not zero. The current peak in DCM can be calculated as

$$i_{peak} = \frac{V_{dc}}{L} P d. \tag{2.28}$$

In order to validate the LC model, a numeric simulation with the commercial simulator SystemModeler of Wolfram Mathematica™, is made. Considering a fixed duty cycle $d = 0.5$ and the parameters given in Table 2.1, where the inductor L is calculated with (2.25) for a DCM operation, the comparison between SystemModeler and LC model is performed.

The simulation results are shown in the Figure 2.7. Additionally, a zoom of the current signal is presented, where the DCM is observed and value of $\beta = 0.875$ can be approaching. The peak of current expected by (2.28) is 7.5 A and the output voltage (2.27) is 28 V. This comparison validates the LC model as an accurate technique for power converters modeling, where all electronic device characteristics are considered.

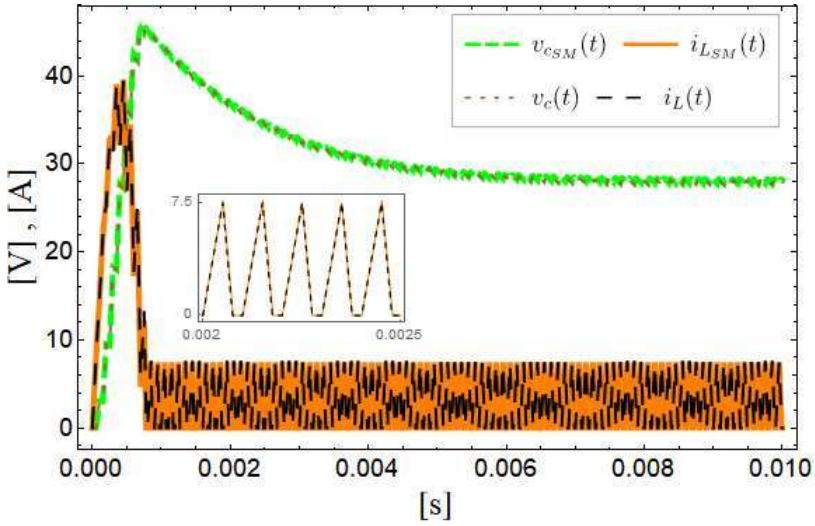

Figure 2.7: Boost converter, compassion of LC model and SystemModeler.

2.4. Mixed logical dynamical system

The LCP is an efficient optimization algorithm that can be used for open loop simulations of power converters. However, if a quadratic objective function is included for control purposes, the resulting quadratic complementarity problem (QCP) has not an efficient solver to handle it. Because of this, it is proposed to transform the LC system to other hybrid systems for control design purposes.

The LC system (2.18) can be reformulated as a MLD system by rewriting the complementarity constraints as a mixed integer linear feasibility problem (MILFP) [Heemels *et al.*, 2001, Bemporad and Morari, 1999, Riyanto and Hakim, 2005]. The MILFP consist in find $y \in \mathbb{R}^{nc} \times \{0,1\}^{nd}$, given a matrix $\mathcal{A}$ and a vector b, such that $\mathcal{A}y \leq b$, where nc and nd are the number of continuous and integer variables, respectively.

For simplicity, consider the scalar case and a variable $\delta(k) \in \{0, 1\}$ for $k = 1, 2, \ldots$. The complementarity condition $0 \leq w(k) \perp z(k) \geq 0$ can be equivalently represented through the following set of inequalities

$$w(k) \leq M_w(1 - \delta(k)), \qquad z(k) \geq 0 \tag{2.29a}$$

$$z(k) \leq M_z\delta(k), \qquad w(k) \geq 0 \tag{2.29b}$$

where $M_w = \max(w)$ and $M_z = \max(z)$. Indeed, from (2.29) it directly follows that for $\delta(k) = 0$, it is $z(k) = 0$ and $0 \leq w(k) \leq M_w$ and for $\delta(k) = 1$, it is $w(k) = 0$ and $0 \leq z(k) \leq M_z$. Then, a power converter, modeled as a LC system, can be represented as a MLD system as

$$\begin{aligned} x(k) &= A_d x(k-1) + B_d z(k) + E_d e(k) + G_d u(k) \\ E_1 x(k) &+ E_2 z(k) + E_3 \delta(k) + E_4 e(k) + E_5 u(k) \leq g, \end{aligned} \tag{2.30}$$

where

$$E_1 = \begin{pmatrix} C \\ -C \\ 0 \\ 0 \end{pmatrix} \quad E_2 = \begin{pmatrix} D \\ -D \\ I \\ -I \end{pmatrix} \quad E_3 = \begin{pmatrix} M_w \\ 0 \\ -M_z \\ 0 \end{pmatrix} \quad E_4 = \begin{pmatrix} F \\ -F \\ 0 \\ 0 \end{pmatrix} \quad E_5 = \begin{pmatrix} H \\ -H \\ 0 \\ 0 \end{pmatrix} \quad g = \begin{pmatrix} M_w \\ 0 \\ 0 \\ 0 \end{pmatrix}$$

2.4.1. Mixed integer problem

In order to performed an open loop simulation, the MLD system can be expressed at each time-step k, as a static mixed integer (MI) problem without objective function. An optimization problem is defined as a MI if the decision variables belongs to a set of continuous and discrete variables. The LCP can be formulated as a MI problem as

$$\begin{aligned} \min_{z(k),\delta(k)} \quad & c' \begin{pmatrix} z(k) & \delta(k) \end{pmatrix} \\ \textit{subject to} \quad & \textit{eq. } (2.30) \\ & z(k) \in \mathbb{R} \textit{ and } \delta(k) \in \{0, 1\}, \end{aligned} \tag{2.31}$$

where $c = 0$. At each time-step k, given $x(k-1)$, $e(k)$ and $u(k)$, the MLD (2.30) can be expressed as a mixed-integer (MI) problem, without objective function, in terms of unknown

variables $z(k)$ and $\delta(k)$. Then, starting from a given $x(0)$ and the knowledge of the inputs $e(k)$ and $u(k)$ for $k = 1, 2, ...$, the whole state evolution can be obtained by iteratively solving for $k = 1, 2, ...$ the sequence of MI problems. This problem can be solved using the solver GUROBI [Gurobi Optimization, 2018], available for Matlab™, which employs an branch-and-bound and algorithm.

2.4.2. Numeric simulation - buck converter

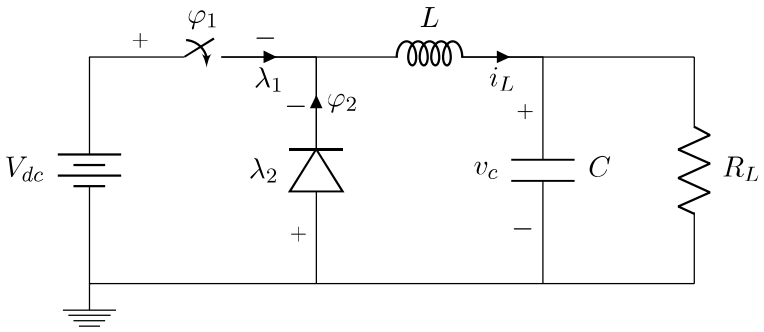

Figure 2.8: Buck converter scheme.

In order to validate the MLD system, consider the buck converter whose circuit scheme is illustrated in Figure 2.8. By applying Kirchoff laws one obtains the following dynamic equations

$$\begin{aligned} L\frac{di_L}{dt} &= V_{dc} - \varphi_1 - v_c \\ C\frac{dv_c}{dt} &= i_L - \frac{v_c}{R_L} \end{aligned}$$

where $\varphi = \begin{pmatrix} \varphi_1 & \varphi_2 \end{pmatrix}^\top$ are the output variables of the complementarity model of the electronic devices, this equations correspond to the (2.15a) with $x = \begin{pmatrix} i_L & v_c \end{pmatrix}^\top$ and the matrices

$$A_c = \begin{pmatrix} 0 & -1/L \\ 1/C & -1/CR_L \end{pmatrix}, \quad E_c = \begin{pmatrix} 1/L \\ 0 \end{pmatrix}, \quad B_c = \begin{pmatrix} -1/L & 0 \\ 0 & 0 \end{pmatrix}.$$

The output equations of the dynamic subsystem can be written as

$$\lambda_1 = i_L - \varphi_2, \qquad \lambda_2 = \varphi_1 - V_{dc}.$$

which correspond to (2.15b) with

$$C_c = \begin{pmatrix} 1 & 0 \\ 0 & 0 \end{pmatrix}, \; D_c = \begin{pmatrix} 0 & -1 \\ -1 & 0 \end{pmatrix} \; F_c = \begin{pmatrix} 0 \\ 1 \end{pmatrix}.$$

The representation (2.1) can be obtained by collecting the switch model (2.9) for (φ_1, λ_1) and the diode model (2.2) for (φ_2, λ_2), thus obtaining the following matrices:

$$B_s = \begin{pmatrix} -1 & 1 & 0 \\ 0 & 0 & 1 \end{pmatrix}, \quad C_s = \begin{pmatrix} 1 & 0 \\ -1 & 0 \\ 0 & -1 \end{pmatrix}, \quad F_s = \begin{pmatrix} 0 \\ I_{\mathrm{M}} \\ 0 \end{pmatrix}$$

$D_s = 0$ and $E_s = 0$. By using the matrices derived above in (2.17), the LC model (2.16) of the buck converter can be directly obtained, and then, the complementarity constraints can be rewritten as MLD system (2.30).

In this case, the buck parameters are selecting for a DCM, this can be done by choosing the inductor value as lower as the critical value $L < L_{cr}$, where

$$L_{cr} = \frac{R_L(1-d)}{2} P. \tag{2.36}$$

The output voltage in DCM is expected to be greater than the output voltage in CCM, $V_{o_{CCM}} < V_{o_{DCM}}$, where

$$V_{o_{CCM}} = dV_{dc} \tag{2.37}$$

and

$$V_{o_{DCM}} = \frac{dV_{dc}}{\beta}, \tag{2.38}$$

being $0 \leq \beta \leq 1$ the time fraction of the duty cycle where the current is not zero. The current peak in DCM can be calculated as

$$i_{peak} = \frac{V_{dc} - V_o}{L} Pd. \tag{2.39}$$

In Figure 2.9, a transient simulation of the buck converter is shown, where a comparison between the MI model and SystemModeler is presented. In the simulation, a fixed duty cycle $d = 0.5$ and the buck parameters from the Table 2.2 are considered, where the inductor L is calculated with (2.36) for a DCM operation. Additionally, a zoom of the

Table 2.2: Buck Converter parameters

Component, Parameter	value
Voltage supply, V_{dc}	12 V
Inductance, L	156 µH
Capacitance, C	120 µF
Load Resistance, R_L	40 Ω
Switching period, P	100 µs
Integration step, α	1 µs

current is presented, where the DCM is observed and value of $\beta = 0.625$ can be approaching. The peak of current expected by (2.39) is 0.76 A and the output voltage (2.38) is 9.6 V. This comparison validates the MLD system and proves that the switching characteristics are conserved, as the same as the LC system.

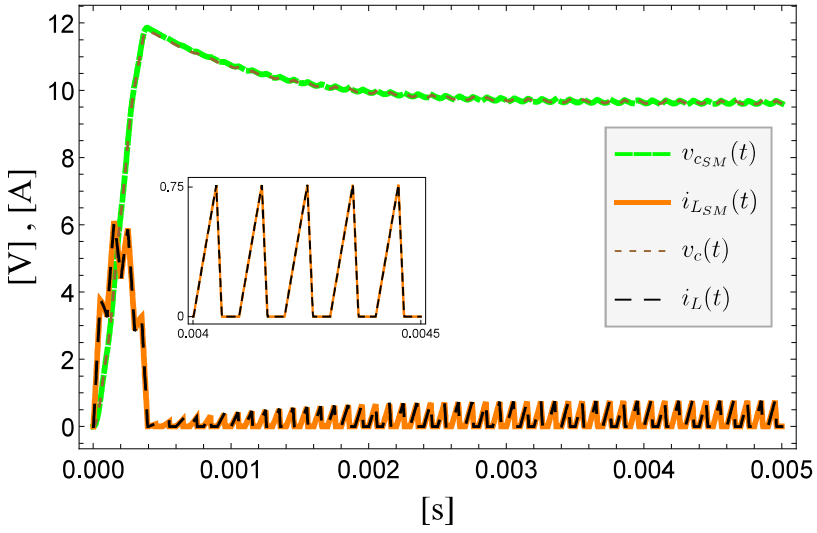

Figure 2.9: Buck converter, compassion of MI model and SystemModeler.

2.5. Piecewise affine system

Other useful transformation of the LC system for control purposes is the piecewise affine (PWA) system. In this case, the solution of LCP (2.19) for $z(k)$ is obtained for a boun-

ded conditions range. This allows simplifying the transient simulation to the single evaluation of conditionals and linear equations, without solving an optimization problem at each time-step k. The piecewise solution of the complementarity variable z is obtained by means of a multi-parametric analysis, in this case named as parametric linear complementarity problem (PCLP). This problem was first formulated by Maier [Maier, 1970] and it consists of the family of the classic Linear complementarity problem [Cottle *et al.*, January 1993b], but differs from LCP by the addition of a parametric term θ [Pang *et al.*, 1979], the PLCP can be written in compact form as

$$\begin{aligned} w(k) = \quad & Mz(k) + q + Q\theta(k) \\ & 0 \leq w(k) \perp z(k) \geq 0 \\ & \theta(k) \in \Theta \end{aligned} \tag{2.40}$$

where $Q \in \mathbb{R}^{n_z \times n_p}$ and $\theta \in \mathbb{R}^{n_p}$ represent a free parameter, which is assumed to be a polytope $\Theta \subset \mathbb{R}^{n_p}$. Concepts as polyhedron and polytope are needed for the geometric interpretation of parametric optimization [Borrelli *et al.*, 2014]. A polyhedron $\mathcal{P}$ in $\mathbb{R}^n$ denotes an intersection of a finite set of closed half-spaces in $\mathbb{R}^n$

$$\mathcal{P} = \{\theta \in \mathbb{R}^n : A\theta \leq b\} \tag{2.41}$$

where $Ax \leq b$ is the usual shorthand form for a system of inequalities, namely $a_i\theta \leq b_i$, $i = 1, ..., m$, $a_1, ..., a_m$ are the rows of A, and $b_1, ..., b_m$ are the components of b. A polytope `P` is a bounded polyhedron. In Figure 2.10 a two dimensional polytope is plotted.

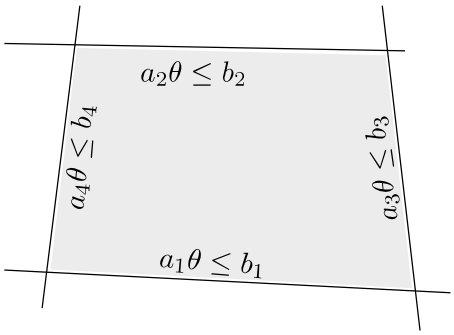

Figure 2.10: Polytope: the planes (lines here) defining the halfspace $a_i\theta - b_i = 0$.

This problem can be effectively solved by employing the lexicographic perturbations algorithm, which is available in free license solvers as the MPT 3.0 [Herceg *et al.*, 2013]. The solution is given by an optimal pair of $z(k)^*$, $w(k)^*$ that forms a piecewise affine (PWA) function of the parameters $\theta(k)$

$$\begin{bmatrix} w(k)^* \\ z(k)^* \end{bmatrix} = F_i\theta(k) + g_i \quad \text{if } \theta(k) \in \mathtt{P}_i. \tag{2.42}$$

where F_i, g_i define the i-th local affine function which determines values of w^* and z^* for any $\theta(k)$ that resides in the i-th polytope $\mathtt{P}_i$.

The LCP (2.19) can be formulated as a PLCP (2.40) by considering the initial conditions $x(k-1)$, the power supplies $e(k)$ and the control inputs $u(k)$ as parameters $\theta(k)$, from which the vector and the matrices of (2.40) can be defined as

$$\begin{aligned} M &= CB_d + D \\ q &= 0 \\ Q &= [CA_d, CG_d + H, CE_d + F] \end{aligned}$$

where $\theta(k) = [x(k-1), u(k), e(k)]^T$. From this formulation a PWA solution (2.42) for $z(k)$ can be obtained by means of PLCP solution. Then, substituting this solution in (2.18a), the power converter can be modeled by a linear system, where $z(k)$ can be considered as an auxiliary input, which is calculated by an exogenous PWA system

$$x(k) = A_d x(k-1) + B_d z(k) + E_d e(k) + G_d u(k) \tag{2.43a}$$

$$z(k) = \begin{cases} F_1\theta(k) + g_1 & \text{if } \theta(k) \in \mathtt{P}_1 \\ F_2\theta(k) + g_2 & \text{if } \theta(k) \in \mathtt{P}_2 \\ \vdots & \vdots \\ F_r\theta(k) + g_r & \text{if } \theta(k) \in \mathtt{P}_r \end{cases} \tag{2.43b}$$

This approach is synthesized in the block diagram, Figure 2.11. The main advantage of this formulation is that, once the PLCP is solved, the open loop simulation of the power converter, can be obtained by solving directly algebraic equations, without any optimization solver.

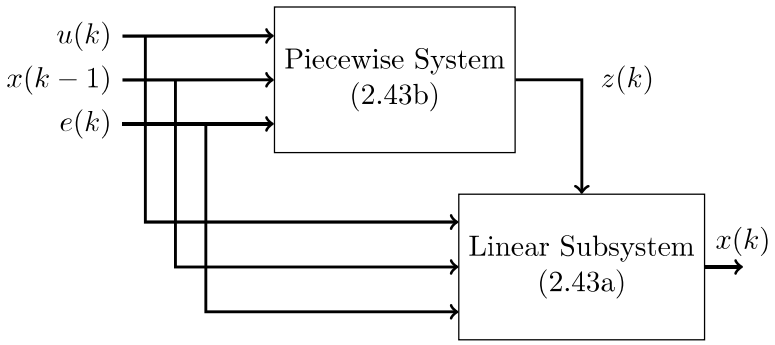

Figure 2.11: Linear model of power converters with an linear piecewise input function.

2.5.1. Numeric simulation - buckboost converter

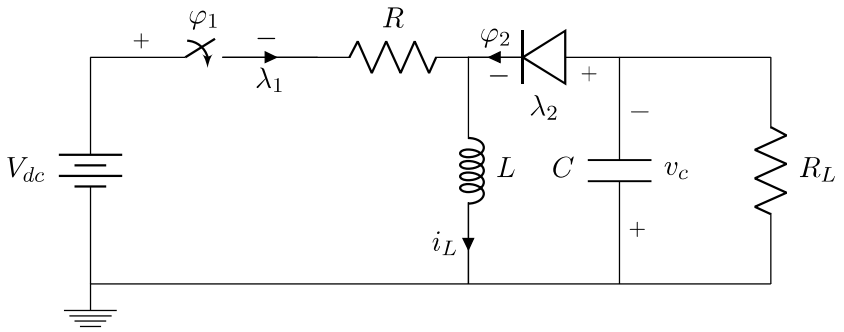

Figure 2.12: Buckboost converter scheme.

In order to validate the PWA system, consider the buck-boost converter, whose circuit scheme is illustrated in Figure 2.12. By applying Kirchoff laws one obtains the following dynamic equations

$$\begin{aligned} L\frac{di_L}{dt} &= V_{dc} - R(i_l + \varphi_2) - \varphi_1 \\ C\frac{dv_c}{dt} &= \varphi_2 - \frac{v_c}{R_L} \end{aligned}$$

where $\varphi = \begin{pmatrix} \varphi_1 & \varphi_2 \end{pmatrix}^\top$ are the output variables of the complementarity model of the electro-

nic devices, this equations correspond to the (2.15a) with $x = \begin{pmatrix} i_L & v_c \end{pmatrix}^\top$ and the matrices

$$A_c = \begin{pmatrix} -R/L & 0 \\ 0 & -1/CR_L \end{pmatrix}, \quad E_c = \begin{pmatrix} 1/L \\ 0 \end{pmatrix}, \quad B_c = \begin{pmatrix} -1/L & -R/L \\ 0 & 1/C \end{pmatrix}.$$

The output equations of the dynamic subsystem can be written as

$$\lambda_1 = i_L - \varphi_2, \qquad \lambda_2 = -R(i_L + \varphi_2) + v_c - \varphi_1 + V_{dc}.$$

which correspond to (2.15b) with

$$C_c = \begin{pmatrix} 1 & 0 \\ -R & 1 \end{pmatrix}, \; D_c = \begin{pmatrix} 0 & -1 \\ -1 & -R \end{pmatrix} \; F_c = \begin{pmatrix} 0 \\ 1 \end{pmatrix}.$$

The representation (2.1) can be obtained by collecting the switch model (2.9) for (φ_1, λ_1) and the diode model (2.2) for (φ_2, λ_2), thus obtaining the following matrices:

$$B_s = \begin{pmatrix} 1 & -1 & 0 \\ 0 & 0 & 1 \end{pmatrix}, \quad C_s = \begin{pmatrix} 1 & 0 \\ -1 & 0 \\ 0 & -1 \end{pmatrix}, \quad F_s = \begin{pmatrix} 0 \\ I_{\mathrm{M}} \\ 0 \end{pmatrix}$$

$D_s = 0$ and $E_s = 0$. By using the matrices derived above in (2.17), the LC model (2.16) of the buck-boost converter can be directly obtained. Then, the parametric linear complementarity problem (2.40) can be formulated in order to obtained the PWA system as (2.43).

The buck-boost parameters are taken form the Table 2.3, where the inductor L is calculated with (2.49) for a DCM operation in buck mode and a CCM operation in boost mode, the PLCP parameters $\theta = (i_L(k), v_c(k), u(k))$ are bounded by the intervals: $0 \leq i_L(k), v_c(k) \leq 100$ for the state variables and $0 \leq u(k) \leq 1$ for the control input, the piecewise system (2.43b) is defined by $r = 3$ and the matrices

$$F_1 = \begin{pmatrix} 0 & 0 & 0 \\ 0 & 0 & 0 \\ 0 & 0 & 0 \end{pmatrix}, \quad F_2 = \begin{pmatrix} 0 & 0 & 0 \\ 200 & 0 & -0.00002 \\ 0 & 0 & 0 \end{pmatrix}, \quad F_3 = \begin{pmatrix} 0 & 0 & 0 \\ -0.0175 & 1 & 7.4748 \\ 1 & -0.005 & -999.9874 \end{pmatrix},$$

$$g_1 = \begin{pmatrix} 0 \\ 0 \\ 0 \end{pmatrix}, \qquad g_2 = \begin{pmatrix} 0 \\ 12 \\ 0 \end{pmatrix}, \qquad g_3 = \begin{pmatrix} 12 \\ 0 \\ 0 \end{pmatrix},$$

and the polytopes

$$P_1 : \begin{pmatrix} 0.01 & -0.99 & 1 \\ 0 & 0 & -1 \\ -1 & 0 & 0 \end{pmatrix} \theta(k) \leq \begin{pmatrix} 12 \\ 0 \\ 0.06 \end{pmatrix},$$

$$P_2 : \begin{pmatrix} 0 & 0 & -1 \\ 0.01 & 0 & -1 \\ 0.01 & 0 & 1 \end{pmatrix} \theta(k) \leq \begin{pmatrix} 0 \\ 0 \\ 0.0005 \end{pmatrix},$$

$$P_3 : \begin{pmatrix} 0 & 0 & -1 \\ 0.0023 & -0.1326 & -0.9912 \\ -0.001 & 0 & 1 \end{pmatrix} \theta(k) \leq \begin{pmatrix} 0 \\ 1.5912 \\ 0 \end{pmatrix}.$$

In this case, the buckboost parameters are selecting for a DCM in buck mode and a CCM in boost mode, this can be done by choosing the inductor value as lower as the critical value $L < L_{cr}$, where

$$L_{cr} = \frac{R_L(1-d)^2}{2} P. \tag{2.49}$$

The output voltage in DCM is expected to be greater than the output voltage in CCM, $V_{o_{CCM}} < V_{o_{DCM}}$, where

$$V_{o_{CCM}} = \frac{-dV_{dc}}{(1-d)} \tag{2.50}$$

and

$$V_{o_{DCM}} = \frac{-dV_{dc}}{(\beta - d)}, \tag{2.51}$$

being $0 \leq \beta \leq 1$ the time fraction of the duty cycle where the current is not zero. The current peak in DCM can be calculated as

$$i_{peak} = \frac{V_{dc}}{L} dP. \tag{2.52}$$

In Figure 2.13 a comparative transient simulation of the buck-boost converter between the PWA system and SystemModeler is shown. This simulation considers two stages: the first with a fixed duty cycle of $d = 0.8$, and the second with $d = 0.2$, which lead the converter to the boost and buck operation mode, respectively. In Figure 2.13a the boost mode is shown, where the converter operates in CCM. Additionally, a zoom is presented of

Table 2.3: Buck-boost converter parameters

Component, Parameter	value
Voltage supply, V_{dc}	12 V
Resistance, R	0.01 Ω
Inductance, L	0.2 mH
Capacitance, C	396 µF
Load Resistance, R_L	20 Ω
Switching period, P	200 µs
Integration step, α	1 µs

the current signal, in this case the output voltage expected by (2.50) is 48 V, value which is achieved by the converter. In Figure 2.13b the buck mode is shown, where the current operates in DCM with $\beta = 0.516$. In this case the peak of current expected by (2.52) is 2.4 A and the output voltage (2.51) is 7.59 V. This comparison validates the PWA system and proves that the switching characteristics are conserved, as the same as the LC system.

2.6. Chapter conclusion

In this chapter the modeling and open loop simulation of power converters is described, using basic power converters as boost, buck and buck-boost. The results are validated by comparing the simulation against a commercial simulator, SystemModeler. The effectives to model power converters of the described models is perfectly proven in the transient simulations and steady-state. The three hybrid systems presented has the same accuracy level to capture non-linear dynamics in power converters. However, the open loop simulation of these system is performed by different numerical method. In Figure 2.14 a flowchart of the presented modeling techniques for power converters are shown, where some advantages of each power converter representation are indicated. In the next chapter, model predictive control (MPC) designs are presented based on these modeling techniques for power converter.

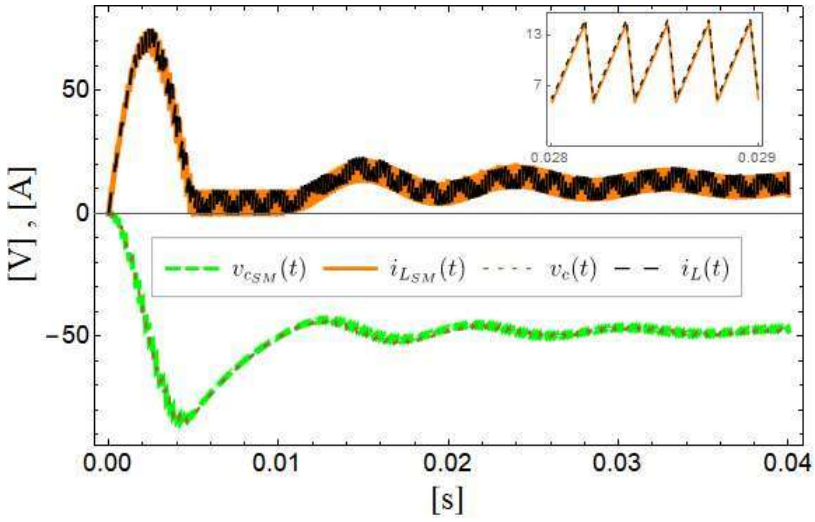

(a)

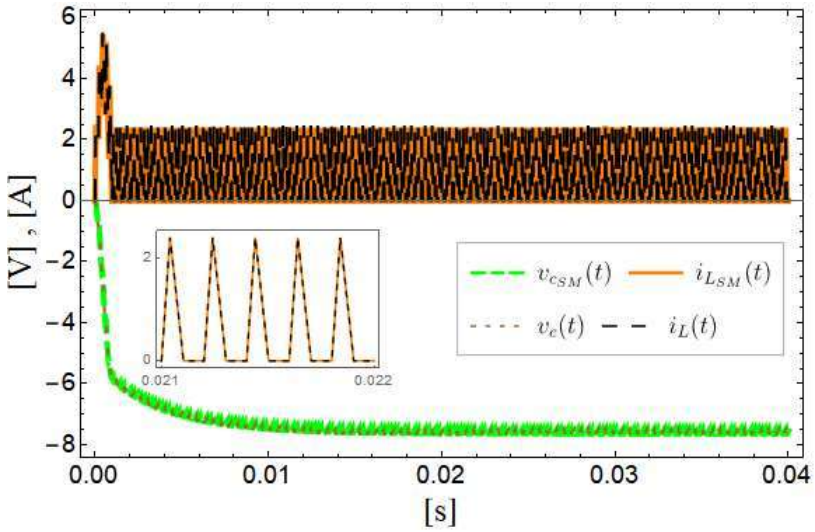

(b)

Figure 2.13: Buckboost converter, compassion of parametric LC model and SystemModeler, (a) Boost mode with $d = 0.8$ and (b) buck mode with $d = 0.2$.

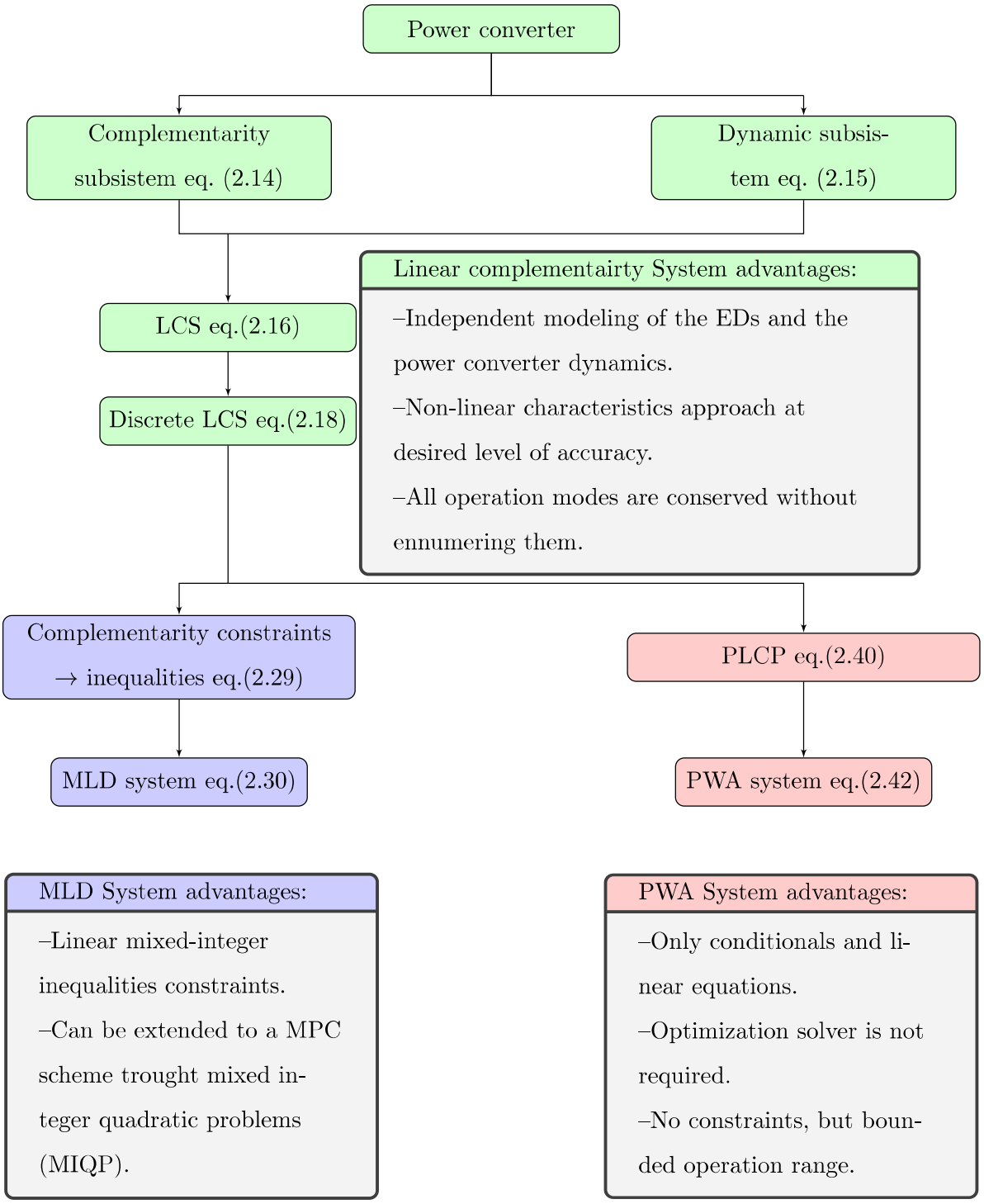

Figure 2.14: Flowchart of the modeling for power converters in the complementarity framework, and the transformations to MLD and PWA systems.

Chapter 3

Model predictive control for power converters in the LC framework

The term MPC does not designate a specific control strategy but rather an ample range of control methods that makes explicit use of a model of the system in order to predict the future behavior of the variables over a time frame (integer multiple of the sample time). These predictions are evaluated based on an objective function, and then, the sequence that minimizes this function is chosen, obtaining, in this way, the sequence of optimized control actions. MPC schemes present several features that make it suitable for controlling power converters. Apart from being intuitive and easy to understand, constraints, nonlinearities, and receding control horizon can easily be included in the formulation. In this chapter, the power converters modeling as hybrid systems (LCS, MLD, and PWA) are used into designs of MPC schemes.

3.1. Model predictive control for power converters

The MPC applied to power electronics have been classified into two main categories: continuous control set MPC (CCS-MPC) and finite control set MPC (FCS-MPC). In the first group, a modulator generates the switching states starting from the continuous output of the predictive controller, in this group, the solution is obtained by the generalized

predictive control (GPC) method [Clarke *et al.*, 1987, Abdeldjebar and Khier, 2008], where the optimization is solved analytically, obtaining a linear controller. Nevertheless, with GPC, a solution that includes system constraints and non-linearities is very difficult to obtain. On the other hand, the FCS-MPC approach takes advantage of the inherently discrete nature of power converters. Since the power converters have a finite number of switching states, the MPC optimization problem can be simplified and reduced to the prediction of the system behavior only for those possible switching states. Then, each prediction is used to evaluate an objective function, and consequently, the state which minimizes this function is selected and generated as input. This thesis is focused only in the FCS-MPC, where the power converter models described in the previous chapter are used in FCS-MPC schemes, particularly three formulations are presented, the first includes the PWA system and a direct search algorithm, the second is based in the MLD system and the optimization problem is formulated as a mixed integer quadratic problem (MIQP), in this formulation the control input is defined as pulse-width modulation (PWM), therefore, a modeling of the PWM in a mixed integer (MI) form is presented. The last FCS-MPC scheme is based in the PWA system and the simplex optimization algorithm Nelder-Mead, this scheme considers a continuous control input associated to an external PWM modulator. The presented FCS-MPC schemes are based in a receding horizon control.

3.1.1. Receding horizon control

In an optimization context, the MPC is an infinite horizon suboptimal controller, designed by repeatedly solving a finite time optimal control law, by online computing an optimization problem at each time-step, in a receding horizon control (RHC) as shown in Figure 3.1. This can be explained as follows: at each sampling time, starting at the current state, an open-loop optimal control problem is solved over a finite time horizon. Then, the computed optimal input signal is applied to the process only during the following sampling interval $[t, t+1]$. At the next time step $t+1$, a new optimal control problem based on new measurements of the current state is calculated over a shifted horizon, and applied to the following sampling interval [Borrelli *et al.*, 2014].

Generally, in FCS-MPC schemes for power converters, the control task is related

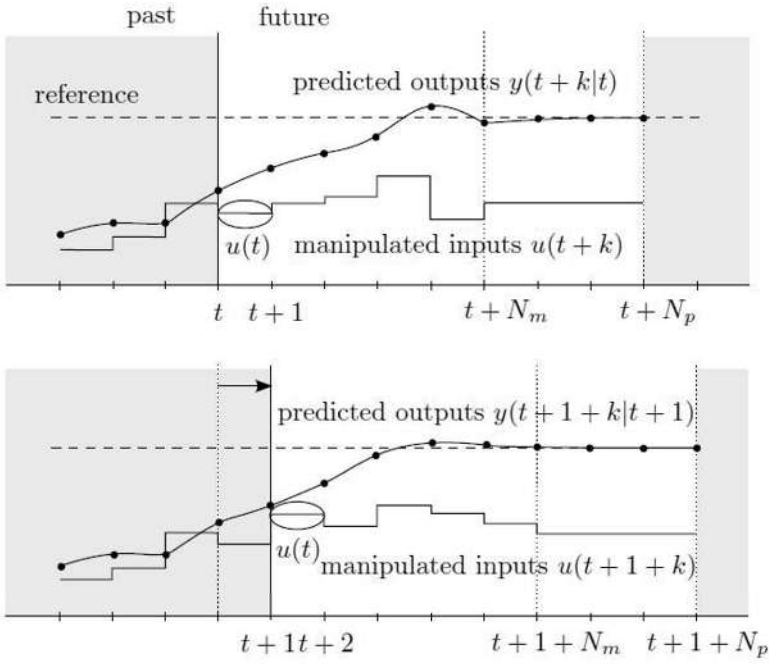

Figure 3.1: Receding horizon control [Borrelli *et al.*, 2014].

to keep the state variables as close as possible in a desired trajectory or value. Because of this, a quadratic function is normally chosen as the objective function, where the difference between the state variable and its respective reference is minimized. In the next sections, different FCS-MPC schemes are presented, where the objective function is always purposed as quadratic, since the control objectives involved regulation and trajectory tracking tasks, and the main difference between these formulations is related to the hybrid system that employs, the optimization algorithm that they used, and how the control input is modeled.

3.2. FCS-MPC - exhaustive search algorithm

In this FCS-MPC scheme the optimized control input for the next time horizon n is obtained by means of numbering all the possible inputs, and choosing the one that minimize a quadratic objective function. This thesis purposes the usage of the PWA system (2.43) under this MPC formulation. In this system, the set of possible control inputs at each time-step k can be defined as $u(k) \in \{0,1\}^{n_u}$, where n_u is the number of controlled

EDs. Note that each input $u(k)$ are directly associated with only one auxiliary input $z(k)$, therefore, the possible control inputs are defined only by $u(k)$. Considering a RHC of n time steps all the possibles control inputs can be numbering as $2^{n\times n_u}$. Then, the FCS-MPC can be formulated as a quadratic optimization problem, which can be stated as follows: given $x(0)$ and the power supplies vector $e(k)$, find the optimized control sequence $u(k)$, for $k = 1, ..., n$, that minimizes

$$\begin{aligned}
&\min_{u(k)} && \textstyle\sum_{k=1}^{n}(x(k) - x_{ref}(k))^T Q(x(k) - x_{ref}(k)) \\
&subject\ to: && \\
& && x(k) = A_d x(k-1) + B_d z(k) + E_d e(k) + G_d u(k) \\
& && z(k) = \begin{cases} F_1\theta(k) + g_1 & \text{if } \theta(k) \in \mathtt{P}_1 \\ F_2\theta(k) + g_2 & \text{if } \theta(k) \in \mathtt{P}_2 \\ \vdots & \vdots \\ F_r\theta(k) + g_r & \text{if } \theta(k) \in \mathtt{P}_r \end{cases} \\
& && \theta(k) = [x(k-1), e(k), u(k)] \\
& && u(k) \in \{0,1\}^{n_u},
\end{aligned} \tag{3.1}$$

where Q is a weighting matrix and $x_{ref}(k)$ is the desired reference trajectory for $x(k)$. Since there are a finite number of possible inputs $u(k)$, this problem can be solved by an exhaustive search. The purposed algorithm for this FCS-MPC scheme can be described in two steps as follows

FCS-MPC Algorithm
– Determine all the $(n \times n_u)$ possibles control inputs $u(k)$ and the associated auxiliary input $z(k)$ from the equation (2.43b).
– Determine which control input $u(k)$ minimizes the objective function (3.1).

Note that since a PWA system (2.43) is used, an additional optimization algorithm for computing the power converter evolve is not required. Therefore, this MPC formulation (3.1) can be easily implemented in devices like a microcontroller or an FPGA; however, the resulting control action usually has a high cost, i.e., the switching frequency in the controlled EDs tend towards infinity. Another aspect to keep in mind with this formulation is the predicted horizon, which is not clearly defined. Because of these drawbacks, in this

thesis, other FCS-MPC schemes are proposed, where the control input includes a PWM modulation.

3.3. FCS-MPC - MIQP

Normally the pulse-width modulation (PWM) is the basis for control of power electronics. An ideal PWM waveform represents a preferred way of driving electronic devices (EDs) when modeling techniques as averaging models are used. With the exception of some resonant converters, the majority of power converters can be controlled by PWM signals of various forms [Vasca and Iannelli, 2012]. When the power converter is modeled into a hybrid format as an LCS, MLD or PWA system, the PWM is not required, however including this control input modulation allows to reduce the control effort, by reducing the number of switchings, or maintaining a constant an smooth ripple at the converter signals, among other advantages. On the other hand including PWM control input requires a more time prediction in multiples of the PWM period which considerably increase the MPC computation time. The PWM signal is characterized by a continuous duty-cycle variable. However, by considering a discrete-time model, the possibles values of the duty-cycle can be numbering. Then, the PWM can be included into an FCS-MPC formulation. In this section, the PWM is modeled by mixed integer (MI) inequalities, and the FCS-MPC is presented as a mixed integer quadratic problem (MIQP).

3.3.1. Modeling of the PWM waveform

Considering a continuous-time horizon multiple of the PWM period, say $t \in [0, \pi P_s]$, where π is a positive integer, and P_s is the PWM period. Since there are N samples for each switching period P_s, in discrete-time the horizon of interest is $k \in [0, \pi N]$. Say p an integer characterizing the p-th period of interval, i.e. $p = \lceil \frac{k}{N} \rceil$. Then, the samples of the p-th period are $k \in [(p-1)N, pN]$, $p = 1, \ldots, \pi$.

We assume that each switch has only one commutation in each switching period.

In particular, for $i = 1, \ldots, N_s + N_a$ define

$$u_i(k) = \begin{cases} 1 & k \in [(p-1)N + \mathcal{S}_{ip}, (p-1)N + \mathcal{F}_{ip}] \\ 0 & \text{otherwise} \end{cases} \tag{3.2}$$

with $\mathcal{S}_{ip}$ and $\mathcal{F}_{ip}$ integers such that

$$0 \leq \mathcal{S}_{ip} \leq \mathcal{F}_{ip} \leq N \tag{3.3}$$

for $k \in [0, \pi N]$, $p = \lceil \frac{k}{N} \rceil$. The i-th switch is turned-on at the sample $\mathcal{S}_{ip}$ of the p-th period and is turned-off at the sample $\mathcal{F}_{ip}$. Then, in continuous time the duty-cycle in the p-th switching period is $d_{ip} = \alpha(\mathcal{F}_{ip} - \mathcal{S}_{ip} + 1)$. The particular case when the switch is turned-on at the beginning of the period can be derived by fixing $\mathcal{S}_{ip} = 0$.

The switching function (3.2) can be defined as the sum of window functions, say $u_{ip}(k) : [0, \pi N] \to \{0, 1\}$, $p = 1, \ldots, \pi$, each one being nonzero and equal to 1 only in the p-th period when the i-the switch must be On. Clearly, for each i, it is $u_{ip}(k) = u_i(k)$ for $k \in [(p-1)N, pN]$ and $u_{ip}(k) = 0$ for $k \notin [(p-1)N, pN]$, $p = 1, \ldots, \pi$. Then, for each $i = 1, \ldots, N_s + N_a$ we can write

$$u_i(k) = \sum_{p=1}^{\pi} u_{ip}(k) \tag{3.4}$$

with $k \in [0, \pi N]$. For given i and p, the signal $u_{ip}(k) : [0, \pi N] \to \{0, 1\}$ can be defined by

$$u_{ip}(k) = \begin{cases} 1 & (p-1)N + \mathcal{S}_{ip} \leq k \leq (p-1)N + \mathcal{F}_{ip} \\ 0 & \text{otherwise.} \end{cases} \tag{3.5}$$

Each signal u_{ip} can be written by introducing two functions which are useful for the MI representation. For each $i = 1, \ldots, N_s + N_a$ let us define π functions, say $\sigma_{ip}(k) : [0, \pi N] \to \{0, 1\}$, $p = 1, \ldots, \pi$, as

$$\sigma_{ip}(k) = \begin{cases} 1 & k \leq (p-1)N + \mathcal{F}_{ip} \\ 0 & \text{otherwise} \end{cases} \tag{3.6}$$

and π functions, say $\phi_{ip}(k) : [0, \pi N] \to \{0, 1\}$, $p = 1, \ldots, \pi$, as

$$\phi_{ip}(k) = \begin{cases} 1 & k \geq (p-1)N + \mathcal{S}_{ip} \\ 0 & \text{otherwise} \end{cases} \tag{3.7}$$

Note that for each function the value of p is fixed. Then one can write $u_{ip}(k)$ as a signal which is equal to 1 for all k such that $\sigma_{ip}(k) = 1$ and $\phi_{ip}(k) = 1$ and zero otherwise, see Figure 3.2. Therefore, for each $i = 1, \ldots, N_s + N_a$ and for each $p = 1, \ldots, \pi$, one can write

$$u_{ip}(k) = \sigma_{ip}(k) + \phi_{ip}(k) - 1, \tag{3.8}$$

for $k \in [0, \pi N]$. By definition $\sigma_{ip}(k)$ and $\phi_{ip}(k)$ are never zero at the same time, i.e. for any k one of the two or both are equal to 1, see (3.3) with (3.6)–(3.7). Therefore, if $\sigma_{ip}(k) = 0$ or $\phi_{ip}(k) = 0$ form (3.8) it is $u_{ip}(k) = 0$, while if $\sigma_{ip}(k) = \phi_{ip}(k) = 1$ then (3.8) implies $u_{ip}(k) = 1$.

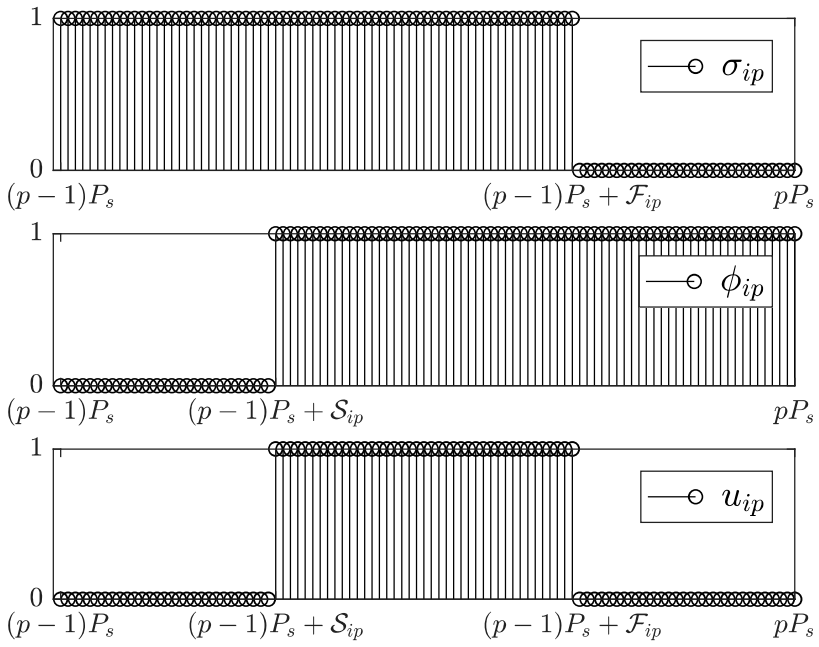

Figure 3.2: Switching signals for the i-th switch in the p-th discrete-time period. Since each triple of switching signals corresponds to a fixed p, the signals have the same values on the left and right time intervals, i.e. $\sigma_{ip}(k) = 1$ for $k \leq (p-1)N$, $\sigma_{ip}(k) = 0$ for $k \geq pN$, and so on. Therefore $u_{ip}(k)$ is nonzero only in the p-th period.

For each pair (i, p) the signal $\sigma_{ip}(k)$ can be written as a solution of a set of linear

inequalities. In particular, $\sigma_{ip}(k)$ must satisfy

$$k-(p-1)N-\mathcal{F}_{ip} \leq M(1-\sigma_{ip}(k)) \tag{3.9a}$$

$$k-(p-1)N-\mathcal{F}_{ip} \geq \varepsilon+(m-\varepsilon)\sigma_{ip}(k) \tag{3.9b}$$

with $k \in [0, \pi N]$, $0 < \varepsilon < 1$, M and m are an upper bound and a lower bound, respectively, of the left hand side of the inequalities. For instance one can choose $M = -m = \pi N$. Indeed, for $\sigma_{ip}(k) = 1$ from (3.9a) it follows $k \leq (p-1)N+\mathcal{F}_{ip}$ (remind that p is fixed) while (3.9b) is automatically verified. Instead, for $\sigma_{ip}(k) = 0$ the inequality (3.9a) is automatically verified and from (3.9b) it follows $k > (p-1)N + \mathcal{F}_{ip}$. By using similar arguments it follows that for each pair (i, p) with $i = 1, \ldots, N_s$ and $p = 1, \ldots, \pi$, the signal $\phi_{ip}(k)$ satisfies

$$-k+(p-1)N+\mathcal{S}_{ip} \leq M(1-\phi_{ip}(k)) \tag{3.10a}$$

$$-k+(p-1)N+\mathcal{S}_{ip} \geq \varepsilon+(m-\varepsilon)\phi_{ip}(k) \tag{3.10b}$$

with $k \in [0, \pi N]$.

3.3.2. Mixed integer quadratic problem

A FCS-MPC that includes a PWM modulation can be formulated by combining the MLD system (2.30) with the PWM switching signal in MI form, thus, considering a quadratic objective function, the resulting FCS-MPC problem can be written as a mixed integer quadratic problem (MIQP) with the (integer) optimization variables $\mathcal{S}_{ip}$, $\mathcal{F}_{ip}$, $i = 1, \ldots, N_s + N_a$, $p = 1, \ldots, \pi$.

The FCS-MPC for the power converter can be written using a RCH approach. In particular, the MIQP can be stated as follows: given $x(0)$ and the exogenous input $e(k)$ for $k = 0, \ldots, \pi N$, find the optimization variables $\mathcal{S}_{ip}$, $\mathcal{F}_{ip}$, $i = 1, \ldots, N_s + N_a$, $p = 1, \ldots, \pi$

according to

$$
\begin{aligned}
&\underset{\mathcal{S}_{ip},\mathcal{F}_{ip}}{\min} && \textstyle\sum_{k=0}^{\pi N}(x(k)-x_{ref}(k))^T Q(x(k)-x_{ref}(k)) \\
&\textit{subject to}: && \\
& && x(k) = A_d x(k-1) + B_d z(k) + E_d e(k) + G_d u(k) \\
& && E_1 x(k) + E_2 z(k) + E_3 \delta(k) + E_4 e(k) + E_5 u(k) \leq g \\
& && u_{ip}(k) = \sigma_{ip}(k) + \phi_{ip}(k) - 1 \\
& && k - (p-1)N - \mathcal{F}_{ip} \leq M(1-\sigma_{ip}(k)) \\
& && k - (p-1)N - \mathcal{F}_{ip} \geq \varepsilon + (m-\varepsilon)\sigma_{ip}(k) \\
& && -k + (p-1)N + \mathcal{S}_{ip} \leq M(1-\phi_{ip}(k)) \\
& && -k + (p-1)N + \mathcal{S}_{ip} \geq \varepsilon + (m-\varepsilon)\phi_{ip}(k),
\end{aligned}
\tag{3.11}
$$

where Q is a weighting matrix and $x_{ref}(k)$ is the desired reference trajectory for $x(k)$, with $\sigma_{ip}(k) \in \{0,1\}$, $\phi_{ip}(k) \in \{0,1\}$, $u_{ip}(k) \in \{0,1\}$, and $\delta(k) \in \{0,1\}^{N_z}$. In this case the MIQP (3.11) can be solved by a branch-and-bound algorithm, which can be implemented by parallel programming.

3.3.3. Branch and bound algorithm

The process to solve a MIQP by a branch-and-bound algorithm can be described as follows: At the begin, all the constraints that contains integer variables are remove of the original problem, resulting in a quadratic problem (QP) relaxation. After, the QP is solved by quadratic programming, if the result happens to satisfy all the integer constraints, even though these are not explicitly imposed, this solution is a optimal for the MIQP original, and the algorithm ends. If this do not occurs, as is usually the case, the procedure is to pick some variable that is restricted to be integer, but whose value in the QP is fractional. For the sake of argument, suppose that this variable is x, which value in the QP relaxation is 5.7. This value can be exclude by, in turn, imposing the restriction $x \leq 5$ and $x \geq 6$. If the MIQP original is denoted P_0, these two new MIQPs can be denoted as P_1, when the imposed constraint is $x \leq 5$, and P_2, where $x \geq 6$ is imposed. The variable x is called as branching variable, and two sub-MIQPs, P_1 and P_2 are produced. Then, both sub-MIQPs are solved by quadratic programming, and the better solution is taken, which is the optimal

of the original MIQP P_0. In this way, the original P_0 is replaced by two simpler (or at least more-restricted) MIQPs. Then, the same idea is applied to these two new problems, i.e., solving each problem by QP relaxations and, if necessary, selecting branching variables. This procedure generates a search tree algorithm, where each MIQPs generated are called as nodes of the tree, with P_0 designates as the root node. The leaves of the tree are all the nodes from which the algorithm have not yet branched. In general, if the algorithm reach a point at which it can solve or otherwise dispose of all leaf nodes, the algorithm will have solved the original MIPQ [Fujita, 2011, Quinn, 1990]. In figure 3.3 a graphic representation branch-and-bound procedure is shown.

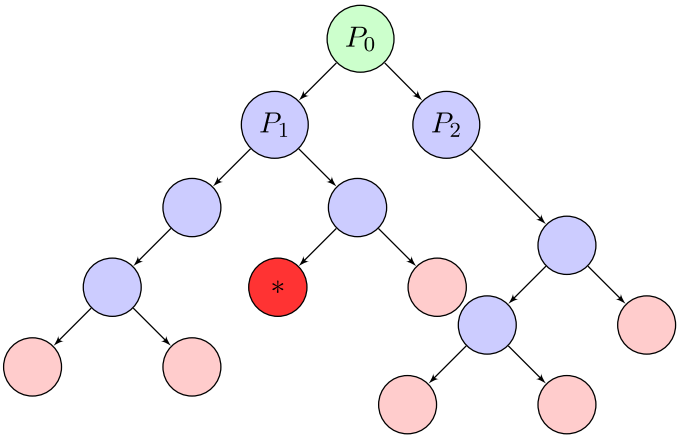

Figure 3.3: Branch-and-bound algorithm, where all leaf nodes are in red color, and the optimal node is indicated by $*$.

3.4. FCS-MPC - Nelder-Mead algorithm

In this section, another FCS-MPC for power converters, controlled by a PWM waveform, is proposed. This MPC scheme differs from the previous one in that the modulator is physically in the power converter circuit. Therefore, the PWM modulator is considered as an exogenous system, that transforms a continuous control input $u(t)$ into a sequence of binary inputs for each time-step k $u(k) \in \{0, 1\}$. For this MPC scheme, the PWA system is proposed to modeling the power converter, since this is a discrete-time system, the MPC

formulation is defined as an FCS-MPC scheme although the control input is continuous.

3.4.1. PWM modulator

The exogenous PWM modulator can be modeled by Heaviside functions. In continuous-time, a Heaviside function can be represented by a piecewise function as

$$h(t) = \begin{cases} 0 & \text{if } t < d \\ 1 & \text{if } t > d \end{cases} \tag{3.12}$$

Considering a finite-time horizon, multiple of the PWM period $t \in \{0, \pi P_s\}$, where P_s is the PWM period and π is a positive integer value, the continuous control input $0 \leq u(t) \leq 1$ can be modeled by means of two shifted Heaviside per period of the PWM signal as

$$u(t) = \sum_{p=1}^{\pi} H_p(t) \tag{3.13}$$

where

$$H_p(t) = h(t-(1-p)P_s) - h(t-((1-p)P_s + d_p P_s)) = \begin{cases} 0 & \text{if } t < ((1-p)P_s + d_p P_s) \\ 1 & \text{if } t > ((1-p)P_s + d_p P_s) \end{cases} \tag{3.14}$$

where $p = 1, ..., \pi$ and $0 \leq d_p \leq 1$ are continuous bounded variables that represents the duty-cycle for each PWM period. This variable are comparing with a modulating signal $s(t)$, normally, a sawtooth or a triangle signal in the PWM modulator. This comparison generates the corresponding control input $u(k)$ for each time-step. In Figure 3.4 the block diagram shows how the discrete input is obtained from a continuous duty-cycle variable.

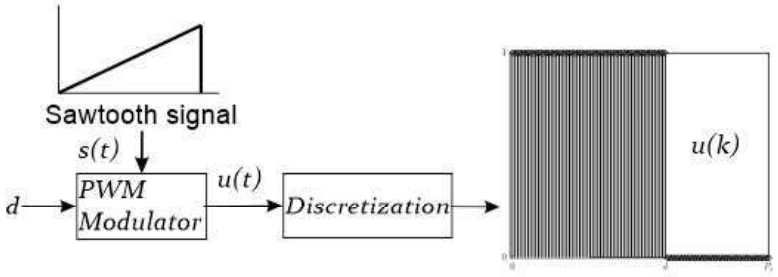

Figure 3.4: PWM signal generator.

3.4.2. Optimization problem

The FCS-MPC can be formulated as a PWA system with a quadratic objective function, where the decision variable is the duty-cycle d_p, for $p = 1, ...\pi$. In particular the problem can be stated as follows: given $x(0)$ and the exogenous signal vector $e(k)$ for $k = 1, ..., \pi P_s$, finding the continuous optimization variables d_p according to

$$\begin{aligned}
&\min_{d_p} && \textstyle\sum_{k=1}^{\pi P_s}(x(k) - x_{ref}(k))^T Q(x(k) - x_{ref}(k)) \\
&subject\ to: && \\
& && x(k) = A_d x(k-1) + B_d z(k) + E_d e(k) + G_d u(k) \\
& && z(k) = \begin{cases} F_1\theta(k) + g_1 & \text{if } \theta(k) \in \mathtt{P}_1 \\ F_2\theta(k) + g_2 & \text{if } \theta(k) \in \mathtt{P}_2 \\ \vdots & \vdots \\ F_r\theta(k) + g_r & \text{if } \theta(k) \in \mathtt{P}_r \end{cases} \\
& && u(k) = \textstyle\sum_{p=1}^{\pi} H_p(k)
\end{aligned} \tag{3.15}$$

In this formulation, the PWA system is proposed to modeling the power converter. Therefore, an optimization solver for the system evolve is not required. Since this FCS-MPC formulation considers a continuous duty-cycle $0 \leq d_p \leq 1$ as decision variable, there is a infinity possible values. In this thesis, the optimization algorithm proposed to solve this FCS-MPC formulation is the Nelder-Mead, which is a multi-variable direct optimization algorithm, where the decision variable is continuous. This algorithm can be efficiently solved by parallel processing, what makes it suitable for control power converters.

3.4.3. Nelder-Mead algorithm

The NelderMead method is a direct search method. For a function of m variables, the algorithm maintains a set of $m + 1$ points forming the vertices of a polytope in m-dimensional space. This method is often termed the simplex method, which should not be confused with the well-known simplex method for linear programming. The Nelder-Mead procedure can be described as follows: at each iteration, $m+1$ points $(p_1, p_2, ..., p_{m+1})$ form a polytope. The points are ordered so that: $f(p_1) \leq f(p_2) \leq ... \leq f(m + 1)$. A new point is then generated to replace the worst point p_{m+1}. Let be c the centroid of the polytope

consisting of the best m points

$$c = \frac{1}{m}\sum_{i=1}^{m} p_i. \tag{3.16}$$

A trial point p_t is generated by reflecting the worst point through the centroid

$$p_t = c + \rho(c - p_{m+1}), \tag{3.17}$$

where ρ is a parameter of reflexion. If the new point p_t is neither a new worst point nor a new best point, i.e. $f(p_1) \leq f(p_t) \leq f(m)$, p_t replaces p_{m+1}.

If the new p_t point is better than the best point, $f(p_t) \leq f(p_1)$, the reflection is very successful and can be carried out further to

$$p_e = c + \beta(p_t - r), \tag{3.18}$$

where $\beta > 1$ is a parameter to expand the polytope. If the expansion is successful, $f(p_e) \leq f(p_1)$, p_e replaces p_{m+1}; otherwise the expansion failed, and p_t replaces p_{m+1}.

If the new point p_t is worse than the second worst point, $f(p_t) \geq f(p_m)$, the polytope is assumed to be too large and needs to be contracted. A new trial point is defined as

$$p_c = \begin{cases} c + \gamma(p_{m+1} - c), & if\ f(p_t) \geq f(P_{m+1}), \\ c + \gamma(p_t - c), & if\ f(p_t) < f(P_{m+1}), \end{cases} \tag{3.19}$$

where $0 \leq \gamma \leq 1$ is a parameter for the contraction. If $f(p_c) < Min(f(p_{m+1}), f(p_t))$, the contraction is successful, and p_c replaces p_{m+1}. Otherwise a further contraction is carried out. The process is assumed to have converged if the difference between the best function values in the new and old polytope, as well as the distance between the new best point and the old best point, are less than the tolerances provided. Strictly speaking, NelderMead is not a true global optimization algorithm; however, in practice it tends to work reasonably well for problems that do not have many local minims. The Nelder-Mead algorithm can be synthesized in the following five steps [Lagarias *et al.*, 1998, Tajjudin *et al.*, 2011]:

1. Randomly initialize $m + 1$ individual points, and order them from the best to the worst.

2. Calculate the reflection point $p(t)$;

   if $f(p_1) \leq f(p_t) < f(p_m)$, accept p_t and terminate.

   if $f(p_t) < f(p_1)$, go to step 3.

   if $f(p_t) \geq f(p_m)$, go to step 4.

3. Generate p_e;

   if $f(p_e) \leq f(p_t)$, accept p_e and terminate.

   if $f(p_e) > f(p_t)$, accept p_t and terminate.

4. if $f(p_t) < f(p_{m+1})$, generate p_c;

   if $f(p_c) \geq f(p_t)$, accept p_c and terminate.

   Else, go to step 5.

   if $f(p_t) \geq f(p_{m+1})$, generate p_c.

   if $f(p_t) \leq f(p_{m+1})$,accept p_c and terminate.

   Else, go to step 5.

5. For each individual point i except for first p_1, evaluate new points as $p_i = p_1 + \gamma(p_i - p_1)$ and terminate.

3.5. FCS-MPC formulation advantages

In this chapter different formulations of the FCS-MPC for the power converters are presented, the characteristics of each FCS-MPC formulation are shown in Table 3.1. In relation to how we can select a formulation over another, the option is clear for the FCS-MPC - Nelder-Mead, which is suitable when a PWM device is physically part of the power converter circuit. However, the better selection between FCS-MPC - exhaustive search and FCS-MPC - MIQP is not clear, this depends on the desired control performance. In the following subsection, these formulations are applied to a power converter circuit, in order to test the control performance of each them.

Table 3.1: FCS-MPC formulations summary.

FCS-MPC, binary search	FCS-MPC, MIQP	FCS-MPC, direct search
Formulation suitable for:		
Control designs without any input modulation.	Control designs with PWM input waveform.	Control designs that the circuit includes a PWM device.
Optimization algorithm used:		
Exhaustive search	Branch and bound	Nelder-Mead
Control input obtained:		
binary input	binary sequence	Continuous input
Advantages:		
Small time-horizon, easy to implement online, intuitive solver method.	Low control effort, smooth ripple, solved by commercial solvers	Low control effort, smooth ripple, solved by simplex algorithm (Nelder-Mead).
Disadvantages:		
High control effort, suitable time-horizon not clearly established	High compute time, difficult to implement online for many independent control inputs.	High compute time, difficult to implement onlinefor many independent control inputs.

3.5.1. PWM waveform

This subsection presents a comparative study of the impact into the controller performance, when the control input is defined by a PWM modulation or not. For this

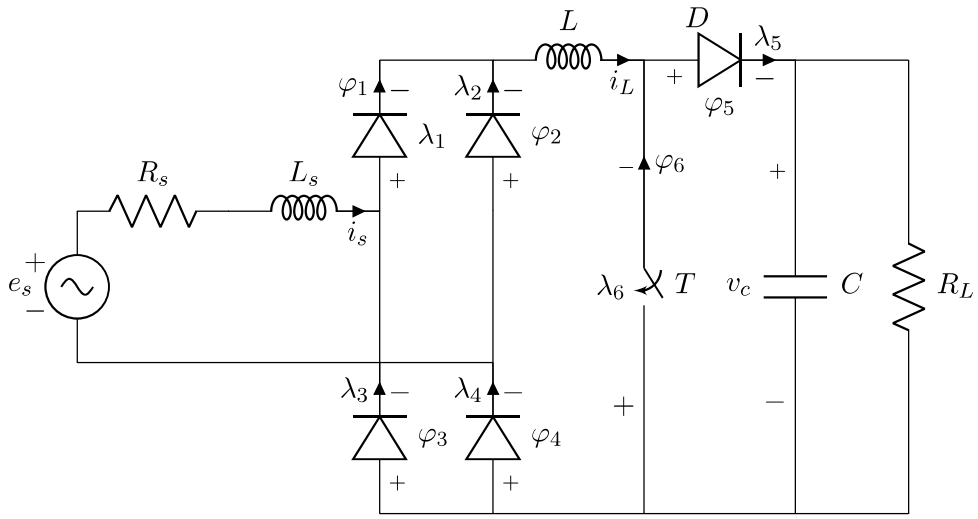

Figure 3.5: Single phase boost rectifier.

comparative case, consider one of the most important high power factor rectifiers, from a theoretical and conceptual point of view, the so-called single-phase boost rectifier, whose circuit scheme is illustrated in Figure 3.5. This circuit is an interesting power converter configuration, since this presents the modeling of a classical H bridge in the complementarity framework, and has only one controlled ED, which simplifies the comparative study of the control inputs. The rectifier is modeling in the complementarity form by cascading a classical H bridge rectifiers with a boost converter composed by a transistor T, a diode D an inductor L and a capacitor C. By applying the Kirchhoff laws one obtains the following dynamic equations

$$
\begin{aligned}
L_s \frac{\mathrm{d}}{\mathrm{d}t} i_s &= -R_s i_s + \varphi_3 - \varphi_4 + e_s \\
L \frac{\mathrm{d}}{\mathrm{d}t} i_L &= -v_c - \varphi_2 - \varphi_4 - \varphi_5 \\
C \frac{\mathrm{d}}{\mathrm{d}t} v_c &= i_L - \frac{1}{R_L} v_c - \varphi_6
\end{aligned}
$$

where $\varphi = \begin{pmatrix} \varphi_1 & \varphi_2 & \varphi_3 & \varphi_4 & \varphi_5 & \varphi_6 \end{pmatrix}^\top$ are the output variables of the complementarity model of the electronic devices, this equations correspond to the (2.15a) with $x = \begin{pmatrix} i_s & i_L & v_c \end{pmatrix}^\top$ and the matrices

$$A_c = \begin{pmatrix} -\frac{R_s}{L_s} & 0 & 0 \\ 0 & 0 & -\frac{1}{L} \\ 0 & \frac{1}{C} & -\frac{1}{R_L C} \end{pmatrix}, \quad E_c = \begin{pmatrix} 1 \\ 0 \\ 0 \end{pmatrix}$$

$$B_c = \begin{pmatrix} 0 & 0 & 1 & -1 & 0 & 0 \\ 0 & -1 & 0 & -1 & -1 & 0 \\ 0 & 0 & 0 & 0 & 0 & -1 \end{pmatrix}.$$

The output equations of the dynamic subsystem can be written as

$$\begin{aligned} \lambda_1 &= \varphi_2 - \varphi_3 + \varphi_4, & \lambda_2 &= i_L - \varphi_1 \\ \lambda_3 &= -i_s + \varphi_1, & \lambda_4 &= i_s + \lambda_2 = i_s + i_L - \varphi_1 \\ \lambda_5 &= i_L - \varphi_6, & \lambda_6 &= v_c + \varphi_5 \end{aligned}$$

which correspond to (2.15b) with

$$C_c = \begin{pmatrix} 0 & 0 & 0 \\ 0 & 1 & 0 \\ -1 & 0 & 0 \\ 1 & 1 & 0 \\ 0 & 1 & 0 \\ 0 & 0 & 1 \end{pmatrix}, \; D_c = \begin{pmatrix} 0 & 1 & -1 & 1 & 0 & 0 \\ -1 & 0 & 0 & 0 & 0 & 0 \\ 1 & 0 & 0 & 0 & 0 & 0 \\ -1 & 0 & 0 & 0 & 0 & 0 \\ 0 & 0 & 0 & 0 & 0 & -1 \\ 0 & 0 & 0 & 0 & 1 & 0 \end{pmatrix}$$

and $F_c = 0$. The representation (2.1) can be obtained by collecting the diode model (2.2) for (φ_1, λ_1), the diode model (2.3) for (φ_i, λ_i), $i = 2, \ldots, 5$, and the switch model (2.7) for (φ_6, λ_6), thus obtaining the following matrices:

$$B_s = \begin{pmatrix} diag(1, -1, -1, -1, -1, 1) & 0_{6\times 1} \end{pmatrix}$$

$$D_s = \begin{pmatrix} 0_{5\times 5} & 0_{5\times 2} \\ 0_{2\times 5} & \begin{pmatrix} 0 & 1 \\ -1 & 0 \end{pmatrix} \end{pmatrix}, \quad F_s = \begin{pmatrix} 0_{6\times 1} \\ I_{\mathrm{M}} \end{pmatrix}$$

Table 3.2: Single phase boost rectifier parameters

Component, Parameter	value
Voltage supply, e_s	$100\sin(100\pi t)$ V
Internal power supply resistance, R_s	$0.1\,\Omega$
Internal power supply Inductance, L_s	1 mH
Inductance, L	12 mH
Capacitance, C	120 µF
Switching period, P	100 µs
Integration step, α	10 µs

$C_s = -B_s^\top$ and $E_s = 0$, where 'diag' stands for a diagonal matrix whose main diagonal elements are indicated in the argument and $0_{i\times j}$ is a zero matrix with i rows and j columns. By using the matrices derived above in (2.17), the LC model (2.16) of the power rectifier can be directly obtained.

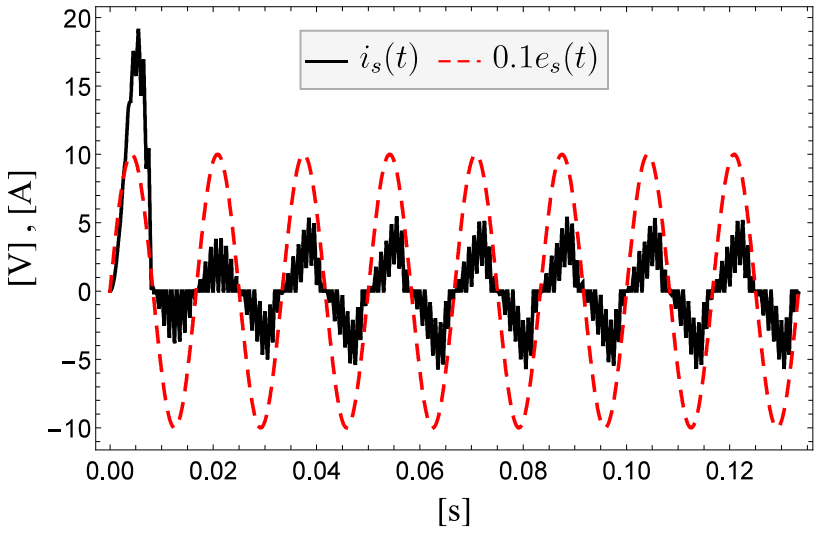

Figure 3.6: Single Phase Boost Rectifier, open-loop simulation for the signals i_s and e_s.

A open-loop simulation is performed with the parameters of the Table 3.2, and a fixed duty-cycle $d = 0.5$. Figure 3.6 shows the voltage source e_s and the current supplied i_s, where the current has a considerable ripple and the current is not in-phase in relation of

the voltage, which means a very low power factor.

A control objective in the boost rectifier is presented in [Rashid, 2007], where the current $i_s(t)$ is supplied with a unitary power factor by changing the conduction state of the transistor T. For this, an FCS-MPC is proposed for trajectory tracking of $i_s(t)$ to a sinusoidal reference $i_{s_{ref}} = A_i \sin(wt)$, which is proposed in phase with the power supply e_s, with a current amplitude $A_i = 2$ is considered. The study considers two FCS-MPC: the formulation (3.1), where the controller defines a binary control input without any PWM modulation, and the formulation (3.11), where the input control is defined as PWM signal.

In Figure 3.7 the control performance of both cases are shown, in Figure 3.7a one step ahead prediction without PWM modulation is presented, and in Figure 3.7b one PWM period prediction. In both cases, the optimal trajectory tracking is achieved, and the current i_s is in-phase with the power supply e_s voltage, which means a unitary power factor. However, the ripple presented by the current signal is not the same as it is shown in Figure 3.8, where the MPC with one step prediction, Figure 3.8a, presents a high-frequency ripple over another non-periodic signal, while MPC with prediction of one PWM period, Figure 3.8b, presents a smooth periodic ripple. This is an important difference between both controls performance, since if the ripple frequency is unknown the design of a filter stage is more complex. Another important difference is related to the control signal, in Figure 3.9 the control input for both MPC schemes are presented, where the control effort required by the MPC with one step prediction, Figure 3.9a, is bigger than the MPC with a PWM prediction, Figure 3.9b, where lower switches are required. This is an important difference since lower switches imply reducing the heating in the controller.

3.6. Chapter conclusion

This chapter presented different FCS-MPC formulations for power converters. The inclusion of a PWM signal reduces the control effort, but demands a longer computation time. Chosen one formulation over another depends on control designs criteria, which is related to the required performance and the available hardware devices. In the next chapter, these formulations are used in control designs for practical cases of power converters.

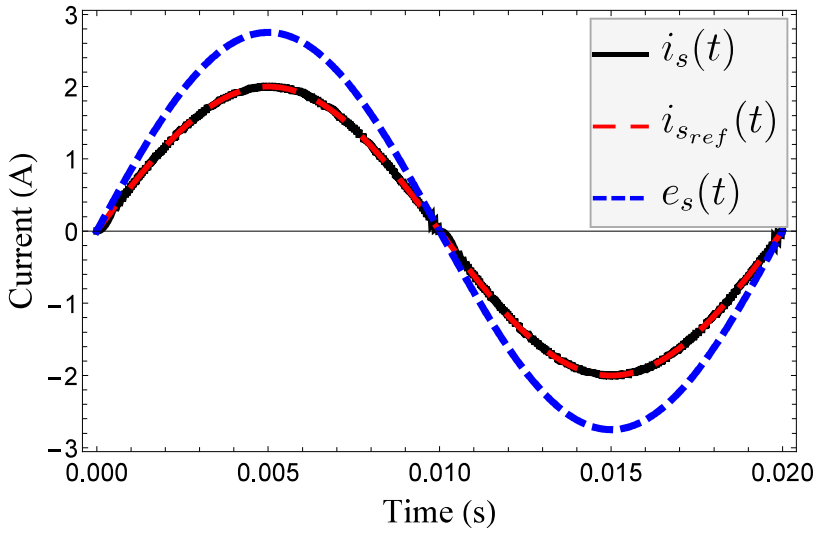

(a)

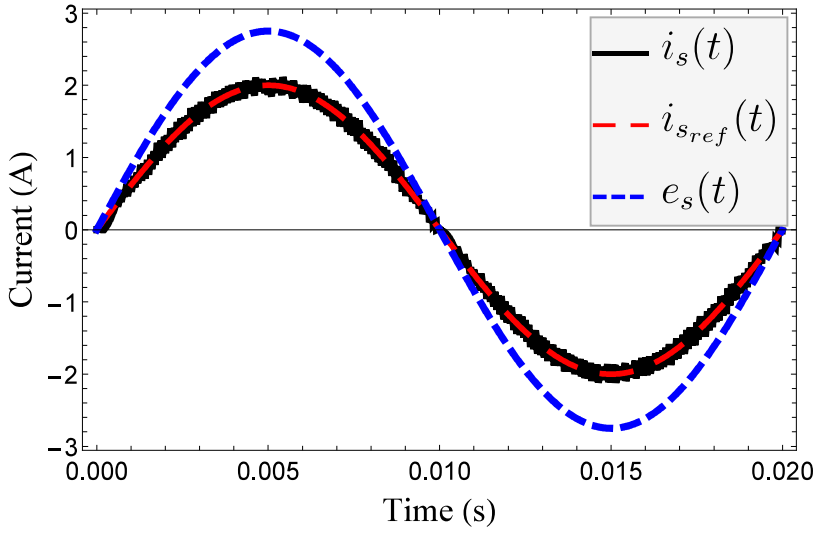

(b)

Figure 3.7: Control performance for: (a) Prediction without PWM, 1 step horizon, and (b) PWM prediction, 1 period horizon.

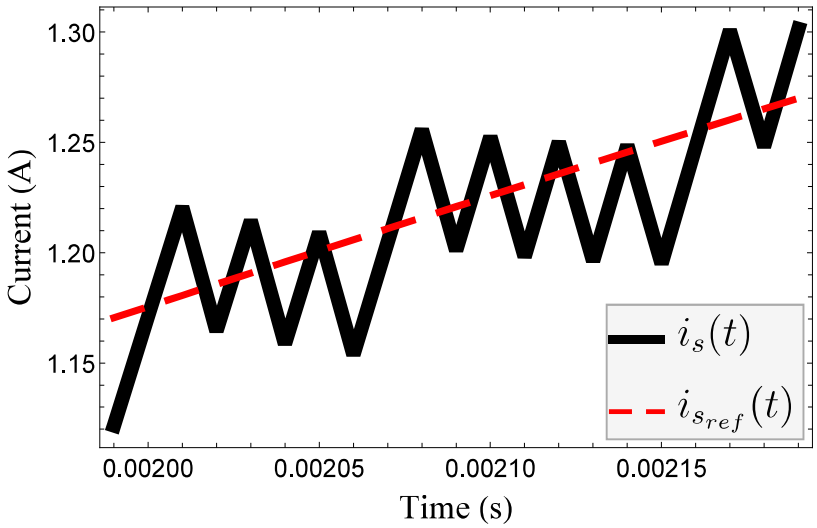

(a)

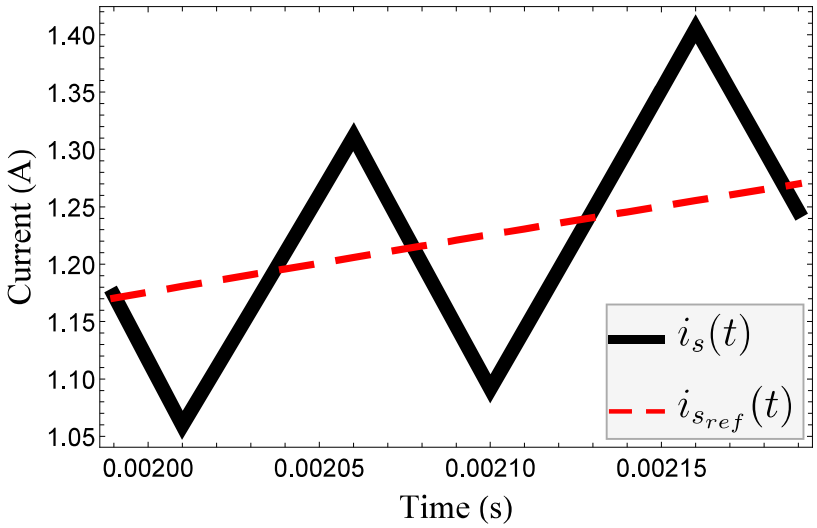

(b)

Figure 3.8: Current signal i_s ripple for: (a) Prediction without PWM, 1 step horizon, and (b) PWM prediction, 1 period horizon.

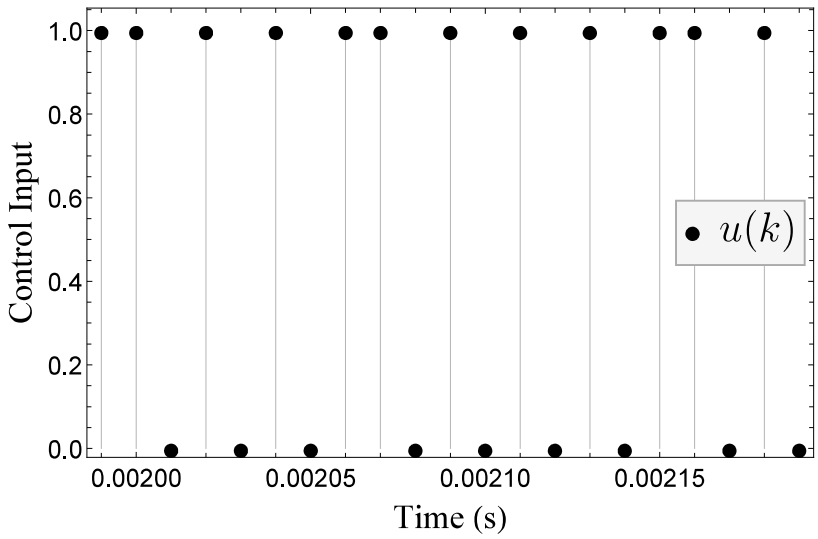

(a)

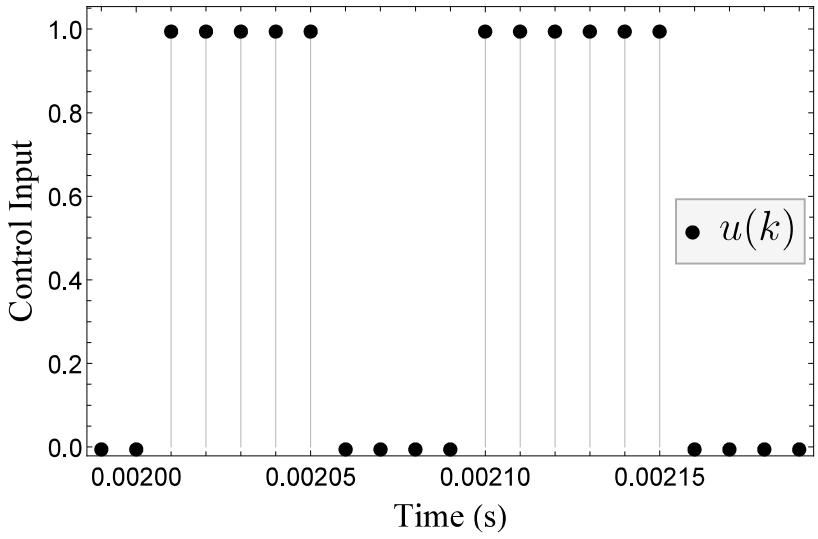

(b)

Figure 3.9: Control signal for: (a) Prediction without PWM, 1 step horizon, and (b) PWM prediction, 1 period horizon.

Chapter 4

Case Studies

This chapter deals with practical sceneries for power converters, where the FCS-MPC schemes described in the previous chapter is used. In order to implement the controller, additional techniques for reducing the computational time and to given robustness to the controller are proposed. The power converters used in this chapter are the boost converter, the AC/DC single-phase power inverter, and a combination of both, into a photovoltaic array connected to the grid. The FCS-MPC controller is implemented in two study cases.

4.1. HIL simulation of a boost converter.

In this section an hybrid controller that involves a FCS-MPC scheme (3.15) and an integral action is presented for a boost converter. A real-time simulation is performed using a hardware in the loop (HIL) methodology, and the controller is implemented in a microcontroller device, which contains a PWM module generator. Since a PWM generator is available, the FCS-MPC - direct search (3.15) formulation is used. This FCS-MPC is solved by the Nelder-Mead algorithm, which can be implemented by means of parallel processing. However, in this case the processing capacity in the microcontroller is limited, then, a parametric analysis is proposed to get explicitly the FCS-MPC controller off-line, whereby the computational cost is drastically reduced.

4.1.1. Hardware in the loop

Digital control designs for power converters, as MPC schemes, are more and more used in modern power electronic circuits. Digital control provides flexibility, high tolerance to noise, and higher robustness against thermal and aging effects. However, the digital-based implementation of the power converter control involves new concerns with respect to analog implementations, mainly due to the time discretization and finite resolution features [Fernndez-lvarez *et al.*, 2017]. In recent years it has been observed that testing digital controllers close to the application conditions is a critical step. Real-time simulation is a fundamental enabler for advanced testing techniques like HIL. In this technique, a part, or all system is modeled and simulated in real-time, normally using a field programmable gate array (FPGA). In this real time simulation, the analog input of the controller and the digital output of the power converter are implemented as close as possible to the actual controller to emulate signal conversion delays. Control signals are connected to the analog and digital inputs of the virtual plant model. From the controller perspective, there is no difference between the real converter and the simulated one. HIL simulation allows a comprehensive evaluation of all modes of operation of the controller under realistic system conditions and offers advantages as reduce cost, fast repeatability of the tests, and the ability to subject the controller to risky contingency situations, [Difronzo *et al.*, 2017, Sanchez *et al.*, 2012, Grgoire *et al.*, 2011, Faruque and Dinavahi, 2010].

4.1.2. MPC design

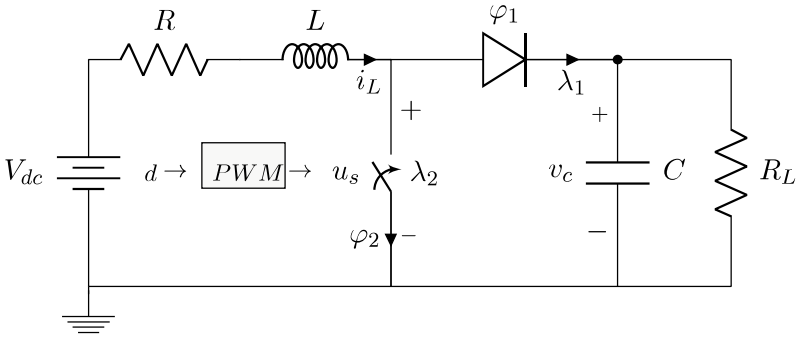

Figure 4.1: Boost converter circuit.

The control task for the boost converter circuit, shown in the Figure 4.1, usually involves the voltage regulation. Depending on the boost parameters, this regulation can be achieved by means of indirect or direct methods, controlling the current or the voltage state variable, respectively [Sriram *et al.*, 2003, Mohamed *et al.*, 2016]. In the first case (indirect method) a current reference i_{ref} can be obtained by means of a voltage reference v_{ref} [Escobar *et al.*, 1997, Ornelas-Tellez *et al.*, 2012], as

$$i_{ref} = \frac{v_{ref}^2}{R_L V_{dc}}. \tag{4.1}$$

In the direct method, the voltage reference v_{ref} is directly taken as reference. With these reference the indirect and direct control method can be design as an FCS-MPC (3.15), where the objective function is to minimize the difference between the state variables and their respective references. The MPC constraints are defined by the PWA system (2.43) of the boost converter, described in the subsection 2.3.1, and the PWM model as

$$\begin{aligned} \min_{d_p} \quad & \textstyle\sum_{k=1}^{\pi P_s} (x(k) - x_{ref}(k))^T Q (x(k) - x_{ref}(k)) \\ subject\ to: & \\ & \text{PWA system (2.43)} \\ & \text{PWM modulator (3.13).} \end{aligned}$$

In this case, the predicted horizon is considered as $\pi = 2$. In order to show different conduction modes of the power converter, two parameter configuration for the boost converter are considered, taken of Table 4.1. In the indirect control method, the power converter operates in continuous conduction mode (CCM). While in the direct control method, the boost operation is expected as discontinuous conduction mode (DCM).

4.1.3. Parametrized solution

In MPC implementation for power converters, the computing time usually is a limiting factor. This limitation can be resolved by transferring the on-line computation to an off-line parametric analysis, where it is considered the power converter state variables as parameters, then a parametric sweep is performed for a finite number of possible converter conditions, taken from a bounded operation range of the controller. This idea has been used

Table 4.1: Boost Converter parameters for MPC.

Component, Parameter	Indirect control	Direct control
Voltage supply, V_{dc}	48 V	12 V
Resistance, R	0.1 Ω	0.1 Ω
Inductance, L	12 mH	0.5 mH
Capacitance, C	15 µF	180 µF
Load Resistance, R_L	220 Ω	20 Ω
Switching period, P	100 µs	1000 µs
Integration step, α	1 µs	10 µs

in [Mariéthoz and Morari, 2009, Mirzaei and Afzalian, 2009], where the optimized duty cycle d^* for each power converter condition is written in a look-up table as result of the parametric analysis and interpolation techniques are used to approach the rest of the values in the operating range. In this work, on the other hand, an original parametric analysis is proposed from which the optimized duty cycle d^* is obtained as a piecewise function.

The parametric analysis purposed consist of an inspection of the slopes between consecutive points in each parameter direction. The algorithm for the parametric analysis can be described in the next five steps

1. Delimit the operation range of the controller for each parameter (i_L, v_c).

2. The FCS-MPC is solved to obtain the optimized duty cycle for a finite set values of one of the parameters, keeping the other parameter into a fixed value.

3. Using the equation of a line passing two points, the slopes between consecutive duty cycles is calculated. Then, a limit point is defined when the difference of two consecutive slopes exceeds a tolerance, as it is show in Figure 4.2.

4. The steps 2 and 3 are repeated for the other parameter until the operation range is completely divided by the limit points into rectangular regions, as it is shows in Figure 4.3.

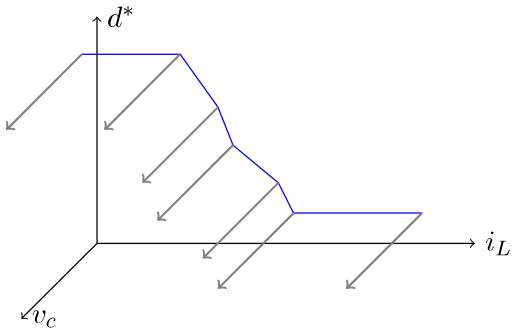

Figure 4.2: Limit points detection.

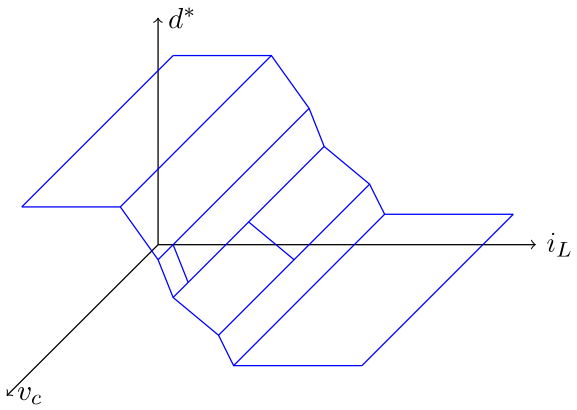

Figure 4.3: Rectangular regions.

Once the rectangular regions are defined, the optimized duty cycle d^* is approach in each region by means of the general equation of a plane as

$$d^* = \frac{\rho i_L + \beta v_c + \delta}{\gamma} \tag{4.2}$$

where the coefficients ρ, β, γ y δ can be approximated by means of a fitting function in Mathematica ™[Wolfram, 2017]. Then, considering the equations of all the regions, the FCS-MPC can be approached as a piecewise function as

$$d^* = \begin{cases} \frac{\rho_1 i_L + \beta_1 v_c + \delta_1}{\gamma_1} & \text{if } i_L, v_c \in R_1 \\ \frac{\rho_2 i_L + \beta_2 v_c + \delta_2}{\gamma_2} & \text{if } i_L, v_c \in R_2 \\ \vdots & \vdots \\ \frac{\rho_r i_L + \beta_r v_c + \delta_r}{\gamma_r} & \text{if } i_L, v_c \in R_r \end{cases} \tag{4.3}$$

where r is the number of regions.

4.1.4. Numeric simulations

The FCS-MPC controller (4.3) is tested in numeric simulations for both control cases: direct and indirect method. In Figure 4.5 the indirect control method is presented, where the voltage regulation to the desired reference $v_{ref} = 100\,\mathrm{V}$ is achieved, and the current operates in CCM. In Figure 4.4 the direct method is presented, where the voltage regulation for $v_{ref} = 16\,\mathrm{V}$ is achieved, and the current operates in DCM.

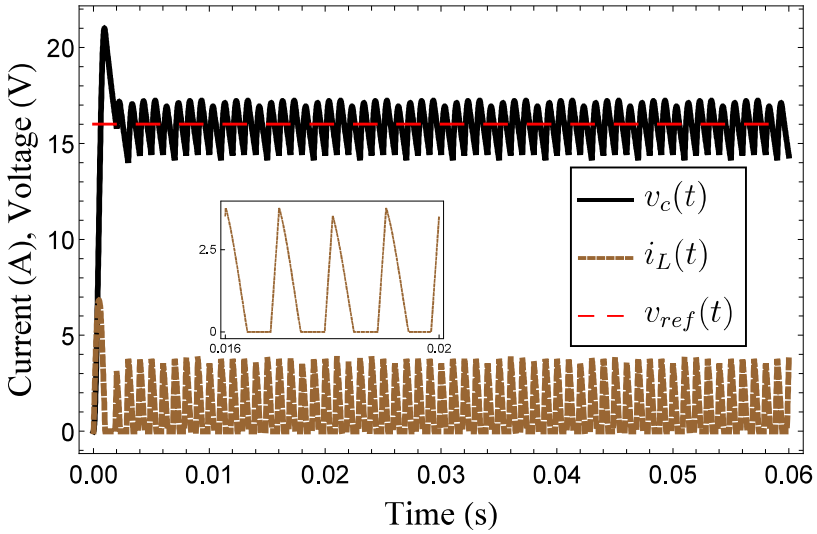

Figure 4.4: Direct control method and DCM.

These controllers approach by piecewise function (4.3) can be easily implemented in a microcontroller. However, any changes in the boost converter parameters, as load variations in the case of the boost, could affect the controller performance, and if this variation remains the control goal is not achievable.

4.1.5. Robustness against load variations

In order to provide of robustness to the controller against the load variations, an integral action is included as

$$d_i = K_i \sum (v_{ref} - v_c)\alpha \tag{4.4}$$

where K_i is a constant gain and α is the sampling time. The resulting robust controller can

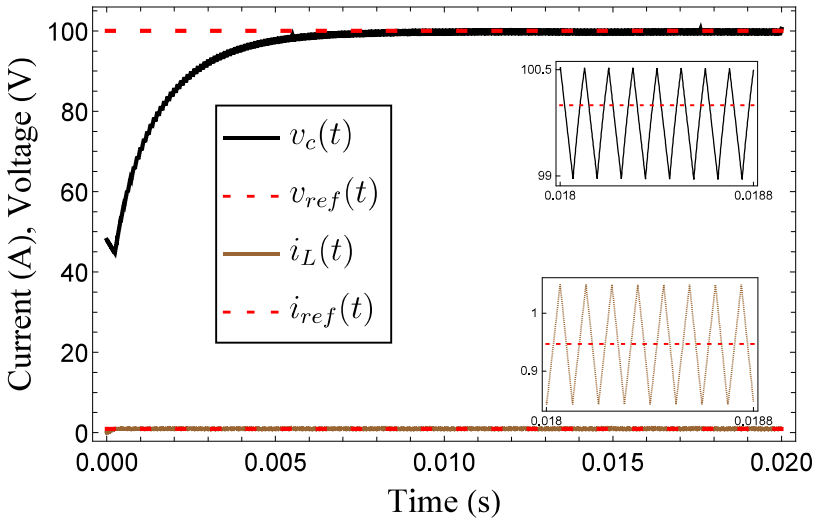

Figure 4.5: Indirect control method and CCM.

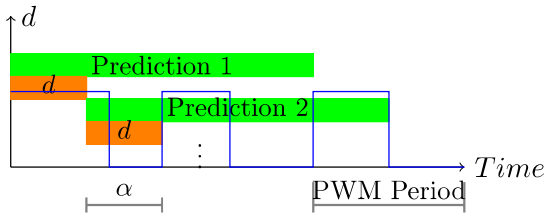

Figure 4.6: Prediction scheme of the controller.

be expressed as the sum of the parametric FCS-MPC (4.3) and the integral action (4.4) as

$$d = d^* + d_i. \tag{4.5}$$

In Figure 4.7, a block diagram of the resulting hybrid controller is shown. The implementation scheme is shown in Figure 4.6, where a prediction horizon is fixed to $\pi = 2$ PWM periods.

4.1.6. HIL real-time simulation

The controller (4.5) performance is tested in a real-time environment by means of HIL method with the development devices shown in Figure 4.8. In this case, the boost converter dynamics are simulated in an FPGA of a CompactRio, which is a device of National

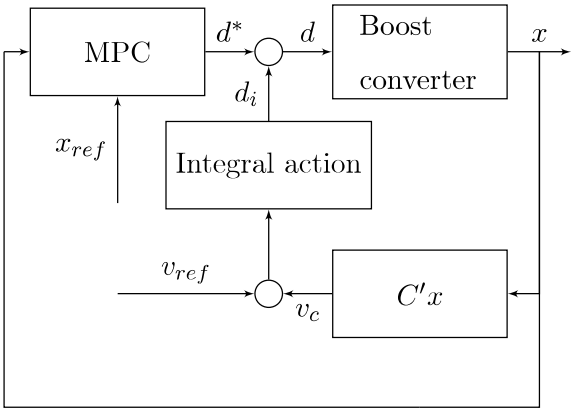

Figure 4.7: Block diagram of the controller

Instruments. In the other hand, the controller (4.5) is implemented in the microcontroller TMS320F28379D of Texas Instruments, which has a PWM output block. The real-time simulation is running by means a Labview interface, where changes in the load resistance can be easily programmed.

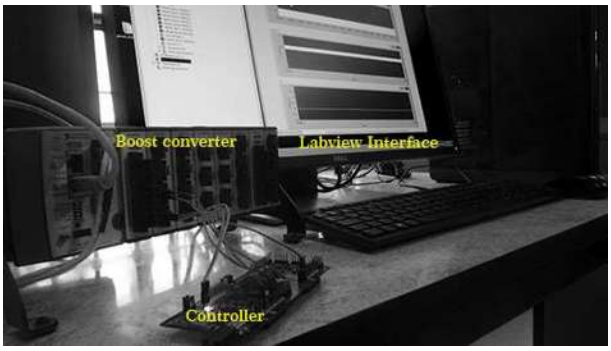

Figure 4.8: Hardware for HIL.

The controller is tested for both cases, the direct control, and the indirect control method. The changes in the load resistance are programmed in Labview as $\pm 20\,\%$ of its nominal value.

The controller performance of the direct control method is presented in Figure 4.9, in Figure 4.9a the regulation voltage is shown, where the voltage reference is achieved even with load variations, which only implies a small transient and a current peak modification

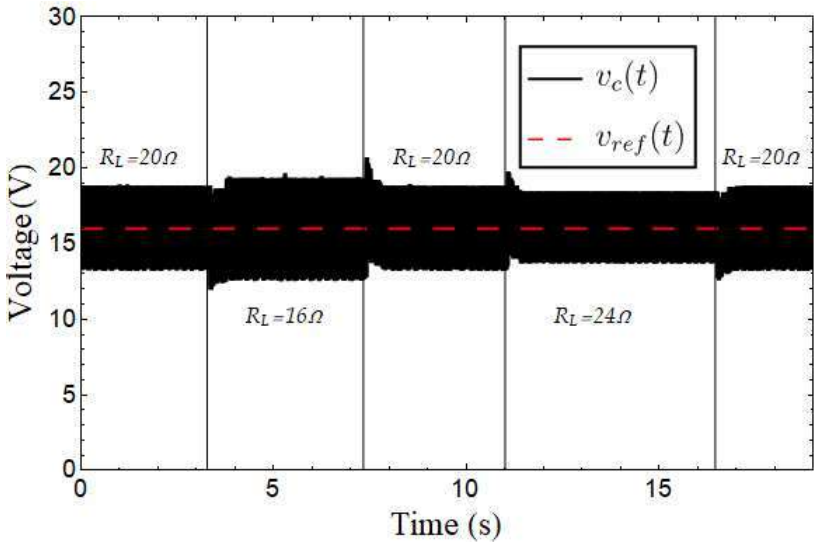

(a)

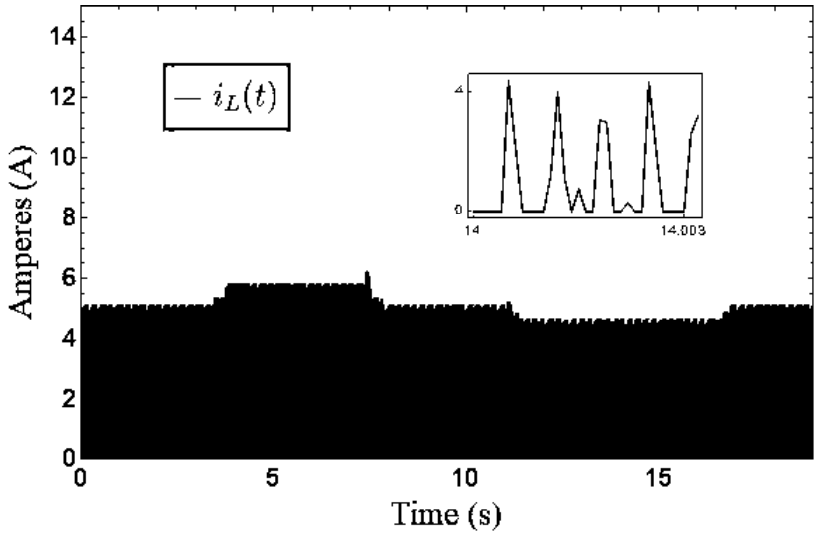

(b)

Figure 4.9: Regulation by direct method against load variations: (a) voltage regutaltion performance, and (b) current time transient.

by the integral action as it is shown in Figure 4.9b, where a zoom of the current signal is presented, in this a DCM operation mode and the signal shows noise due to the sampling process.

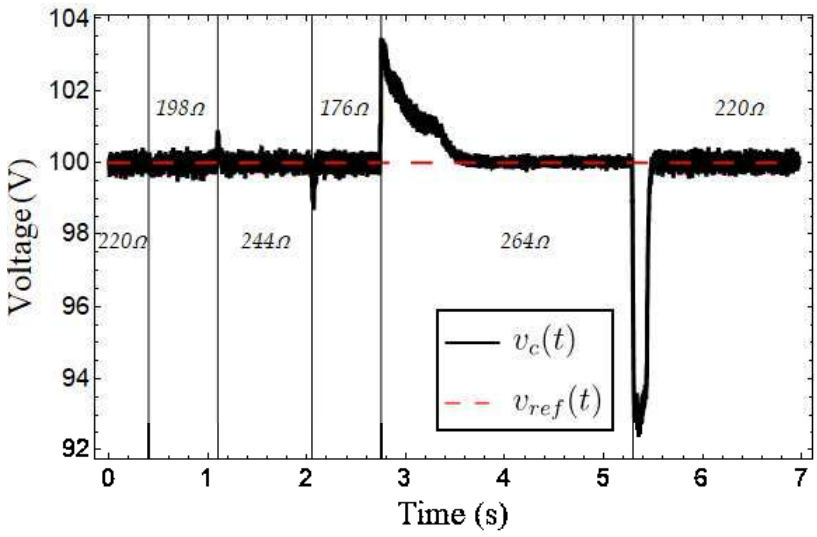

(a)

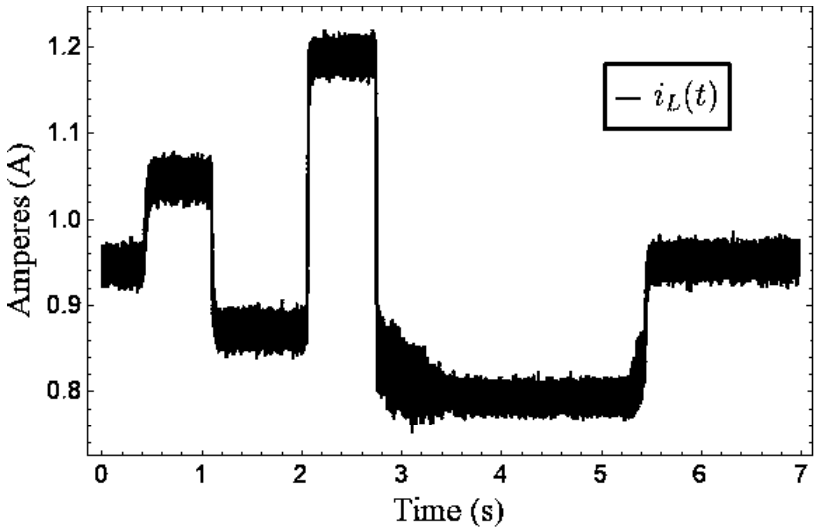

(b)

Figure 4.10: Regulation by indirect method against load variations: (a) voltage regutaltion performance, and (b) current time transient..

The control performance of the indirect control method is presented in Figure 4.10,

in Figure 4.10a the voltage regulation performance is shown, where the voltage reference is achieved even with load variations, Figure 4.10b shows the current modifications by the integral action in order to ensure the voltage convergence to the reference.

The implementation of an MPC design in an economic commercial device is one of the most important challenges of model predictive control, because one of the main limitations for its implementation is the high hardware demand. However, in this case, using a parametric analysis and incorporating classic control techniques to given of robustness the controller, allows to implement the synthesized hybrid controller (4.5) into a low profile microcontroller.

4.2. Implementation of a grid connected single-phase full bridge inverter

In this section, an FCS-MPC is implemented for a grid-connected, single phase full bridge inverter system, depicted in Figure 4.11. This power inverter is widely used for the DC/AC conversions, and in this implementation their formulation in the complementarity framework is presented. In this case, the control design considers the FCS-MPC formulation (3.1), where the control inputs are defined without any PWM modulation. As the same as the previous case, it is important to given of robustness to the controller in a implementation. In this case, a recursive least squares (RLS) algorithm is proposed. This algorithm estimates the coefficients of the linear system (2.43a), which adjust the system model when small variations in the inverter parameters are presented.

4.2.1. MPC design

The system, Figure 4.11 can be modeled in the complementarity framework using the corresponding electronic device models. Thus, by applying Kirchhoff laws the following

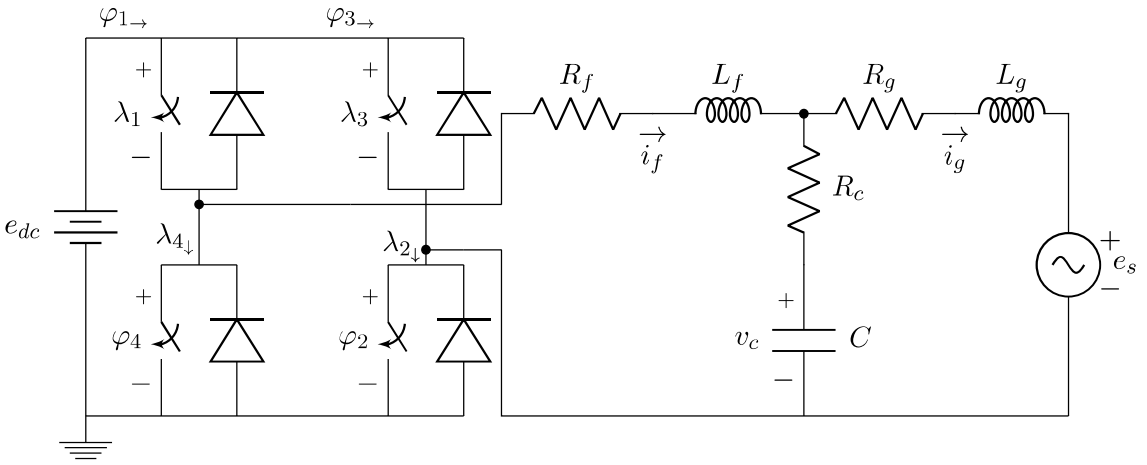

Figure 4.11: Grid connected single phase inverter with LCL filter.

dynamic equations can be obtained

$$L_f\dot{i_f} = -(R_f + R_c)i_f + R_c i_g - v_{cf} - \varphi_2 + \varphi_4$$
$$L_g\dot{i_g} = R_c i_f - (R_g + R_c)i_g + v_{cf} - e_s$$
$$C\dot{v_c} = i_f - i_g$$

which correspond to the (2.16) with $x = \begin{pmatrix} i_f & i_g & v_c \end{pmatrix}^\top$ and $e = \begin{pmatrix} e_{dc} & e_s \end{pmatrix}^\top$ and the matrices

$$A_c = \begin{pmatrix} -\frac{R_f+R_c}{L_f} & \frac{R_c}{L_f} & -\frac{1}{L_f} \\ \frac{R_c}{L_g} & -\frac{R_g+R_c}{L_g} & \frac{1}{L_g} \\ \frac{1}{C_f} & -\frac{1}{C_f} & 0 \end{pmatrix},\ B_c = \begin{pmatrix} 0 & -\frac{1}{L_f} & 0 & \frac{1}{L_f} \\ 0 & 0 & 0 & 0 \\ 0 & 0 & 0 & 0 \end{pmatrix},\ E_c = \begin{pmatrix} 0 & 0 & 0 \\ 0 & -\frac{1}{L_g} & 0 \end{pmatrix}^T.$$

The output equations of the dynamic subsystem can be written as

$$\lambda_1 = e_s - \varphi_4, \qquad \lambda_2 = i_f + \varphi_3$$
$$\lambda_3 = e_s - \varphi_2 \qquad \lambda_4 = -i_f + \varphi_1$$

which correspond to (2.15b) with

$$C_c = \begin{pmatrix} 0 & 0 & 0 \\ 1 & 0 & 0 \\ 0 & 0 & 0 \\ -1 & 0 & 0 \end{pmatrix},\ D_c = \begin{pmatrix} 0 & 0 & 0 & -1 \\ 0 & 0 & 1 & 0 \\ 0 & -1 & 0 & 0 \\ 1 & 0 & 0 & 0 \end{pmatrix} \qquad F_c = \begin{pmatrix} 1 & 0 & 1 & 0 \\ 0 & 0 & 0 & 0 \end{pmatrix}^T.$$

The representation (2.1) can be obtained by collecting the antiparallel switch models (2.12) for (φ_1, λ_1) and (φ_3, λ_3), the model (2.13) for (φ_2, λ_2) and (φ_4, λ_4). By assuming the same value of the maximum current for all switches and by defining $u = \begin{pmatrix} u_1 & u_2 & u_3 & u_4 \end{pmatrix}^\top$, the following matrices are obtained

$$B_s = \begin{pmatrix} -1 & 0 & 0 & 0 \\ 0 & 1 & 0 & 0 \\ 0 & 0 & -1 & 0 \\ 0 & 0 & 0 & 1 \end{pmatrix} \quad E_s = \begin{pmatrix} I_M & 0 & 0 & 0 \\ 0 & 0 & 0 & 0 \\ 0 & 0 & I_M & 0 \\ 0 & 0 & 0 & 0 \end{pmatrix} \quad F_s = \begin{pmatrix} 0 & 0 & 0 & 0 \\ 0 & I_M & 0 & 0 \\ 0 & 0 & 0 & 0 \\ 0 & 0 & 0 & I_M \end{pmatrix},$$

$C_s = -B_s^\top$ and $D_s = 0$. By using the matrices derived above, the LC model (2.15) of the grid-connected single phase inverter can be directly obtained. The discrete LC model (2.18)

Table 4.2: grid-connected, single phase inverter parameters

Component, Parameter	value
Input LCL filter resistance, R_f	$1\,\mathrm{m\Omega}$
Input LCL filter Inductance, L_f	$3.2\,\mathrm{mH}$
LCL filter Resistance, R_c	$4\,\mathrm{m\Omega}$
LCL filter Capacitance, C	$180\,\mu\mathrm{F}$
Output LCL filter Resistance, R_g	$1\,\Omega$
Output LCL filter Inductance, L_g	$80\,\mu\mathrm{H}$
Grid voltage, e_s	$297\sin(120\pi t)$ V
Switching period, P	$100\,\mu\mathrm{s}$
Integration step, α	$1\,\mu\mathrm{s}$

can be obtained, considering the power converter parameters of Table 4.2. The parameters $\theta(k)$ in the PLCP (2.40) are bounded by the limits: $-500 \leq i_f, i_g, v_c \leq 500$, $200 \leq e_{dc} \leq 800$, $-300 \leq e_s \leq 300$ and $0 \leq u \leq 1$. After, by solving the PLCP the power converter is modeled as (2.43). Then, the FCS-MPC (3.1) can be formulated. Additionally, in this case, it is necessary to including the constraints

$$u_1 + u_3 \leq 1 \quad \textit{and} \quad u_2 + u_4 \leq 1. \tag{4.11}$$

for the control inputs. These constraints avoid a possible short circuit in the controlled ED's. In this circuit the objective control is to supply active and reactive power to the grid. This objective can be included in the FCS-MPC through the current reference

$$i_{g_{Ref}} = \frac{S}{0.707 e_{s_{RMS}}} \sin(wt + \phi) \tag{4.12}$$

with

$$\begin{aligned} S = &\quad \sqrt{P^2 + Q^2}, \\ \phi = &\quad \cos^{-1}(PF), \\ PF = &\quad \tfrac{P}{S}. \end{aligned}$$

where PF is the power factor, S, P and Q are the apparent, active and reactive power, respectively. In this case, the control objective is considered as supply only active power, which can be done by set up $PF = 1$, and $Q = 0$. A necessary condition to be available for supply power to the grid in this circuit is that the magnitude of direct voltage e_{dc} must be 1.5 times that the grid e_s amplitude, or bigger. A FCS-MPC (3.1) can be formulated considering the minimum horizon prediction $n = 1$, where the number of possible inputs are $2^{n \times n_u} = 8$, and the objective function is to minimize the difference between the state variable i_g and its respective reference $i_{g_{ref}}$ (4.32), subject to the PWA system (2.43), and the additional constraints to avoid the possible short circuit (4.11), written as

$$\begin{aligned} &\min_{z(k)} \qquad (i_g(k) - i_{g_{Ref}}(k))^T Q (i_g(k) - i_{g_{Ref}}(k)) \\ &subject\ to: \\ &\qquad\qquad \text{PWA system (2.43)} \\ &\qquad\qquad \text{Input constraints (4.11)} \end{aligned} \tag{4.13}$$

As it was mentioned in the chapter 3, this MPC can be solved by means of exhaustive search method, where all the possible inputs are numbering. Then, the input that minimizes the objective function is chosen.

4.2.2. Recursive least squares algorithm

The proposed FCS-MPC is based on a deterministic model of the power converter. The main challenge in this formulation is to obtain the values of the power converter parameters (inductors, capacitors, and resistors), which usually is not possible, due to parameter

uncertainties or because the power converter is physically a black box. In order to address this drawback, in this paper is purposed a method to give robustness to the FC-MPC against parameter variations based on a recursive least square (RLS) estimation. Considering that at this point the power converter model (2.43) has already obtained with some expected values of the power converter parameters, the RLS algorithm is applied only for the matrices A_d, B_d and E_d of the linear system (2.43a). Note that, since the matrices coefficients of the PWA (2.43b) are not estimated, the system robustness only remains for the bounded operation range of the parameters $\theta(k)$ in (2.43), and it is important to mention that the estimated coefficients of the difference equation (2.43a) approach the system dynamics, not the power converter parameters. The RLS algorithm estimates on-line the coefficient values of the matrices A_d, B_d and E_d, at each sampling time [Astrom and Wittenmark, 1994], where the coefficients of the state variables of the power converter can be estimates as

$$\hat{a}^i(k) = \hat{a}^i(k-1) - K^i(k)(X^i(k) - \chi(k)^\top \hat{a}^i(k-1)) \tag{4.14}$$

where

$$\begin{aligned}
X^i(k) =& [x^i(k-1), x^i(k-2), x^i(x-3)]^\top, \\
\chi(k) =& \begin{bmatrix} x^1(k-1) & x^1(k-2) & x^1(k-3) \\ \vdots & \vdots & \vdots \\ x^{n_v}(k-1) & x^{n_v}(k-2) & x^{n_v}(k-3) \\ z^1(k) & z^1(k-1) & z^1(k-2) \\ \vdots & \vdots & \vdots \\ z^{n_c}(k) & z^{n_c}(k-1) & z^{n_c}(k-2) \\ e^1(k) & e^1(k-1) & e^1(k-2) \\ \vdots & \vdots & \vdots \\ e^{n_e}(k) & e^{n_e}(k-1) & e^{n_e}(k-2) \end{bmatrix}^\top \\
K^i(k) =& P^i(k-1)\chi(k)(I + \chi(k)^\top P^i(k-1)\chi(k))^{-1}, \\
P^i(k) =& (1 - K^i(k)\chi(k)^\top)P^i(k-1),
\end{aligned}$$

where $i = 1, ..., n_v$, and $P(k)$ is normally referred as the covariance matrix. In Figure 4.12 a block diagram of the resulting controller is shown.

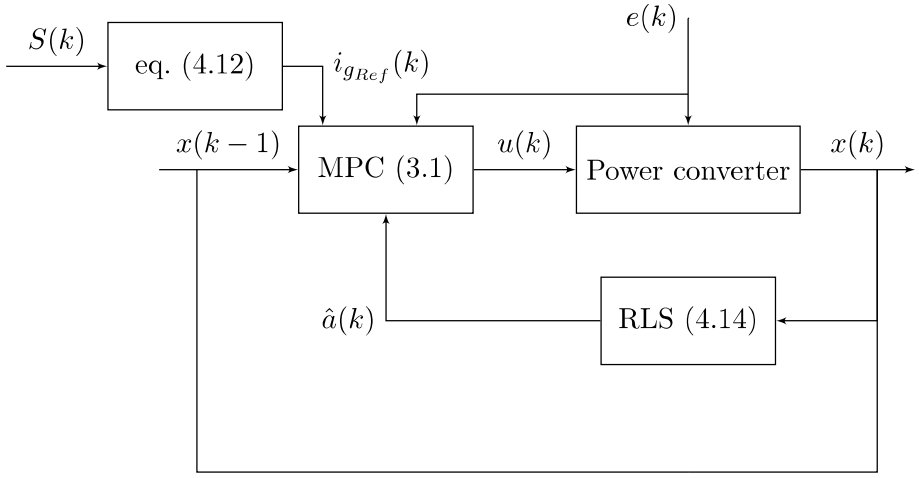

Figure 4.12: Block diagram of the controller.

4.2.3. Numeric simulation

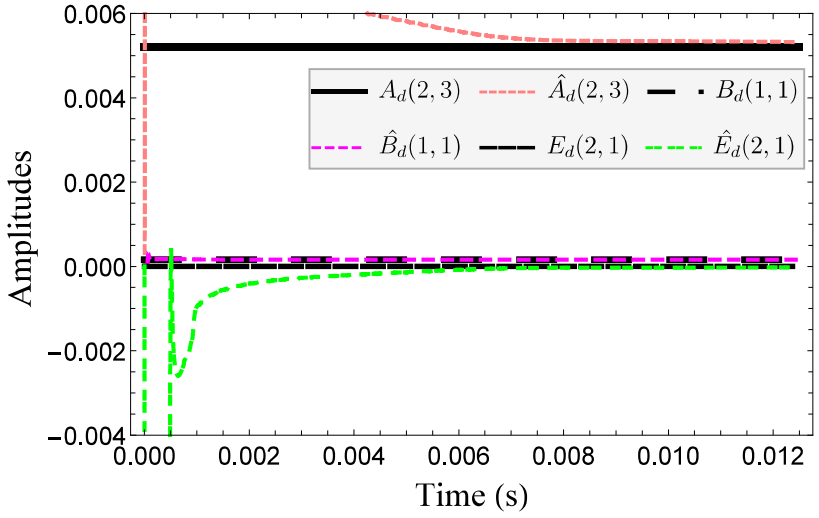

Figure 4.13: Convergence of the recursive least square algorithm.

In order to show the coefficient convergence of the RLS algorithm and the control performance, the resulting controller is tested in a numeric simulation. In this, all coefficients

in the matrices A_d, B_d and E_d of the model (2.43a) are initialized to zero, and then, their values are estimates at each sampling time by the RLS algorithm (4.14), while the FCS-MPC (4.13) obtains the optimized control input, using these estimate matrices.

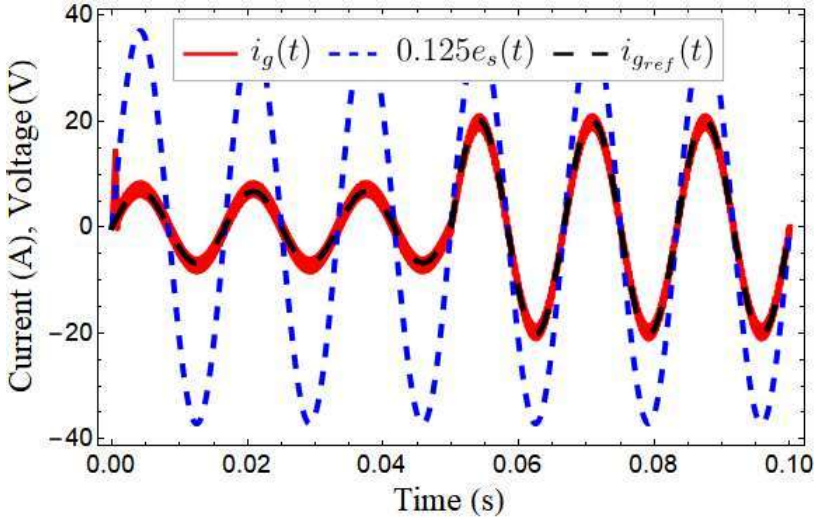

Figure 4.14: Optimal trajectory tracking performance of i_g to $i_{g_{ref}}$ and the grid $e_s(t)$.

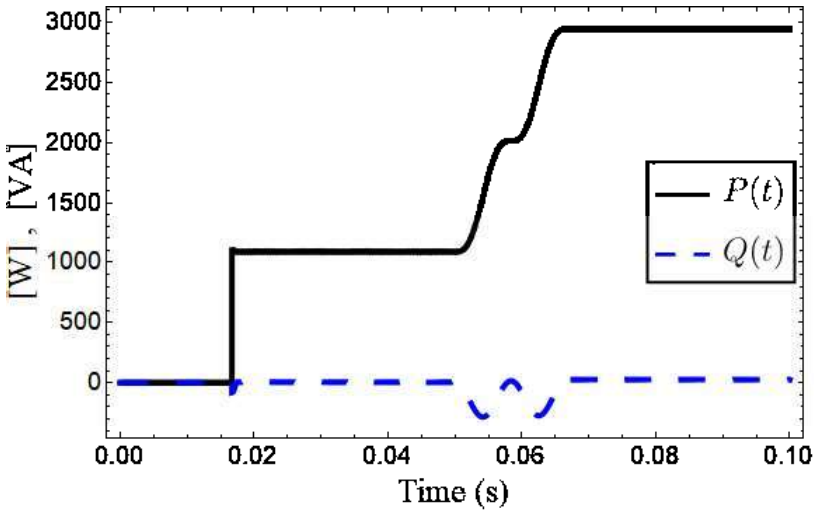

Figure 4.15: Active and reactive power supplied to the grid.

In Figure 4.13 the RLS convergence, where a coefficient of each matrix is shown, the time convergence is about 0.1 seconds. After this time, the system is identify and the optimal trajectory tracking task is achieved as it is shown in Figure 4.14, where the current

i_g converges to its reference $i_{g_{ref}}$ until the coefficients converge to the system matrix values, the simulation considers a increment in the active power at time 0.05 s,which implies an increment in the reference $i_{g_{ref}}$. Additionally, the grid voltage e_s is shown, which is in-phase with the current i_g. Therefore, the power is supplied to the grid with an unitary power factor. The active and reactive power supplied to the grid are shown in Figure 4.15, where only active power is supplied in steady-state, which is the control task.

This numeric simulation allows to test the RLS algorithm performance, which can be implemented into a microcontroller or similar devices for on-line estimation, as same as the FCS-MPC (4.13).

4.2.4. Implementation

In order to test the FCS-MPC controller in a real-time environment, the controller is implemented in the laboratory by means of Lab-Volt equipment and an OPAL-RT system. Figure 4.16 shows the practical scenario for testing the controller. In this implementation,

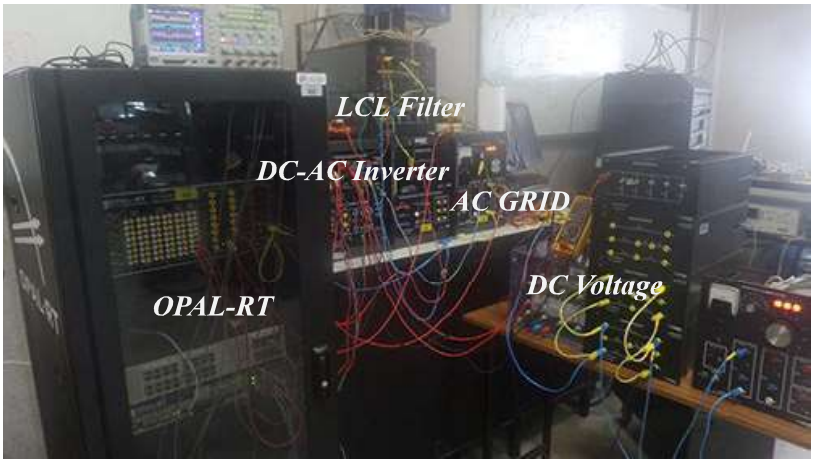

Figure 4.16: Implementation scenario.

the equipment used is chosen by considering the components available in the laboratory. Even though the FCS-MPC resulting controller can be implemented in lower profile device as a digital signal processor (DSP), OPAL-RT equipment is used, due to its sensing interface and because it is available in the laboratory. Similarly, the power inverter parameters are chosen considering the available equipment of Lab-Volt, which in this case the power

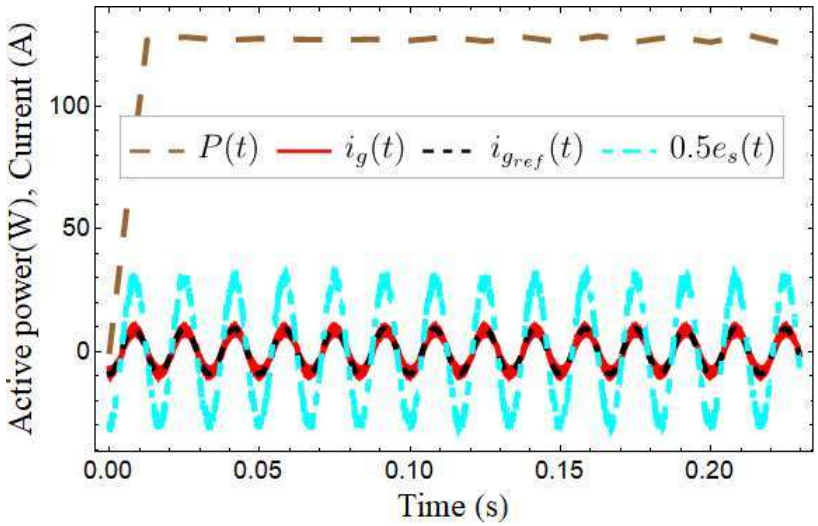

Figure 4.17: Real-time implementation. Active power supplied to the grid, and FCS-MPC performance.

converter parameters are: $e_{dc} = 160\,\text{V@8 A}$, $L_f = 14.98\,\text{mH}$, $R_f = 0.37\,\Omega$, $R_c = 6.82\,\Omega$, $C = 190\,\text{mF@250 V}$, $R_g = 0.06\,\Omega$, $L_g = 98\,\mu\text{F}$, $e_s = 40\,\text{V@15 A}$, and $\alpha = 25\,\mu\text{s}$. This parameters differs from the numeric simulation. However, the same PWA system (2.43b) is used, and the parameter variation is compensated by the matrices of the linear model (2.43a), which are estimated by the RLS algorithm. Figure 4.17 shows the FCS-MPC performance for optimal control tracking of the current i_g to the reference $i_{g_{ref}}$, and the active power supplied to the grid, this value is calculated form the root mean square (RMS) values of the voltage e_s and the current i_g since the sampling proccess in the OPAL-RT could lost information. Additionally, the voltage of the grid e_s is presented, in order to prove that is in-phase with the current i_g, which means that only active power is supplied.

An control objective of interest could be to supply a varying active power to the grid. In the FCS-MPC scheme, this can be achieve by varying the amplitude of the current reference $i_{g_{ref}}$, which is obtained by means of equation (4.32). In Figure (4.18) is presented a fictional case where a slow sinusoidal variation of the active power is required, and how the current reference is modifying. With this the capabilities of the FCS-MPC controller for supplied active power according to the requirements of the grid, trough the current reference (4.32), is proven. In relation of the three FCS-MPC formulations presented in

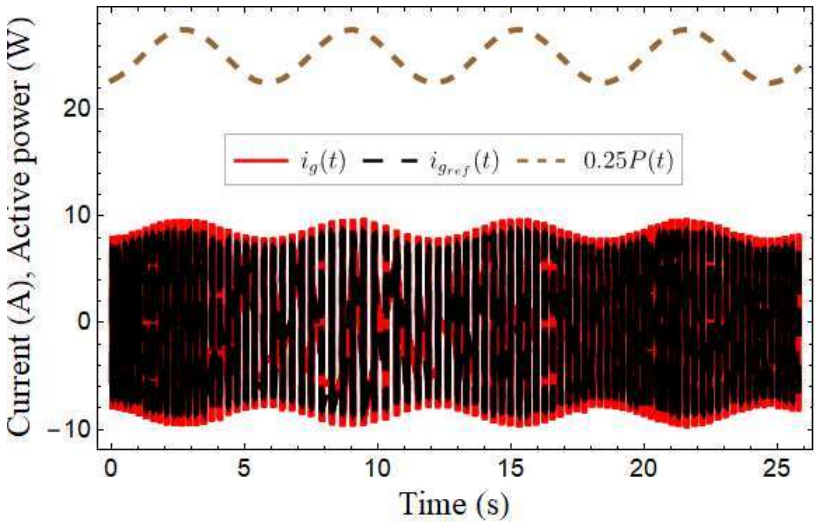

Figure 4.18: Real-time implementation. Variations of active power supplied to the grid.

this thesis, this FCS-MPC formulation (3.1) without any PWM modulation is easier to be implemented, since a pretty small prediction time can be considered (25 µs), which reduce the compute time and, therefore, the hardware requirements.

4.3. Residential microgrid applications

In this section, the FCS-MPC scheme is applied to the field of renewable energies. Nowadays, on issues of energy generation, the urgency of a change to renewable energies, such solar energy, is evident. However, the integration of photovoltaic (PV) generation demands not only modern power electronic equipment, but also state-of-the-art techniques, that through modeling and control design would ensure the compatibility of renewal sources with the existing electronic power systems. The complementarity formalism constitutes a suitable framework to support the integration of PV generations into electric power grids. In this case, a typical circuit for residential microgrid integration is presented. Figure 4.19 depicts a single-phase photovoltaic generator with a two-stage power conversion subsystem and LCL filter for a residential microgrid. The solar energy is obtained from an array of PV cells, the power inversion subsystem includes a DC-DC boost converter that step up the voltage of PV cell to the required levels in the integration of a renewable resource and

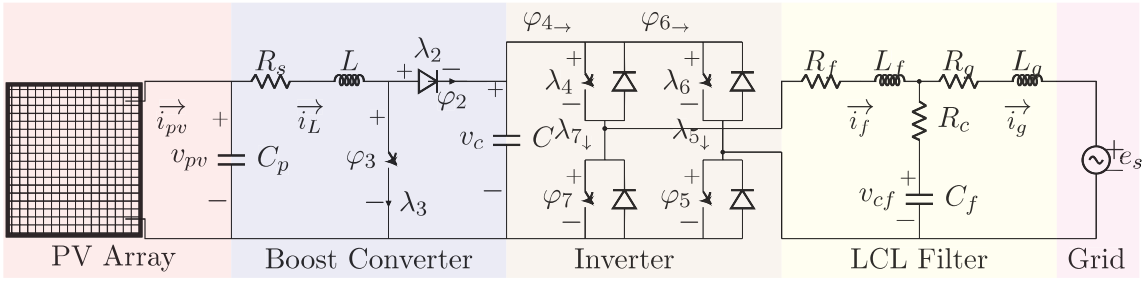

Figure 4.19: A single-phase photovoltaic generator with a two-stage power conversion subsystem and and LCL filter for a residential microgrid.

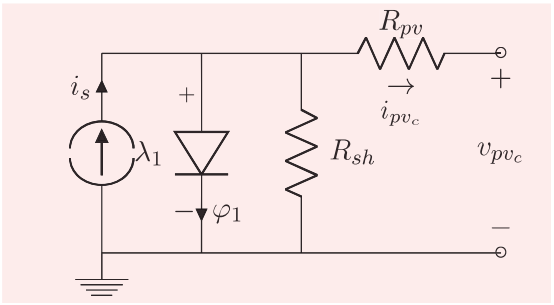

Figure 4.20: The equivalent circuit for a solar cell.

the utility grid. It also includes a power inverter that provides ac power to the microgrid. A passive LCL filter between the inverter and the utility grid is considered to reduce the injection of harmonic pollution into the utility grid. The entire system can be modeled in the complementarity framework using the corresponding electronic device model.

4.3.1. PV system model in complementarity form

First the PV power electronic system, which is shown in Figure 4.19, is modeled in the complementarity framework. For this, let us first consider the dynamic equation of the voltage on the capacitor C_p, which can be written as follows

$$C_p \frac{\mathrm{d}}{\mathrm{d}t} v_{pv} = i_{pv} - i_L. \tag{4.16}$$

The PV array consists of a series-parallel connection of n_s and n_p solar cells, respectively, whose equivalent circuit is shown in Figure 4.20. By applying the Kirchhoff laws, the diode

voltage λ_1 and the PV cell current i_{pv_c} can be written as

$$\lambda_1 = \rho R_{pv} i_s - \rho R_{pv} \varphi_1 + \rho v_{pv_c}, \tag{4.17a}$$

$$i_{pv_c} = \rho i_s - \rho \varphi_1 - \frac{\rho}{R_{sh}} v_{pv_c} \tag{4.17b}$$

where $\rho = R_{sh}/(R_{sh}+R_{pv})$. By assuming that all cells are equal, the voltage v_{pv} and current i_{pv} of the PV array model can be written in terms of the voltage v_{pv_c} and current i_{pv_c} of the solar cell as follows

$$v_{pv} = n_s v_{pv_c} \tag{4.18a}$$

$$i_{pv} = n_p i_{pv_c}. \tag{4.18b}$$

By combining (4.17)–(4.18) the dynamic equation (4.16) can be rewritten as

$$C_p \frac{\mathrm{d}}{\mathrm{d}t} v_{pv} = -\frac{n_p \rho}{n_s R_{sh}} v_{pv} - i_L - n_p \rho \varphi_1 + n_p \rho i_s. \tag{4.19}$$

The remaining dynamic equations can be obtained by applying the Kirchhoff laws to the circuit in Figure 4.19:

$$L \frac{\mathrm{d}}{\mathrm{d}t} i_L = v_{pv} - R_s i_L - \varphi_3 \tag{4.20a}$$

$$C \frac{\mathrm{d}}{\mathrm{d}t} v_c = \varphi_2 - \varphi_4 - \varphi_6 \tag{4.20b}$$

$$L_f \frac{\mathrm{d}}{\mathrm{d}t} i_f = -(R_f + R_c) i_f + R_c i_g - v_{cf} - \varphi_5 + \varphi_7 \tag{4.20c}$$

$$L_g \frac{\mathrm{d}}{\mathrm{d}t} i_g = R_c i_f - (R_g + R_c) i_g + v_{cf} - e_s \tag{4.20d}$$

$$C_f \frac{\mathrm{d}}{\mathrm{d}t} v_{cf} = i_f - i_g. \tag{4.20e}$$

The dynamic equations (4.19)–(4.20) correspond to (2.15a) with the state vector $x = \begin{pmatrix} v_{pv} & i_L & v_c & i_f & i_g & v_{cf} \end{pmatrix}^\top$, the exogenous input vector $e = \begin{pmatrix} i_s & e_s \end{pmatrix}^\top$ and the

following matrices

$$A_c = \begin{pmatrix} -\frac{\rho}{R_{sh}C_p} & -\frac{1}{C_p} & 0 & 0 & 0 & 0 \\ \frac{1}{L} & -\frac{R_s}{L} & 0 & 0 & 0 & 0 \\ 0 & 0 & 0 & 0 & 0 & 0 \\ 0 & 0 & 0 & -\frac{R_f+R_c}{L_f} & \frac{R_c}{L_f} & -\frac{1}{L_f} \\ 0 & 0 & 0 & \frac{R_c}{L_g} & -\frac{R_g+R_c}{L_g} & \frac{1}{L_g} \\ 0 & 0 & 0 & \frac{1}{C_f} & -\frac{1}{C_f} & 0 \end{pmatrix},$$

$$B_c = \begin{pmatrix} -\frac{\rho}{C_p} & 0 & 0 & 0 & 0 & 0 & 0 \\ 0 & 0 & -\frac{1}{L} & 0 & 0 & 0 & 0 \\ 0 & \frac{1}{C} & 0 & -\frac{1}{C} & 0 & -\frac{1}{C} & 0 \\ 0 & 0 & 0 & 0 & -\frac{1}{L_f} & 0 & \frac{1}{L_f} \\ 0 & 0 & 0 & 0 & 0 & 0 & 0 \\ 0 & 0 & 0 & 0 & 0 & 0 & 0 \end{pmatrix},$$

$$E_c = \begin{pmatrix} \frac{1}{C_P} & 0 & 0 & 0 & 0 & 0 \\ 0 & 0 & 0 & 0 & -\frac{1}{L_g} & 0 \end{pmatrix}^T.$$

The output equations of the dynamic subsystem can be written as

$$\lambda_1 = \frac{\rho}{n_s} v_{pv} - \rho R_{pv} \varphi_1 + \rho R_{pv} i_s, \tag{4.21a}$$

$$\lambda_2 = -v_c + \varphi_3, \quad \lambda_3 = i_L - \varphi_2, \quad \lambda_4 = v_c - \varphi_7, \tag{4.21b}$$

$$\lambda_5 = i_f + \varphi_6, \quad \lambda_6 = v_c - \varphi_5, \quad \lambda_7 = \varphi_4 - i_f, \tag{4.21c}$$

which correspond to (2.15b) with the matrices

$$C_c = \begin{pmatrix} \rho & 0 & 0 & 0 & 0 & 0 \\ 0 & 0 & -1 & 0 & 0 & 0 \\ 0 & 1 & 0 & 0 & 0 & 0 \\ 0 & 0 & 1 & 0 & 0 & 0 \\ 0 & 0 & 0 & 1 & 0 & 0 \\ 0 & 0 & 1 & 0 & 0 & 0 \\ 0 & 0 & 0 & -1 & 0 & 0 \end{pmatrix},$$

$$D_c = \begin{pmatrix} -\rho R_{pv} & 0 & 0 & 0 & 0 & 0 & 0 \\ 0 & 0 & 1 & 0 & 0 & 0 & 0 \\ 0 & -1 & 0 & 0 & 0 & 0 & 0 \\ 0 & 0 & 0 & 0 & 0 & 0 & -1 \\ 0 & 0 & 0 & 0 & 0 & 1 & 0 \\ 0 & 0 & 0 & 0 & -1 & 0 & 0 \\ 0 & 0 & 0 & 1 & 0 & 0 & 0 \end{pmatrix}$$

$$F_c(1,1) = \rho R_{pv}, \quad F_c(i,j) = 0 \; \forall i, j \neq 1$$

The representation (2.1) can be obtained by collecting the piecewise linear approach of the diode (2.6) for (φ_1, λ_1), the diode model (2.2) for (φ_2, λ_2), the switch model (2.7) for (φ_3, λ_3), the antiparallel switch model (2.7) for (φ_4, λ_4), (φ_6, λ_6), and the antiparallel switch model (2.13) for (φ_5, λ_5) and (φ_7, λ_7). By assuming the same value of the maximum current

for all switches and by defining $u = \begin{pmatrix} u_3 & u_4 & u_5 & u_6 & u_7 \end{pmatrix}^\top$, and the matrices

$$B_s = \begin{pmatrix} 1_{1\times 9} & 0_{1\times 3} & 0_{1\times 4} \\ 0_{2\times 9} & \begin{pmatrix} 1 & 0 & 0 \\ 0 & -1 & 1 \end{pmatrix} & 0_{2\times 4} \\ 0_{4\times 9} & 0_{4\times 3} & diag(-1,1,-1,1) \end{pmatrix},$$

$$C_s = \begin{pmatrix} -1_{1\times 9} & 0_{1\times 3} & 0_{1\times 4} \\ 0_{2\times 9} & \begin{pmatrix} -1 & 0 & 0 \\ 0 & 1 & -1 \end{pmatrix} & 0_{2\times 4} \\ 0_{4\times 9} & 0_{4\times 3} & diag(1,-1,1,-1) \end{pmatrix}^\top,$$

$$D_s = \begin{pmatrix} diag\begin{pmatrix} 1/g_1 \dots 1/g_9 \end{pmatrix} & 0_{9\times 7} \\ 0_{7\times 9} & 0_{7\times 7} \end{pmatrix},$$

$$E_s = \begin{pmatrix} 0_{3\times 3} & 0_{3\times 2} \\ \begin{pmatrix} 0 & I_M & 0 \end{pmatrix} & 0_{1\times 2} \\ 0_{3\times 3} & \begin{pmatrix} 0 & 0 \\ I_M & 0 \\ 0 & 0 \end{pmatrix} \end{pmatrix},$$

$$F_s = \begin{pmatrix} 0_{11\times 2} & 0_{11\times 3} \\ \begin{pmatrix} I_M & 0 \end{pmatrix} & 0_{1\times 3} \\ 0_{4\times 2} & \begin{pmatrix} 0 & 0 & 0 \\ I_M & 0 & 0 \\ 0 & 0 & 0 \\ 0 & 0 & I_M \end{pmatrix} \end{pmatrix},$$

$$hs = \begin{pmatrix} \begin{pmatrix} V_1 \dots V_9 \end{pmatrix} & 0_{1\times 7} \end{pmatrix}^\top.$$

4.3.2. Current source of the PV cell

A temperature dependent expression for the photo-generated current i_s can be obtained by considering the solar cell in Figure 4.20. To this aim let us consider the current-voltage diode characteristic

$$\varphi_1 = I_0(T)\left(e^{\frac{\sigma\lambda_1}{T}} - 1\right) \tag{4.24}$$

where T is the PV temperature, $I_0(T)$ is the temperature dependent diode saturation current, $\sigma = q/(nK)$ with q the electron charge, n the diode ideality factor and K the Boltzmann constant [Sera *et al.*, 2007]. The expression for I_0 can be obtained by substracting the diode current φ_1 in the circuit in Figure 4.20 under open-circuit ($i_{pv_c} = 0$, $v_{pv_c} = V_{oc}$) and short circuit ($i_{pv_c} = I_{sc}$, $v_{pv_c} = 0$) operating conditions, thus obtaining

$$\varphi_1|_{oc} - \varphi_1|_{sc} = I_0(T)\left(e^{\frac{\sigma V_{oc}(T)}{T}} - e^{\frac{\sigma R_{pv} I_{sc}(T)}{T}}\right) = -\frac{1}{R_{sh}} V_{oc}(T) + \frac{R_{pv} + R_{sh}}{R_{sh}} I_{sc}(T). \quad (4.25)$$

The temperature dependence of I_{sc} and V_{oc} can be approximated through the following functions

$$I_{sc}(T) = I^*_{sc}\left[1 + K_i(T - T^*)\right] \quad (4.26a)$$

$$V_{oc}(T) = V^*_{oc}\left[1 + K_v(T - T^*)\right], \quad (4.26b)$$

where I^*_{sc}, V^*_{oc}, T^* are the short circuit current, the open circuit voltage and the temperature in standard test conditions, respectively, and K_i and K_v are suitable temperature coefficients for the short circuit current and open circuit voltage variations, respectively [Villalva *et al.*, 2009]. Then, by computing $I_0(T)$ form (4.25) one can write

$$I_0(T) = \frac{(R_{pv} + R_{sh})I_{sc}(T) - V_{oc}(T)}{R_{sh}\left(e^{\frac{\sigma V_{oc}(T)}{T}} - e^{\frac{\sigma R_{pv} I_{sc}(T)}{T}}\right)}. \quad (4.27)$$

The photo-generated current i_s can be expressed in terms of the short circuit current and the open circuit voltage by considering the open circuit operating conditions. In particular, from Figure 4.20 with $i_{pv_c} = 0$ and by using (4.24) one obtains

$$i_s(T, S) = \left[I_0(T)\left(e^{\frac{\sigma V_{oc}(T)}{T}} - 1\right) + \frac{V_{oc}(T)}{R_{sh}}\right]\frac{S}{S^*} \quad (4.28)$$

where S^* is the irradiance in standard test conditions, the ration S/S^* takes into account the photo-generated current variations under not standard irradiance, the saturation current $I_0(T)$ is given by (4.27) and $I_{sc}(T)$ and $V_{oc}(T)$ are given by (4.26) [Sera *et al.*, 2007].

4.3.3. Modelling of a PV array

In this work, an PV cell with a single diode, described in Figure 4.20 is used, i.e. a PV array composed of a set of n_s series and n_p parallel connected PV cells. The relevant

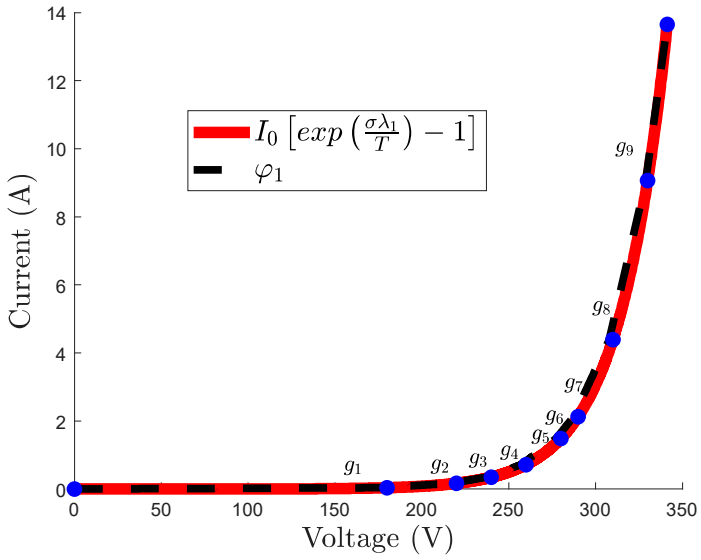

Figure 4.21: LC model approach of the PV cell exponential part.

parameters parameters are given in Table 4.3. Figure 4.21 shows a typical $V-I$ characteristic where the blue dots mark the pieces that can be approximated by straight line segments in order to obtained a LC model of the PV array. In this case, the diode characteristic has been approximated by nine linear segments which allows to obtain a very accurate approximation for small temperature variations, as it is shown in Figure 4.22 (a) and (b), where the simulation results of the curves $I-V$ and $P-V$ show the changes according to the variations of ambient temperature for a constant irradiance of 1000 W/m^2. It must be noticed that each temperature conditions requires a particular piece-wise approximation. However, the models can be obtained from a prescribed number of linear segments. It is important to say also, that a fewer number of segments is used without a significant lose of accuracy of the results. From Figure 4.22, it can be observed that voltage and power of the PV module decreases with increasing the cell temperature.

Note that the PV model depicted in Figure 4.20 allows for the full consideration of the PV losses through both R_{pv} and R_{sh}. Let us define $\rho = \frac{R_{sh}}{R_{sh}+R_{pv}}$ and, applying Kirchhoff laws the diode voltage λ_1 and the PV array current i_{pv} can be obtained as

$$\lambda_1 = \rho R_{pv} i_s - \rho R_{pv}\varphi_1 + \rho v_{pv}, \tag{4.29}$$

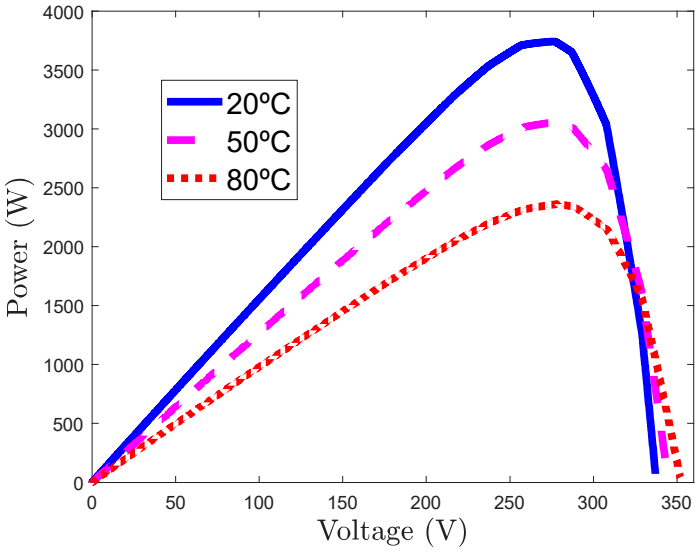

(a) V–I characteristic.

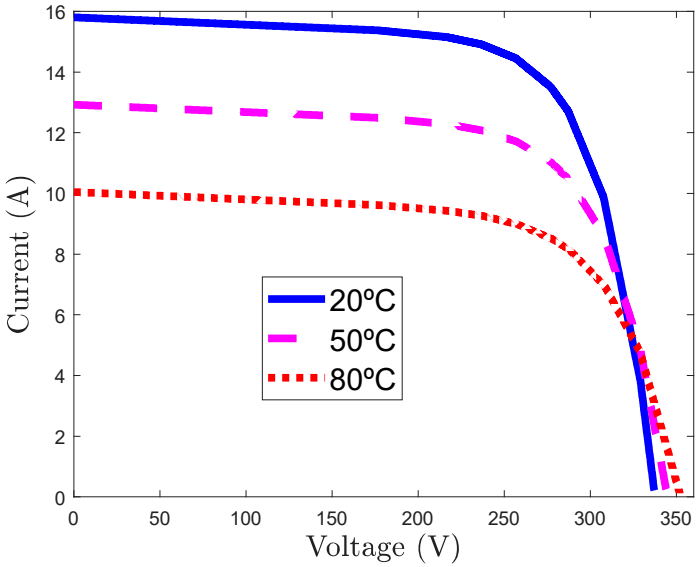

(b) V–P characteristic.

Figure 4.22: Linear complementarity approach of the PV array characteristics: (a) voltage-current characteristic, and (b) voltage-power characteristic.

Table 4.3: Photovoltaic array parameters.

Parameter	Value	Parameter	Value
n_s	600	n_p	2
I^*_{sc}	5.27 A	V^*_{oc}	310 V
K_i	0.0032	K_v	0.123
T	308 K	T^*	293 K
S	1000 W/m^2	S^*	1000 W/m^2
R_{sh}	500 Ω	R_{pv}	0.221 Ω
σ	1.3		

$$i_{pv} = \rho(n_p i_s - n_p \varphi_1) - \frac{\rho}{R_{sh}} v_{pv}. \tag{4.30}$$

Then the LC model (2.16) for the PV array can be completed considering that the corresponding matrices are defined as: $A_c = 0$, $B_c = 0$, $E_c = 0$, $C_c = \rho$, $D_c = -\rho R_{pv}$, $F_c = \rho R_{pv}$, with the state $x = \begin{pmatrix} v_{pv} \end{pmatrix}$ and the exogenous input $e = \begin{pmatrix} i_s \end{pmatrix}$. While the complementarity subsystem (2.1) matrices are defined as

$$\begin{aligned} B_s &= \begin{pmatrix} 1_{1\times 9} \end{pmatrix}, \\ D_s &= \begin{pmatrix} diag \begin{pmatrix} 1/g_1 \dots 1/g_9 \end{pmatrix} \end{pmatrix}, \\ hs &= \begin{pmatrix} V_1 \dots V_9 \end{pmatrix}^\top, \end{aligned}$$

and $C_s = -B_s^\top$.

4.3.4. P&O MPPT Algorithm

The efficient operation of any PV array requires implementing a suitable control strategy to force the panel to work in an operating point that would ensure that the maximum power is extracted from the solar irradiance. Accordingly, it is necessary to compute the panel voltage at the point of maximum power transfer V_{MPPT} and the corresponding panel current I_{MPPT}, according to the measured voltage v_{pv} and current i_{pv}. Many techniques have been developed to determine the maximum power that a PV array can deliver, being

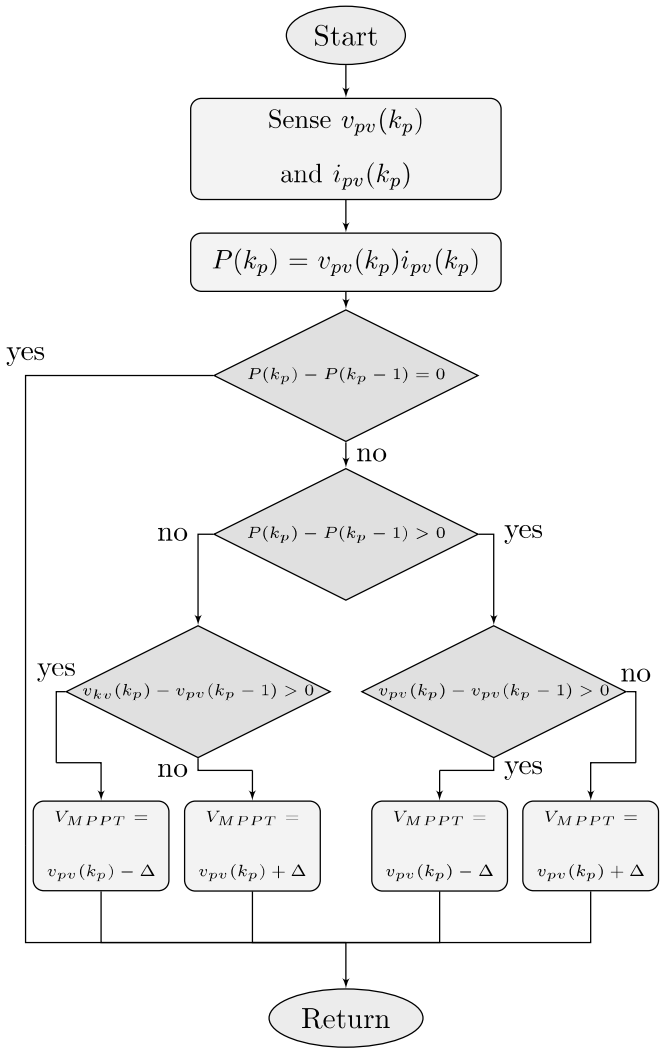

Figure 4.23: P&O Algorithm for direct search of V_{MPPT}, where Δ is the incremental/decremental step and k_p is the sampling step.

the perturb and observe (P&O) algorithm [Esram and Chapman, 2007] one of them. The basic P&O MPPT algorithm consists in the calculation of the PV array power $P = i_{pv}v_{pv}$ at each sample time, which in this case can be considered as the PWM period P_s. Then, by comparing the calculated power against a previous one, the algorithm moves the V_{MPPT} reference an incremental/decremental step Δ in direction of the maximum power point. An adequate value for Δ is selected considering that high values produce steady-state oscillations and for small values, the convergence to steady-state is slower. In Figure 4.23 a flowchart of this algorithm is shown.

4.3.5. The PI controller

As it has been shown before, an efficient *P&O* algorithm is essential to operate the panel at its maximum power transfer point; however, an additional and dedicated PI controller is required to indicate to the FCS-MPC controller the amplitude of the current to be injected into the utility grid to achieve such maximum power injection, by means of regulating the DC-link voltage v_c. In Figure 4.24, the PI controller is in an outer loop, which in combination with the phase-locked loop (PLL), provides the current reference $i_{g_{ref}}$ in-phase with the voltage utility grid, this is

$$i_{g_{ref}} = A_p \sin(wt) \tag{4.32}$$

where the amplitude A_p is defined by means of the PI as

$$A_p = \mathcal{K}_p(v_c - v_{c_{ref}}) + \mathcal{K}_i \sum (v_c - v_{c_{ref}}) \tag{4.33}$$

where the reference value $v_{c_{ref}}$ is assumed o be 1.5 times the nominal peak voltage expected at the grids common coupling point and $\mathcal{K}_p$ and $\mathcal{K}_i$ are the controller parameters, which are selected by simulation tests to achieve a short transient response and a zero steady-state error. Simulation experiments carried out during the development of this work have shown that appropriate values are those presented in Table 4.4. The integration process can be executed at discrete times, e.g. at every period of the carrier signal, as done in this work, nonetheless other time periods are possible.

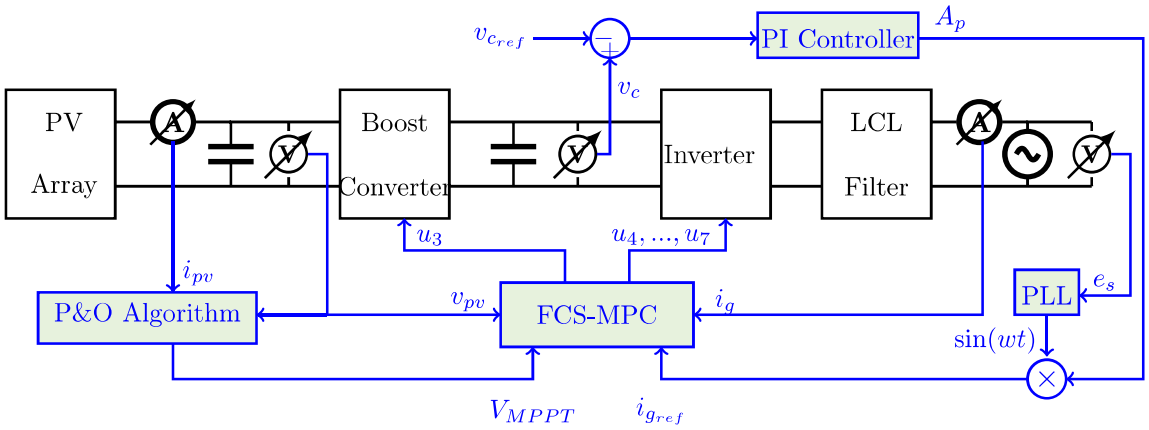

Figure 4.24: Schematic representation of a two-stage, grid-connected PV generator and control system. Blue lines represent control signals.

4.3.5.1. The Finite Set control-Model Predictive Control Scheme

The FCS-MPC is design to ensure that the PV array sticks to the operating point of maximum power transfer by pushing the $v_{pv}(t)$ voltage and $i_g(t)$ current to their respective references V_{MPPT} and $i_{g_{ref}}$. The discrete LCS (2.18) is obtained by considering the system parameters of the Table 4.4. Where the sampling period α directly influences on the electrical wave-forms ripples, that is, a higher switching frequency reduces the ripple and at same time the required components of the circuits can be selected of small values, by the contrary, a lower frequency requires high components values to reduce the produced ripples.

The MPC based on the formulation (3.11) is proposed for the operation of the grid-connected single-phase inverter. The control strategy assumes independent signals for each ideal switch, but it is necessary to consider the additional constraints

$$u_4 + u_7 \leq 1 \quad and \quad u_5 + u_6 \leq 1 \tag{4.34}$$

for the control inputs. These constraints avoid a possible short-circuit in the DC-link. The main purpose of the scheme in Figure 4.19 is to pull out the maximum power to the PV source and supply the available power to the grid as active power. Note the salient multi-tasking feature of MPC schemes. Indeed, multiple constraints and objectives can be included

Table 4.4: Single phase boost grid-connected PV generator.

Parameter	value	Parameter	value
C_p	4.7 mF	R_s	1 mΩ
L	5.2 mH	C	4.7 mF
R_f	10 mΩ	L_f	12 mH
R_c	0.4 Ω	C_f	180 µF
R_g	50 mΩ	L_g	0.12 mH
α	$10\mu s$	P_s	$100\mu s$
e_s	110 $\sin(2\pi 50t)$ V	$\mathcal{K}_p$	0.5
$\mathcal{K}_i$	0.0015	Δ	1

in the cost function (3.11) for instance to transfer the maximum power form the PV array and keep the dc-link voltage balanced. As presented in Figure 4.24, the MPC is set to regulate the voltage v_{pv} to the reference V_{MPPT} provided by the P&O algorithm and to track of sinusoidal current reference $i_{g_{ref}}$ which amplitude is provided by the PI controller. Figure 4.25 shows the time evolution of the main state variables in the PV array, i.e. the current $i_{pv}(t)$ and the voltage $v_{pv}(t)$. At time $t = 0$ the initial conditions of the PV array do not correspond to the MPPT and a transient behavior is observed until the reference provided by the P&O algorithm reaches the V_{MPPT} value. To proof that the P&O algorithm tracks the changes in irradiation, the simulation set up considers that at time $t = 0.8$ the solar irradiance increases from $S = 1000$ W/m^2 to $S = 1600$ W/m^2, which changes the MPPT. Also, a reduction of the solar irradiance $S = 800$ W/m^2 is consider to happen at time $t = 1.6$. Figure 4.26 also shows a zoom of the current i_{pv} where the characteristic curve V–I of the PV cell is observed, it revels the piece-wise linear approximation of the LC model of the PV array. Figure 4.26 shows the time evolution of the main state variables in the boost converter, i.e. the current $i_L(t)$ and the voltage $v_c(t)$. where the indirect regulation to the voltage reference $v_{c_{ref}} = 300$ V is achieved. Additionally, a zoom of each state variable is presented, where a ripple is exhibit, in the case of $i_L(t)$ is the characteristic switching ripple and, in $v_c(t)$ a sinusoidal ripple generated by the current $i_g(t)$. In the Figure 4.27, the

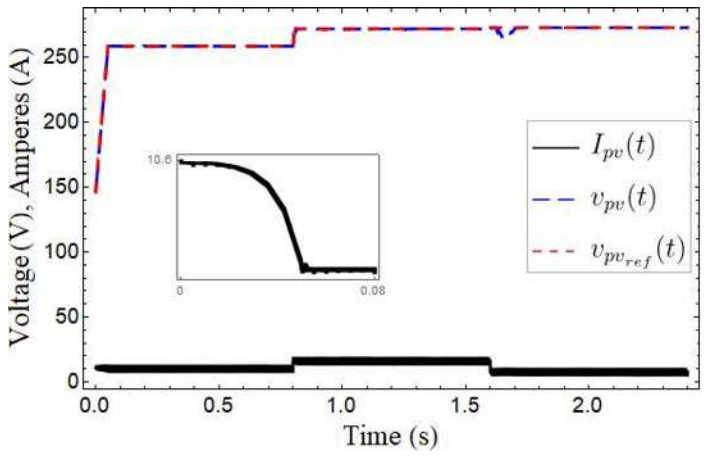

Figure 4.25: Convergence of the voltage $v_{pv}(t)$ to the reference V_{MPPT}, provided by the P&O MPPT algorithm.

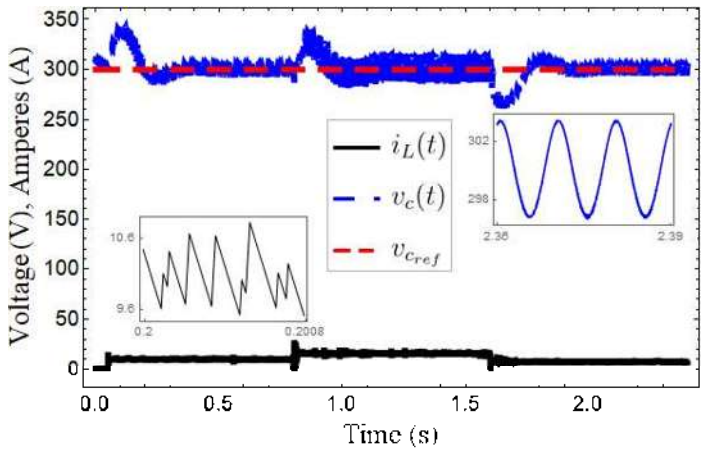

Figure 4.26: Regulated voltage $v_c(t)$ across the DC link capacitor C.

current tracking control of i_g is shown, it varies according to the irradiation and available power at the PV array. Additionally, a close view of the trajectory tracking is presented, where the MPC tracking capabilities make difficult to distinguish $i_{g_{ref}}(t)$ and $i_g(t)$. Figure

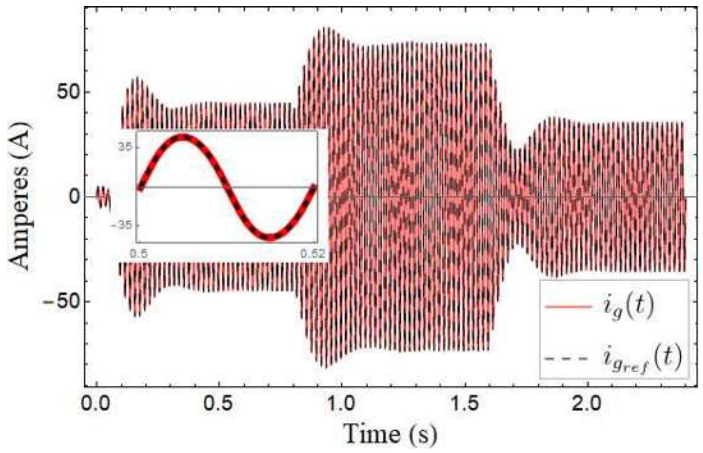

Figure 4.27: Current $i_g(t)$ delivered to the residential microgrid and it dynamical evolution as irradiation changes at $t_1 = 0.8s$ and $t_2 = 1.6$. Inserted window shows that the FCS-MPC perfectly trackes $i_g(t)$ references provided by the PI controller

4.28 shows the behavior of the supplied current to the utility together with scaled version of the utility voltage within a time window. The wave-forms are in-phase, meaning that in this case only active power is provided to the system, i.e., a unitary power factor. However, the PV generator may be required to deliver reactive power and thus providing ancillary services to the system. The later can be achieved by time-shifting the current $i_g(t)$ accordingly. It must be said that in this case the prediction horizon was set to be equal to one period of the carrier signal but the experiments with larger prediction horizons were simulated, e.g., 2 and 3 periods of the carrier signal.The main effects of this variations were visualized as changes in the amplitude of the ripple of current $i_g(t)$. Also, it must be considered that the computational effort increases exponentially with the length of the prediction horizon. In the Figure 4.29 the active power supplied to the grid is shown, which varies according to the irradiation and available power at the PV array. It is not shown here but the power factor at the point of common coupling was unitary during the whole experiment.

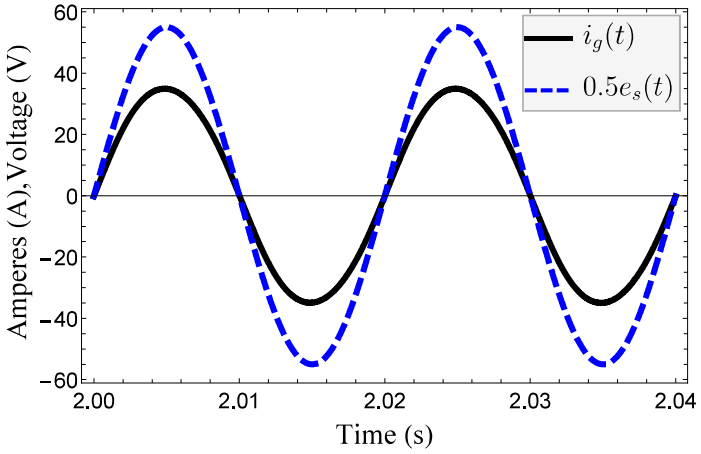

Figure 4.28: PV-generator and microgrid synchronization through the FCS-MPC demonstrated by the in-phase time response of the delivered $i_g(t)$ current and the point of coupling utility system voltage e_s (here scaled for comparison purposes).

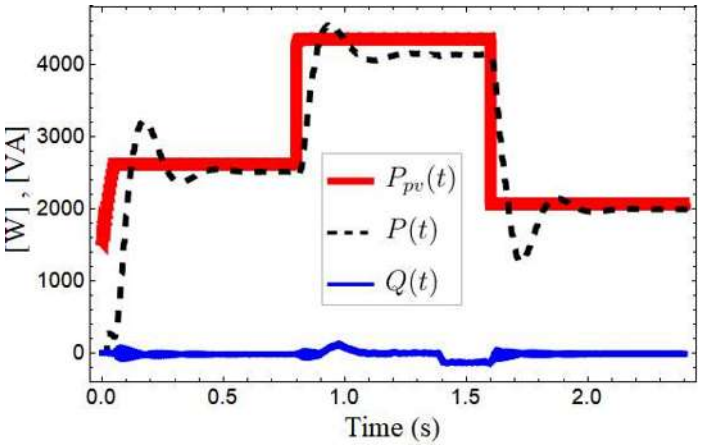

Figure 4.29: Active power supplied by the PV array at the maximum point of power transfer(MPPT) in red line, and active power delivered to the microgrid in dashed black line. The differences in input and output power correspond to the power losses caused by resistive components of the PV generator

4.4. Chapter conclusion

In this chapter, the described methodology in the previous chapters is applied to practical cases of power converters. Through the addressed cases, the FCS-MPC shows its effectiveness for control tasks, as regulation and trajectory tracking for power converters. The additional methodologies presented for implementation purposes, guarantees the success of the controllers at real environments.

Chapter 5

Conclusions

5.1. General conclusions

The guideline for modeling and control design of power converters in the complementarity framework, presented in this thesis has proven to be a very suitable method for switched systems. In chapter 3, open loop simulations and the comparisons with SystemModeler demonstrated that the LC framework can model all the operation modes of the power converters in compact linear models. The MPC scheme based in the LC system as the same as other hybrid systems allows to control power converters without PWM signals, but it is described in chapter 4, the PWM signal present advantages for the controller performance as a lower control effort and a smoother ripple, due to this, in general, it is preferable to include a PWM signal in the control design. One of the main drawbacks of the model-based control design as the MPC is the parameter variations, such can affect the control performance, this can be attended by the including strategies to given robustness to the controller in the control design as it is proved in the implementations of chapter 4. Finally, in the grid-connected photovoltaic array presented in chapter 4, the LC model proves that can be a suitable framework for the analysis of power converters circuits, capable of incorporating additional techniques for the control as P & O algorithms and PI controllers. For the above, this thesis presents the complementarity framework as the better choice for analysis circuits that involved power converters.

5.2. Future work

The model predictive control, based on the linear complementarity system, is a framework recently proposed to analysis, study and control of power converters. In this thesis, a guideline for modeling and control of power converters is presented. However, the complementarity framework is an area of research with too many opportunities, in the following points, some possible future works from this thesis are mentioned.

- The development of a software for efficiently modeling power converters in the complementarity framework. Since this procedure do not required numbering the operation modes or given a time sequence. Therefore, a general method to model any power converter topology can be programmed in a software platform.

- Exploring the advantages and benefits of modeling power converters directly as another hybrid system class, as MLD, PWA, hybrid automata, among others. This thesis focused on modeling power converters in an LCS format and their transformation to MLD and PWA systems. However, exploiting these frameworks directly can be present other advantages for specific power converters topologies.

- Study and analysis of general techniques for reducing the compute time and, to endowed of robustness the FCS-MPC, in order to be implemented in real time environments. In this thesis, some techniques are addressed with these purposes (Parametric analysis, integral gains, and RLS algorithm), for the presented study cases. However, a general procedure to implement an FCS-MPC in a real-time environment is not proposed.

- Expand the study cases to three-phase power converter systems. In this thesis are presented in different power converter systems, but all power converters addressed are single-phase systems.

- In this thesis is considered as a study case the PV energy generation in residential microgrids, A next step could expand the use of FCS-MPC designs method to another microgrid configurations, i.e. including wind generation systems, battery charge system, among others possible stages in a microgrid.

5.3. Publications list

R. Morfín-Magaña, J. Rico-Melgoza and F. Ornelas-Tellez, Control predictivo para sistemas lineales complementarios: Aplicación a convertidores de potencia", Memorias del Congreso Nacional de Control Automático 2016, Querétaro, México, Septiembre 28-30, 2016.

R. Morfín-Magaña, J. Rico-Melgoza and F. Ornelas-Tellez, "Modeling of Switched Systems in the Complementarity Framework and PWM Controller Design as a Mixed Integer Quadratic Problem", 3rd. Electric Vehicles International Symposium (EVIS), 2018.

R. Morfín-Magaña, R. Rodriguez-Flores, S. Ramos-Paz, J. Rico-Melgoza and F. Ornelas-Tellez, "Model Predictive Control for Linear Parameter-Varying Systems", 2018 IEEE International Autumn Meeting on Power, Electronics and Computing (ROPEC 2018). Ixtapa, México.

F. Ornelas-Tellez, J. Rico-Melgoza, S. Ramos-Paz and R. Morfín-Magaña, "Método para la Estimación y Supresión Dinámica y Óptima de Armónicos para Aplicaciones Industriales", Solucitud de patente, Instituto Mexicano de la Propiedad Industrial (IMPI), 2019.

F. Ornelas-Tellez, J. Rico-Melgoza, R. Morfín-Magaña and S. Ramos-Paz, "Dynamic Harmonic Extraction and Suppression in Industrial Applications", IEEE Transactions on Industrial Electronics, 2019. (under review)

R. Morfín-Magaña, J. Rico-Melgoza, F. Ornelas-Tellez and F. Vasca, Complementarity Model of a Photovoltaic Power Electronic System with Model Predictive Control", IEEE Transactions on Circuits and Systems I, 2019. (under review)

References

[Abdeldjebar and Khier, 2008] Abdeldjebar B., Khier B. "Generalized predictive control: Application of the Induction Motor." In "2008 International Conference on Smart Manufacturing Application," pages 526–529. 2008.

[Acary *et al.*, 2011] Acary V., Bonnefon O., Brogliato B. *Nonsmooth Modeling and Simulation for Switched Circuits.* London, U.K.: Springer-Verlag, 2011.

[Addi and Goeleven, 2017] Addi K., Goeleven D. *Complementarity and Variational Inequalities in Electronics.* Springer International Publishing, 2017.

[Ahmed *et al.*, 2018] Ahmed A.A., Koh B.K., Lee Y.I. "A Comparison of Finite Control Set and Continuous Control Set Model Predictive Control Schemes for Speed Control of Induction Motors." *IEEE Transactions on Industrial Informatics*, volume. 14(4):pages 1334–1346, 2018.

[Almer and Morari, 2013] Almer S., Morari M. "Efficient online solution of multi-parametric mixed-integer quadratic problems." *International Journal of Control*, volume. 86(8):pages 1386–1396, 2013.

[Astrom and Wittenmark, 1994] Astrom A., Wittenmark B. *Adaptive Control.* Addison-Wesley series, 2nd edition, 1994.

[Batlle *et al.*, 2005] Batlle C., Fossas E., Merillas I., Miralles A. "Generalized Discontinuous Conduction Modes in the Complementarity Formalism." *IEEE Trans. Circuits Syst. II, Exp. Briefs*, volume. 52(8):pages 447–451, 2005.

[Bemporad and Morari, 1999] Bemporad A., Morari M. "Control of systems integrating logic, dynamics, and constraints." *Automatica*, volume. 35(3):pages 407 – 427, 1999.

[Bordons and Montero, 2015] Bordons C., Montero C. "Basic Principles of MPC for Power Converters: Bridging the Gap Between Theory and Practice." *IEEE Industrial Electronics Magazine*, volume. 9(3):pages 31–43, 2015.

[Borrelli *et al.*, 2014] Borrelli F., A. B., Morari M. *Predictive Control for linear and hybrid systems.* Cambridge University Press, first edition, 2014.

[Branicky, 1998] Branicky M.S. "Multiple Lyapunov functions and other analysis tools for switched and hybrid systems." *IEEE Transactions on Automatic Control*, volume. 43(4):pages 475–482, 1998.

[Burdio and Martinez, 1995] Burdio J.M., Martinez A. "A unified discrete-time state-space model for switching converters." *IEEE Transactions on Power Electronics*, volume. 10(6):pages 694–707, 1995.

[Camlibel, 2001] Camlibel M.K. *Complementarity Methods in the Analysis of Piecewise Linear Dynamical Systems.*

Doctoral thesis, Tilburg University, School of Economics and Management, 2001.

[Camlibel *et al.*, 2003] Camlibel M.K., Heemels W.P.M.H., van der Schaft A.J., Schumacher J.M. "Switched networks and complementarity." *IEEE Transactions on Circuits and Systems I: Fundamental Theory and Applications*, volume. 50(8):pages 1036–1046, 2003.

[Cavalcanti, 2001] Cavalcanti G. *Design And Analysis Of Multivariable Predictive Control Applied To An Oil-Water-Gas Separator: A Polynomial Approach.* Doctoral thesis, 2001.

[Cheng *et al.*, 2018] Cheng L., Acuna P., Aguilera R.P., Jiang J., Wei S., Fletcher J.E., Lu D.D.C. "Model Predictive Control for DCDC Boost Converters With Reduced-Prediction Horizon and Constant Switching Frequency." *IEEE Transactions on Power Electronics*, volume. 33(10):pages 9064–9075, 2018.

[Clarke *et al.*, 1987] Clarke D., Mohtadi C., Tuffs P. "Generalized predictive controlPart I. The basic algorithm." *Automatica*, volume. 23(2):pages 137 – 148, 1987.

[Cortes *et al.*, 2008] Cortes P., Kazmierkowski M.P., Kennel R.M., Quevedo D.E., Rodriguez J. "Predictive Control in Power Electronics and Drives." *IEEE Transactions on Industrial Electronics*, volume. 55(12):pages 4312–4324, 2008.

[Cortes *et al.*, 2009] Cortes P., Ortiz G., Yuz J.I., Rodriguez J., Vazquez S., Franquelo L.G. "Model Predictive Control of an Inverter With Output *LC* Filter for UPS Applications." *IEEE Transactions on Industrial Electronics*, volume. 56(6):pages 1875–1883, 2009.

[Cottle *et al.*, 1992a] Cottle R., Pang J., Stone R. *The Linear Complementarity Problem.* Press Academic, first edition edition, 1992a.

[Cottle *et al.*, January 1993b] Cottle R., Pang J., Stone R. "The Linear Complementarity Problem." *Bulletin (New Series) of The American Mathematical Society: Book Review*, volume. 28(1), January 1993b.

[Difronzo *et al.*, 2017] Difronzo M., Milton M., Davidson M., Benigni A. "Hardware-in-the-loop testing of high switching frequency power electronics converters." In "2017 IEEE Electric Ship Technologies Symposium (ESTS)," pages 299–304. 2017.

[Dirkse and Ferris, 1995] Dirkse S.P., Ferris M.C. "The path solver: A nonmonotone stabilization scheme for mixed complementarity problems." *Optimization Methods and Software*, volume. 5(2):pages 123–156, 1995.

[Escobar *et al.*, 1997] Escobar G., Ortega R., Sira-Ramirez H., Vilian J., Zein I. "An experimental comparison of several non- linear controllers for power converters." (1):pages 66–82, 1997.

[Esram and Chapman, 2007] Esram T., Chapman P.L. "Comparison of Photovoltaic Array Maximum Power Point Tracking

Techniques." *IEEE Transactions on Energy Conversion*, volume. 22(2):pages 439–449, 2007.

[Faruque and Dinavahi, 2010] Faruque M.O.O., Dinavahi V. "Hardware-in-the-Loop Simulation of Power Electronic Systems Using Adaptive Discretization." *IEEE Transactions on Industrial Electronics*, volume. 57(4):pages 1146–1158, 2010.

[Fernndez-lvarez *et al.*, 2017] Fernndez-lvarez A., Portela-Garca M., Garca-Valderas M., Lpez J., Sanz M. "HW/SW Co-Simulation System for Enhancing Hardware-in-the-Loop of Power Converter Digital Controllers." *IEEE Journal of Emerging and Selected Topics in Power Electronics*, volume. 5(4):pages 1779–1786, 2017.

[Frasca *et al.*, 2010] Frasca R., Camlibel M.K., Goknar I.C., Iannelli L., Vasca F. "Linear Passive Networks with Ideal Switches: Consistent Initial Conditions and State Discontinuities." *IEEE Transactions on Circuits and Systems*, volume. 57(12):pages 3138–3151, 2010.

[Fujita, 2011] Fujita S. "A Branch-and-Bound Algorithm for Solving the Multiprocessor Scheduling Problem with Improved Lower Bounding Techniques." *IEEE Transactions on Computers*, volume. 60(7):pages 1006–1016, 2011.

[Garcia and Morshedi, 1986] Garcia C.E., Morshedi A. "Quadratic Programming Solution of Dynamic Matrix Control

(QDMC)." *Chemical Engineering Communications*, volume. 46(1-3):pages 73–87, 1986.

[Geyer *et al.*, 2015] Geyer T., Darivianakis G., van der Merwe W. "Model predictive control of a STATCOM based on a modular multilevel converter in delta configuration." In "2015 17th European Conference on Power Electronics and Applications (EPE'15 ECCE-Europe)," pages 1–10. 2015.

[Grgoire *et al.*, 2011] Grgoire L., Al-Haddad K., Nanjundaiah G. "Hardware-in-the-Loop (HIL) to reduce the development cost of power electronic converters." In "India International Conference on Power Electronics 2010 (IICPE2010)," pages 1–6. 2011.

[Gurobi Optimization, 2018] Gurobi Optimization L. "Gurobi Optimizer Reference Manual." 2018.

[Hai-Peng *et al.*, 2015] Hai-Peng R., Miao-Miao Z., Jie L. "A simplified mixed logical dynamic model and model predictive control of boost converter with current reference compensator." *2015 IEEE 24th International Symposium on Industrial Electronics (ISIE)*, pages 61–65, 2015.

[Han *et al.*, 2009] Han L., Tiwari A., Camlibel K., Pang J. "Convergence of Time-Stepping Schemes for Passive and Extended Linear Complementarity Systems." *SIAM Journal on Numerical Analysis*, volume. 47(5):pages 3768–3796, 2009.

[Heemels and Schutter, 2000] Heemels W., Schutter B. "On the equivalence of classes of hybrid systems: Mixed logical dynami-

cal and complementary systems." technique report 04, Delft University of Technology, 2000.

[Heemels *et al.*, 1999] Heemels W., Schumacher J., Weiland S. "The rational complementarity problem." *Linear Algebra and its Applications*, volume. 294(1):pages 93 – 135, 1999.

[Heemels *et al.*, 2001] Heemels W., Schutter B.D., Bemporad A. "Equivalence of hybrid dynamical models." *Automatica*, volume. 37(7):pages 1085–1091, 2001.

[Hejri and Giua, 2011] Hejri M., Giua A. "Hybrid modeling and control of switching DC-DC converters via MLD systems." In "IEEE International Conference on Automation Science and Engineering," Trieste, Italy, 2011.

[Herceg *et al.*, 2013] Herceg M., Kvasnica M., Jones C., Morari M. "Multi-Parametric Toolbox 3.0." In "Proc. of the European Control Conference," pages 502–510. Zürich, Switzerland, 2013. `http://control.ee.ethz.ch/ mpt`.

[Hyatt *et al.*, 2008] Hyatt W., Kemmerly J., Durbin S. *Análisis de Circuitos en Ingeniería.* Mcgraw-hill, seventh edition, 2008.

[Iannelli *et al.*, 2011] Iannelli L., Vasca F., Angelone G. "Computation of Steady–state oscillations in power converters through complementarity." *IEEE Trans. Circuits Syst. I, Reg. Papers*, volume. 58(6):pages 1421–1432, 2011.

[James and Kenneth, 1993] James R., Kenneth M. "The Stability of Constrained Receding Horizon Control." *IEEE Transactions on Automatic Control*, volume. 30(10):pages 1512–1516, 1993.

[Kouro *et al.*, 2009a] Kouro S., Cortes P., Vargas R., Ammann U., Rodriguez J. "Model Predictive ControlA Simple and Powerful Method to Control Power Converters." *IEEE Transactions on Industrial Electronics*, volume. 56(6):pages 1826–1838, 2009a.

[Kouro *et al.*, 2009b] Kouro S., Cortes P., Vargas R., Ammann U., Rodriguez J. "Model Predictive ControlA Simple and Powerful Method to Control Power Converters." *IEEE Transactions on Industrial Electronics*, volume. 56(6):pages 1826–1838, 2009b.

[Lagarias *et al.*, 1998] Lagarias J., Reeds J., Wright M., Wright P. "Convergence properties of the Nelder-Mead simplex method in low dimensions." *SIAM J. Optim.*, volume. 9(1):pages 112–147, 1998.

[Lee, 2011] Lee J.H. "Model predictive control: Review of the three decades of development." *International Journal of Control, Automation and Systems*, volume. 9(3):page 415, 2011.

[Li *et al.*, 2014] Li N., Li Y.H., Zhu X.H., Hei H.L. "The FCS-MPC research for a new inverter." *International Journal of Electronics Letters*, volume. 4(1):pages 93–107, 2014.

[Linder *et al.*, 2010] Linder A., Kanchan R., Kennel R., Stolze P.

Model-Based Predictive Control of Electric Drives. Germany: Cuvillier Verlag Gttingen, 2010.

[Lopez-Castillo and Rico-Melgoza, 2014] Lopez-Castillo F., Rico-Melgoza J.J. "Modeling and analysis of switched networks as mixed linear complementarity systems." In "IEEE Int. Autumn Meeting on Power, Electronics and Computing," pages 1–6. Xtapa, Mexico, 2014.

[Maier, 1970] Maier G. "A matrix structural theory of piecewise linear elasto-plasticity with interacting yield planes." *Meccanica*, volume. 5:pages 54–66, 1970.

[Maksimovic *et al.*, 2001] Maksimovic D., Stankovic A.M., Thottuvelil V.J., Verghese G.C. "Modeling and simulation of power electronic converters." *Proceedings of the IEEE*, volume. 89(6):pages 898–912, 2001.

[Mariéthoz and Morari, 2009] Mariéthoz S., Morari M. "Explicit Model-Predictive Control of a PWM Inverter With an LCL Filter." volume. 56(2):pages 389–399, 2009.

[Middlebrook and Cuk, 1976] Middlebrook R.D., Cuk S. "A general unified approach to modelling switching-converter power stages." In "1976 IEEE Power Electronics Specialists Conference," pages 18–34. 1976.

[Mirzaei and Afzalian, 2009] Mirzaei M., Afzalian A.A. "Hybrid modelling and control of a synchronous DC-DC converter." volume. 1(4):pages 414–433, 2009.

[Mohamed *et al.*, 2016] Mohamed H.A., Khattab H.A., Mobarka A., Morsy G.A. "Design, control and performance analysis of DC-DC boost converter for stand-alone

PV system." In "2016 Eighteenth International Middle East Power Systems Conference (MEPCON)," pages 101–106. 2016.

[Morari and Lee, 1999] Morari M., Lee J.H. "Model predictive control: past, present and future." *Computers and Chemical Engineering*, volume. 23(4):pages 667 – 682, 1999.

[Ornelas-Tellez *et al.*, 2012] Ornelas-Tellez F., Rico J.J., Zuniga G.C., Casarrubias G. "Inverse Optimal Trajectory Tracking for Discrete-Time Nonlinear Systems: Application to the Boost Converter." *IEEE ROPEC INTERNACIONAL, Morelia, Mexico*, 2012.

[Pang *et al.*, 1979] Pang J.S., Kaneko I., Hallamn W. "On the solution of some (parametric) linear complementarity problems with applications to portafolio selection, structural engineering and actuarial graduation." *Mathematical Programming*, volume. 16:pages 325–347, 1979.

[Quinn, 1990] Quinn M.J. "Analysis and implementation of branch-and-bound algorithms on a hypercube multicomputer." *IEEE Transactions on Computers*, volume. 39(3):pages 384–387, 1990.

[Rashid, 2007] Rashid M.H., editor. *Power Electronics Handbook*. Engineering. Academic Press, Burlington, second edition edition, 2007.

[Richalet *et al.*, 1978] Richalet J., Rault A., Testud J., Papon J. "Model predictive heuristic control: Applications to indus-

trial processes." *Automatica*, volume. 14(5):pages 413 – 428, 1978.

[Rico-Melgoza *et al.*, 2009] Rico-Melgoza J.J., Suarez J.P., Cardiel E.B., Martinez M.M. "Modeling and Analysis of Three-phase Diode Bridge Rectifiers as Linear Complementarity Systems." *Electric Power Components and Systems*, volume. 47(15):pages 1639–1655, 2009.

[Riyanto and Hakim, 2005] Riyanto B., Hakim I. "Model Predictive Control for Linear Complementarity and Extended Linear Complementarity Systems." *ITB Journal of Engineering Science*, volume. 37(2):pages 121–140, 2005.

[Rodriguez and Cortes, 2012] Rodriguez J., Cortes P. *Predictive Control of Power Converters and Electrical Drives*. New Jersey: Wiley, 2012.

[Rodriguez *et al.*, 2013] Rodriguez J., Kazmierkowski M.P., Espinoza J.R., Zanchetta P., Abu-Rub H., Young H.A., Rojas C.A. "State of the Art of Finite Control Set Model Predictive Control in Power Electronics." *IEEE Transactions on Industrial Informatics*, volume. 9(2):pages 1003–1016, 2013.

[Sanchez *et al.*, 2012] Sanchez A., de Castro A., Garrido J. "A Comparison of Simulation and Hardware-in-the- Loop Alternatives for Digital Control of Power Converters." *IEEE Transactions on Industrial Informatics*, volume. 8(3):pages 491–500, 2012.

[Sera *et al.*, 2007] Sera D., Teodorescu R., Rodriguez P. "PV panel model based on datasheet values." In "2007 IEEE International Symposium on Industrial Electronics," pages 2392–2396. 2007.

[Sessa *et al.*, 2014] Sessa V., Iannelli L., Vasca F. "A complementarity model for closed-loop power converters." *IEEE Trans. Power Electron.*, volume. 29(12):pages 6821–6835, 2014.

[Sessa *et al.*, 2016] Sessa V., Monteiro L.F.C., Dias D.M. "A single-phase active filter with cascaded multilevel inverter modelled as a complementarity problem." In "42nd Annual Conf. IEEE Industrial Electronics Soc.", pages 1075–1080. Florence, Italy, 2016.

[Shi *et al.*, 2013] Shi X., Wang Z., Ma Y., Hang L., Tolbert L.M., Wang F. "Modeling and control of an LCL filter based three-phase active rectifier in grid emulator." In "2013 Twenty-Eighth Annual IEEE Applied Power Electronics Conference and Exposition (APEC)," pages 992–998. 2013.

[Sriram *et al.*, 2003] Sriram V.B., SenGupta S., Patra A. "Indirect current control of a single-phase voltage-sourced boost-type bridge converter operated in the rectifier mode." *IEEE Transactions on Power Electronics*, volume. 18(5):pages 1130–1137, 2003.

[Sun and Grotstollen, 1992] Sun J., Grotstollen H. "Averaged modelling of switching power converters: reformulation and theoretical basis." In "PESC '92 Record. 23rd

Annual IEEE Power Electronics Specialists Conference," pages 1165–1172 vol.2. 1992.

[Tajjudin *et al.*, 2011] Tajjudin M., Ishak N., Ismail H., Rahiman M.H.F., Adnan R. "Optimized PID control using Nelder-Mead method for electro-hydraulic actuator systems." In "2011 IEEE Control and System Graduate Research Colloquium," pages 90–93. 2011.

[Tant *et al.*, 2012] Tant J., Driesen J., Michiels W. "Event-driven simulation of power electronics in the complementarity systems framework." In "13th IEEE Workshop on Control and Modeling for Power Electronics," pages 1–7. Kyoto, Japan, 2012.

[van der Schaft, 1999] van der Schaft A. *An Introduction to Hybrid Dynamical Systems*. Doctoral thesis, Faculty of Mathematical Sciences: University of Twente, 1999.

[van der Schaft and Schumacher, 1998] van der Schaft A.J., Schumacher J.M. "Complementarity modeling of hybrid systems." *IEEE Transactions on Automatic Control*, volume. 43(4):pages 483–490, 1998.

[Vandenberghe *et al.*, 1989] Vandenberghe L., de Moor B.L., Vandewalle J. "The generalized linear complementarity problem applied to the complete analysis of resistive piecewise-linear circuits." *IEEE Transactions on Circuits and Systems*, volume. 36(11):pages 1382–1391, 1989.

[Vasca and Iannelli, 2012] Vasca F., Iannelli L. *Dynamics and control of*

switched electronic systems. London: Springer-Verlag, 2012.

[Vasca *et al.*, 2009] Vasca F., Iannelli L., Camlibel M.K., Frasca R. "A New Perspective for Modeling Power Electronics Converters: Complementarity Framework." *IEEE Transactions on Power Electronics*, volume. 24(2):pages 456–468, 2009.

[Vazquez *et al.*, 2014] Vazquez S., Leon J.I., Franquelo L.G., Rodriguez J., Young H.A., Marquez A., Zanchetta P. "Model Predictive Control: A Review of Its Applications in Power Electronics." *IEEE Industrial Electronics Magazine*, volume. 8(1):pages 16–31, 2014.

[Villa-Villaseor and Rico-Melgoza, 2018] Villa-Villaseor N., Rico-Melgoza J.J. "Complementarity framework formulation from bond graphs to model a class of nonlinear systems and hybrid systems with fixed causality." *SIMULATION*, volume. 94(9):pages 783–795, 2018.

[Villalva *et al.*, 2009] Villalva M.G., Gazoli J.R., Filho E.R. "Comprehensive Approach to Modeling and Simulation of Photovoltaic Arrays." *IEEE Transactions on Power Electronics*, volume. 24(5):pages 1198–1208, 2009.

[Wolfram, 2017] Wolfram. "Curve FittingWolfram Language & System Documentation Center." `http://reference.wolfram.com/language/tutorial/CurveFitting.html`, 2017. Accessed: 2017-04-20.